CONSOLIDATION OF COPPER AND ALUMINUM MICRO AND NANOPARTICLES VIA EQUAL CHANNEL ANGULAR EXTRUSION

A Thesis

by

CATHLEEN RUTH HUTCHINS

Submitted to the Office of Graduate Studies of
Texas A&M University
in partial fulfillment of the requirements for the degree of

MASTER OF SCIENCE

August 2007

Major Subject: Mechanical Engineering

CONSOLIDATION OF COPPER AND ALUMINUM MICRO AND NANOPARTICLES VIA EQUAL CHANNEL ANGULAR EXTRUSION

A Thesis

by

CATHLEEN RUTH HUTCHINS

Submitted to the Office of Graduate Studies of
Texas A&M University
in partial fulfillment of the requirements for the degree of

MASTER OF SCIENCE

Approved by:

Chair of Committee, Ibrahim Karaman
Committee members, Amy Epps-Martin
Karl T. Hartwig
Head of Department, Dennis L. O'Neal

August 2007

Major Subject: Mechanical Engineering

ABSTRACT

Consolidation of Copper and Aluminum Micro and Nanoparticles via Equal Channel Angular Extrusion. (August 2007)

Cathleen Ruth Hutchins, B.S., Marquette University

Chair of Advisory Committee: Dr. Ibrahim Karaman

Ultrafine grained (UFG), and nanocrystalline (nc) materials are of interest because of the high strength, compared with coarse grained counterparts. Several current methods to fabricate UFG and nc materials result in samples too small for practical use. In addition, the fabrication of nc materials, in particular, is difficult, and defects in the material causes significant reduction in strength and ductility of these materials. The present study uses Equal Channel Angular Extrusion (ECAE) to produce relatively large consolidates of UFG and nc materials.

ECAE has been used to consolidate micro and nanocrystalline powders. The behavior of consolidated pure Cu and aluminum alloys in the nano and micron size were explored. The effects of different routes, extrusion temperature, and post-ECAE processing on microstructure and mechanical behavior were studied. Processing parameters were explored to determine the influence of each parameter on the consolidation performance. The goals of experimenting with different processing parameters were to increase the ductility of the material, while maintaining relatively strong specimens. Comparisons were made with a recently developed powder compaction constitutive model and corresponding simulations.

ECAE of microcrystalline powders produced relatively ductile materials, with high strength. Swaging of these consolidated powders produced samples which were softer and less ductile in tension, than the non-swaged samples.

ECAE produced effective consolidation of Cu nanoparticles with average sizes of 100 nm, with an ultimate tensile strength of 680 MPa, with a fracture strain as much as 10%, which is higher than previously reported 7% [Haouaoui, 2005].

ACKNOWLEDGEMENTS

My master's thesis was a not just a study in consolidating material, but a means for me to gain experience in hands-on experimentation. Many people helped me to complete my research, and I would like to thank them for their support and their patience.

First, I would like to thank Dr. Karaman for his guidance and support. Under his direction I was able to perform this study and understand more about metallurgy and materials science. I would also like to thank Dr. Haouaoui, who pushed me to start my thesis early and provided advice in turning data into a thesis. Dr. Haouaoui also helped me to perform experiments more efficiently with his extensive knowledge in the Equal Channel Angular Extrusion process. Also, I would like to thank Dr. Hartwig and Dr. Epps-Martin for reviewing this work and being on my advisory committee.

Thanks are especially in order for Mr. Robert Barber for his efforts in processing my materials, acting as general fabrication consultant, and cutting tension samples in an efficient manner. I would also like to thank Vickie Weir from the College of Veterinary Medicine Large Animal Hospital and Jim Jobling from the Nautical Archeology Program at Texas A&M for their efforts in taking radiographic images of my samples.

This thesis would not have been made possible without the support of my husband, Jeffrey. I would like to thank all of the other students in Dr. Karman's research group: Majid Al-Maharabi, Sadegh Badakshan, Burak Basaran, Andy Brewer, Ersin Karaca, Benat Kockar, Hans Gerd Lamberts, Andre Leifield, Ji Ma, James Monroe, and

Guven Yapici for their advice and help. Also, I would like to thank Anshul Kaushik, from Dr. Srinivasa's group, for providing me with simulations of ECAE.

This research was supported by a grant from the Office of Naval Research Laboratories.

Mahalo Nui Loa, a me ke aloha,

Thank you very much and best regards.

TABLE OF CONTENTS

Page

Page

LIST OF FIGURES

FIGURE Page

FIGURE Page

FIGURE Page

FIGURE Page

FIGURE Page

LIST OF TABLES

TABLE Page

I. INTRODUCTION

1.1 Motivation and Significance

Ultra-fine grained (UFG) and nanocrystalline (NC) materials have the potential for significant improvement in mechanical properties, as compared to coarse grained conventional materials. Ultrafine grains are defined as having grain sizes between 100 nm and 1 μm. Materials that are nc have grain sizes below ~100 nm.

UFG and NC materials can be fabricated using severe plastic deformation (SPD), either in a bulk form or via powder consolidation. Continuous grain refinement can be accomplished by a SPD technique called Equal Channel Angular Extrusion (ECAE). ECAE is also known as equal channel angular pressing (ECAP) [1-12]. Another SPD technique for grain refinement is high pressure torsion (HPT). The advantage of ECAE over HPT is the capability of processing large samples and the uniformity of the strain.

Conventional consolidation techniques are capable of consolidating nanopowders by using heat and pressure. However, they usually result in grain growth, which leads to loss of the nanostructure [4]. SPD techniques can consolidate the powders at room temperature, decreasing the potential for grain growth [23]. HPT and ECAE can consolidate nanoparticles resulting in nc materials, and refine grain size during powder consolidation [13]. On the other hand, it is difficult to obtain nanocrystals using ECAE when starting with bulk coarse grained material [14-19]. However, consolidation of powders via ECAE results in bulk materials with nano to micron sized grains [8, 10]. The problem with HPT consolidation of nanoparticles is the difficulty of obtaining large samples and non-uniform strain distribution. Thus, the present study is being conducted

---

This thesis follows the style of Acta Materialia.

in consolidating nano-sized and micron-sized powder using ECAE at low temperatures. The benefit of using ECAE over other consolidation techniques is that

1) The possibility of consolidation below dynamic recovery temperatures

2) Large product cross-sections, and

3) Easy incorporation of second phase components such as other powder, filaments, or wire/ rod dispersoids [11].

ECAE also allows for a wide range of deformation routes to be applied to the material thru multiple passes and orientations, without changing the cross-section of the material [11]. Routes can be changed by altering the orientation of the billet with respect to the extrusion axis between passes [11].

The challenges of working with nanosized and micron sized powder are agglomeration of the powder, and the elimination of residual porosity. Defects that can arise in nc metals include [20]:

- Porosity- usually comparable to the grain size of the material, degassing and warm compaction can improve the purity and density of the compact
- Large flaws of 1 micron or larger are more detrimental to nc materials than pores, and prevent strong bonding
- Recrystallized grains: Nc Cu powder is especially subject to grain growth due to ambient temperatures being relatively high homologous temperatures.

These flaws may be the cause of the brittle behavior of nc metals in tension [20], even though many nc metals are strong. Higher strengths are usually achieved in

compression tests [21]. This may be due to the fact that the specimen is not significantly influenced by internal flaws in this mode [20].

Several parameters in ECAE can be changed, such as route type, the number of passes, the extrusion temperature, and pre- or post-ECAE processing. Heat treatments, annealing, and cold working can be applied before or after ECAE. Thus, ECAE provides a vast selection of parameters, which in turn, can yield a wide range of material properties and microstructures. It has also been suggested [21] that the use of back pressure during ECAE, in which pressure is applied at the opposite end of the billet as it is pressed thru the extrusion channel, can provide high hydrostatic pressure levels on the powder to break down agglomerates, in order to achieve higher ductility levels on nc consolidates.

Pure Cu and Al-10.5 Mg particles were chosen in the present study to show that ECAE as a method of powder consolidation can be applied to different materials and powder precursors. Pure Cu particles can be effectively consolidated at room temperature [21], and is a simple material to model. Recent research on Cu processed via ECAE at Texas A&M University, has resulted in fully dense nc materials. Tensile strengths as high as 479 MPa for bulk Cu, 470 MPa for mc Cu powder consolidate, and 728 MPa for nc Cu powder, processed at room temperature via ECAE [22]. However, consolidated nanopowders exhibited low ductility.

Aluminum alloys is the next step of complexity from Cu. Previous studies [23-28] have been performed on consolidation of Al alloys using conventional extrusion, though few studies [17, 29-32] have examined using ECAE to consolidate the Al alloy

particles. The use of back pressure during ECAE to consolidate pure Al particles showed promising results in strong, fully consolidated materials extruded at temperatures well below sintering temperatures, with ultimate tensile strengths as high as 160 MPa, and strain to fracture at 11% [17, 33]. Several studies show that using ECAE on bulk Al alloys can improve the toughness and strength of the material [34-37]. Comparisons of mechanical properties between ECAE and conventional extrusion techniques (which already exist in literature) in consolidating Al alloy particles will show if there are advantages of using ECAE, other than the preservation of the specimen cross section.

Additional experiments were performed for comparison with a finite element analysis model developed at Texas A&M University, by Kaushik and Srinivasa [38]. Two different porous media models were used to model the consolidation of powder via ECAE. The efficacy of the two models was evaluated, based on how accurately the models predicted the resulting shape and densities of the experimentalpowder consolidate.

1.2 Objectives

The specific objectives of the present study are stated below:

1. Determine optimal processing parameters to increase the ductility of mc and nc Cu consolidates, while maintaining strength levels, by altering the following parameters:
    a. Powder size: Determining if there are differences between Cu micronsized powder and nanosized powder.

b. Powder type: Determining the mechanical properties of Cu and Al alloy powder
c. Can material: The effect of using OFHC Cu and Ni cans.
d. ECAE route (*i.e*. strain path changes)
e. Number of ECAE passes (*i.e.* strain/ deformation levels)
f. Back pressure
g. Elevated temperature ECAE: compare room temperature extrusions to elevated temperature extrusions, in terms of extrusion performance and mechanical properties.
h. Post ECAE processing deformation: compare as-ECAEd samples to samples swaged at room temperature.

2. Determine the effect of initial density on the strength and ductility of the consolidated powder. This is important to understand, since strength and ductility in consolidated nanoparticles are inherently hindered by internal flaws such as porosity and powder agglomerates.
3. Determine if nanograins can be achieved without starting off with nanoparticlesl, since nanoparticles tends to form agglomerations and thus possess bimodal porosity distribution, which causes low ductility in consolidates. This can be achieved by consolidating cryomilled Al-10.5 Mg with initial nanostructure, and determining if nc grains can be achieved. Cryomilled Al alloy particles have been consolidated using Cold Isostatic Pressing and conventional extrusion in the past, but at high temperatures. This can cause grain growth. It is desirable to

consolidate the Al alloy at low temperatures, to preserve the nanostructure. In addition, ECAE results in large samples due to the conservation of sample cross section during extrusion. The preserved nanostructure of consolidated Al alloys is expected to result in high strength behavior, but equitable ductility as compared with a coarse-grained counterpart.

4. Determine if a Finite Element Analysis model, developed by Kaushik and Srinavasa [38] accurately predicts powder behavior during ECAE.

II. LITERATURE REVIEW

2.1 Ultrafine Grained and Nanocrystalline Materials

Ultrafine grained (UFG) materials have grain sizes in the submicrometer range, usually between 100-1000 nm. They have been of interest in recent years because of the enhanced mechanical properties upon grain size refinement. Several studies have found that UFG materials have significantly higher tensile strengths, compared to their conventional grain-sized counterparts [6, 39]. High cycle fatigue properties in UFG materials have been found to be superior to their conventional grained counterparts [2, 40]. High cycle fatigue resistance is attributed to high strength of materials- which UFG materials exhibit.

Ductility generally relies on the ability of a material to sustain plastic deformation. Several studies have been performed to evaluate the cyclic response of UFG materials produced by grain refinement via Severe Plastic Deformation (SPD) [1-9, 12, 40-43] in which grain refinement is achieved by subjecting a material to SPD. A study by Maier *et al.* [41] found that ultrafine microstructures demonstrated excellent cyclic stability in strain-controlled fatigue test.

Nanocrystalline (nc) materials have average grain sizes of less than 100 nm. These materials are of interest due to the enhanced mechanical properties that they exhibit. Properties include high strength, high hardness, increased resistance to damage, increased strength/ ductility with increasing strain rate, and enhanced super plastic deformation at lower temperatures and faster strain rates [44]. It is expected that with higher hardness, nc materials would have increased wear resistance [19].

Nanocrystalline materials fatigue behavior is similar to that of UFG materials. Studies for some nc materials formed by SPD show reduced low cycle fatigue behavior, even though the materials have enhanced high cycle fatigue behavior [19, 45]. This is expected, since low cycle fatigue is influenced by ductility, and high cycle fatigue is influenced by strength. NC materials so far have generally high strength- thus good high cycle fatigue properties; but low ductility- resulting in poor low cycle fatigue properties.

Due to the nature of nc materials, at high defect densities, the volume fraction of defects can become comparable to the volume fraction of the crystalline areas [46]. According to Gleiter's review of nanostructured materials [46], nc materials which are produced by different methods display vastly different mechanical properties. One example he used was the production of nc Ni prepared by two different methods: consolidation of powder, and by electrodeposition. The Ni produced by consolidation had very little ductility (<3%), and the Ni produced by electrodeposition was very ductile (>100% deformation) [46]. Gleiter [46] explains that this is due to the differences in the interfacial structures. Therefore, mechanical response depends not only on the grain size of the material, but also on other characteristics of the grain boundaries. Thus, mechanical response of a nc material can be altered by the processing conditions and methods applied to the initial material. The present study will investigate a specific method of producing nc materials by consolidating nc powders via ECAE.

Porosity can cause a decrease in tensile strength and ductility [45]. Therefore, it is important to increase the density of the powder before consolidation, called the green density, to achieve the highest possible density. A study performed by Agnew *et al.* [20]

examines the impact of porosity and flaws on mechanical behavior of nc metals. The study found that while crack-like pores affect the material's ability to withstand tensile stresses, large (>1 μm) flaws were more detrimental to the material's strength [20]. Tensile tests revealed that the material was strong, but brittle [20], which is expected, since many nc materials tests in various studies have exhibited similar behavior [44-46], due mainly to the processing induced defects.

Materials selected for the present study are based on the simplicity of the material, as well as the potential of grain refinement to enhance its mechanical behavior. For example, consolidated nc aluminum alloy powder produced by cryomilling and consolidated by high pressure torsion has been found to produce significant increases in microhardness [25], and tensile strength [27]. However, the consolidated material exhibits low ductility [25], which currently makes the material unsuitable for structural applications. Research by Wu and Xia [33] shows promising fully dense bulk samples (approximately 9mm in cross section) of mc and nc aluminum alloy powder using ECAE with back pressure. The mc Al sample reached an ultimate tensile strength (UTS) of 179 MPa and an elongation of greater than 10%, after 4 passes. Nanocrystalline consolidated Al had a compressive strength of 270 MPa, but with approximately 1-2% plastic deformation. Coarse grained pure Al has an UTS of 50 MPa, and UFG pure Al produced via other SPD techniques has a strength of 100-150 MPa. While Al is not as strong as Cu, in this study, we choose to extrude Al-10.5 Mg because it is one step higher in complexity than Cu. Also, many previous consolidations with conventional extrusion

have been performed, so it is simple to compare these results to see if there is an advantage of using ECAE.

Cu powder was selected for this study because it is simple to model, and easy to deform.

2.1.1 Hall-Petch Relationship in UFG Metals

The Hall-Petch relationship relates the grain size of a material to yield stress. Generally, the Hall-Petch relationship predicts that as grain size decreases, yield strength increases. However, the validity of the Hall-Petch relationship below 100 nm is still being debated [45, 47-52]. The Hall-Petch relationship indicates a strengthening of the material with grain refinement [44]. The main mechanism causing the Hall-Petch relationship is the pileup of dislocations at grain boundaries. Smaller grains results in more grain boundaries which causes enhanced resistance to plastic flow.

It is expected that nc materials will exhibit significantly higher strengths than an microcrystalline (mc) material. However, unlike UFG materials, the deformation mechanisms in nc materials is not well understood. In many cases, further decreases of grain size below 10 nm results in weakening of the metal [44]. Furthermore, while the Hall-Petch relationship is a straight line in the micron range, it cannot be extrapolated for grain sizes below approximately 1 micron [47]. Conventional grain sized Cu follows the Hall- Petch relationship given in Equation 2.1 [47]

$$\sigma = \sigma_0 + \frac{f}{\sqrt{d}} \qquad \text{Equation 2.1}$$

where σ is the yield stress, σ_o is the lattice friction stress required to move individual dislocations, f is a material constant, and d is the grain size.

Nanocrystalline Cu showed a negative slope for a hardness- grain size$^{-1/2}$ plot, and the Hall-Petch relationship is given in Equation 2.2 [47].

$$H(VPH) = 375(VPH) + \frac{625(VPH/\sqrt{nm})}{\sqrt{d(nm)}} \qquad \text{Equation 2.2}$$

where VPH is the hardness of the material, and d is the grain size.

This equation characterizes what was found in [47]. However, in their overview of nc Cu and Ni, Siow *et al.* [45] remark that there are several studies that found contradicting results. Thus, the applicability of the Hall-Petch relationship to nc materials is still under contention, and further studies are needed to understand nc behavior.

One particular examination of the validity of the Hall-Petch relationship in nc materials was performed by Chokshi *et al.* [47] in 1989. Chokshi *et al*. theorized that the volume fraction of interfaces with in an nc material becomes comparable to the volume fraction of the crystal, due to its extremely small size. This relationship between volume fraction of interfaces and crystals may introduce a factor that causes the different deformation behavior. Thus, a different explanation of deformation mechanisms than conventional materials is needed.

Chokshi *et al.* used the theory of Armstrong [53] that hardness measurements was a convenient means of establishing the Hall-Petch relationships in fine grained materials. The study by Chokshi *et al.* concluded that for nc Cu and Pd, the Hall-Petch

equation resulted in a negative slope. Materials with a grain size above 1 μm had a Hall-Petch equation with a positive slope. Chokshi *et al.* rationalized that the change in the slope of the Hall-Petch relationship is due to the change of the strength of grain boundaries at low and high temperatures. They argue that at high temperatures, grain boundaries weaken crystalline materials, due to the onset of diffusional creep and grain boundary sliding [47]. The concept of diffusional creep is supported by studies performed by Cai *et al.* [54].

The concept of grain boundary sliding as a mechanism for deformation in nc materials is supported by Kumar *et al.* [44]. In a similar study, Schiotz, Di Tolla, and Jacobsen [55] simulated a nc Cu sample going thru deformation. Computer simulation shows that the reverse Hall-Petch relationship occurs due to grain boundary sliding. This may, however be due to assumptions made during the simulations.

A study on the grain size dependence of the plastic deformation kinetics in Cu by Conrad [49] separated the flow stress of Cu into three regimes. Regime I is between 1 μm to 1 mm, Regime II is between 0.01 μm to 1 μm, and Regime III less than 0.01 μm. Conrad found that Cu in Regime I (conventional sized- grains) obeys the Hall-Petch relationship, since these grain sizes influences the average slip distance of the dislocations, which is expected. No analysis of the Hall-Petch relationship was made for Regime II. It can be concluded that Regime II provides a transition area, as claimed by Conrad and Narayan [56]. In this regime, the grain sizes become smaller than the cell size, so no dislocation cells are expected to form during plastic deformation, but intragranular dislocation activity continues until the separation of dislocations becomes

greater than the grain size [49]. In Regime III, the spacing between dislocations becomes larger than the grain size, and that the Hall-Petch predicts softening as grain size is refined.

A study by Carsley *et al.* [52] on the mechanical behavior of bulk nc iron alloy found that the Hall-Petch relationship remains valid in fine grained Fe alloy with grain sizes between 30 nm and 2 μm. Though, plasticity was extremely limited and shear fracture occurred after small amounts of deformation [52]. Carsley *et al.* notes differences in nc Fe alloy behavior, compared to conventional Fe alloys. These consist of inhomogeneous deformation with the onset of shear banding at the yield point, along with a large tension- compression asymmetry in the strength. The differences between these findings and those previously mentioned are drastic.

2.2 Methods of Creating UFG and Nanocrystalline Materials

Several methods exist to create both UFG and nc materials. This section will describe some of the most common methods and strategies. Also, several strategies involve using a combination of two or more methods. Each has unique advantages and disadvantages.

2.2.1 Top-Down and bottom-up Approaches

There are several methods of fabricating nc materials. Most methods fall under two main approaches: bottom-up and top-down. The bottom-up approach refers to nc materials that are assembled from individual atoms or nanoscale building blocks [19]. Inert gas condensation, electrodeposition, and chemical or physical depositions, are techniques that fall under this approach. The top-down approach involves refining the

grain size of coarse grained materials [19]. Severe plastic deformation (SPD) techniques such as Equal Channel Angular Extrusion (ECAE) and high pressure torsion (HPT) use the top-down approach to achieve nc structures. The disadvantage of SPD techniques, using a coarse-grained bulk material, is that grain sizes can only be refined into the range of 100-1000 nm [19]. Karaman *et al.* [21] have been successful at achieving grain sizes of less than 80 nm, by using ECAE as a bottom-up approach to consolidate nanoparticles. This study focuses on using ECAE as a combination of bottom-up and top-down approaches to consolidate nano and micronsized powders to achieve nc and UFG materials.

Cryomilling is a top-down method of producing UFG material. Cryomilling is the mechanical attrition of powders with micrometer range grain sizes in a slurry form by milling balls in a cryogenic liquid [57]. The cryomilled material needs to be warm or hot pressed into a compact to form bulk structures. This method has been successful in aluminum alloys, in particular, however, the purity of the material can not be controlled and it is difficult to obtain full density [44].

Gas-phase condensation is another bottom-up method to produce nc materials. Powder particles typically 5-50 nm in size are produced by condensing materials from the vapor phase [44]. The powders can then be consolidated in a die using high pressure. Gas-phase condensation has many advantages, in that it produces texture-free microstructures and equiaxed grains, and density can be improved by cold rolling, without affecting texture and grains [44]. Disadvantages of this method include the

production of carbon and sulfur impurities which are inherent with in the process, nano bubbles in the structure, and changes in the texture with decreasing grain size [44].

A similar method to gas-phase condensation is cryomelting. Nanocrystalline powders in sizes 30-100 nm are obtained by condensing a metal vapor with a cryogenic medium [58]. The study by Champion *et al.* [58] found that nc Cu produced by cryomelting had the same modulus of elasticity as coarse grained Cu, but had significantly higher strength than the coarse grained Cu. The benefit of cryomelting is the production of small powder sizes in relatively large yields for bulk consolidation.

Electrodeposition lays a layer of powdered metal onto a bulk substrate. Ebrahimi, Zhai, and Kong [59] studied the mechanical properties of electrodeposited Cu. The sizes of crystals near the substrate were smaller than crystals near the solution. Electro-deposited Cu films exhibited a high strain hardening rate, very small maximum uniform strain, no detectable post-neck elongation, and low ductility [59]. The low ductility was attributed to the early onset of plastic instability due to in-plane residual stresses and surface roughness by Ebrahimi, Zhai, and Kong [59].

2.2.2 Severe Plastic Deformation (SPD)

Several SPD techniques use both top-down, and bottom-up approaches. In addition, several combinations of the powder production techniques and consolidation techniques can be combined as one technique [16-18, 22, 31-33, 57, 60-63]. Several studies have been performed in which the two approaches are combined. Works on using Hot Isostatic Pressing/ Cold Isostatic Pressing (HIP/CIP) and Severe Plastic Torsion/

High pressure torsion (SPT/HPT) combine the top-down and bottom-up fabrication approaches.

Severe plastic torsion (SPT), also known as high pressure torsion (HPT), is a specific SPD technique, which involves large plastic shear deformation under high applied pressures at room temperature [13, 23, 24]. SPT can be used to create bulk nc materials from powder. Botta Filho *et al*. theorized that SPD causes the partial crystallization of amorphous phases [24]. The HPT processed aluminum powder exhibited high Vicker's hardness, which can correspond to high tensile strength. In a similar study, Yavari *et al*. [26] studied the behavior of a gas atomized Al powder consolidated via SPT. The strength of the material was exceptionally high, but the ductility was limited, mainly due to the high levels of internal stresses generated by the SPD [26]. Cryomilled powders can be consolidated via HPT, to create bulk (0.3 mm by 1 cm wide disks) nc samples. Xu and McMeeking [25] consolidated cryomilled Al-7.5 Mg alloy using HPT, with an applied pressure of 6 GPa. These results were compared with bulk Al-7.5 Mg alloy produced by hot isostatic pressing (HIP) and warm extrusion. The microhardness of the HPT alloy was significantly higher than that of the HIPed sample. The disadvantage of SPD/HPT over other consolidation or SPD techniques is that the sample size obtained is relatively small, so is not practical for industry use.

Equal Channel Angular Extrusion (ECAE), which is also commonly known as Equal Channel Angular Pressing (ECAP), is a process in which a material is deformed through simple shear with the shear taking place without any concomitant change in the

cross-sectional area of the sample [10]. As the present study is on ECAE, Section 2.3 will detail the ECAE process.

2.2.3 Hot Isostatic Pressing (HIP)/ Cold Isostatic Pressing (CIP)

Isostatic pressing, whether cold or hot, generally requires that a powder be packed into a container. The container is usually a thin-walled metal can with a desired shape, and is evacuated, sealed, and put under high pressure, with or without high temperatures, until the powder is compacted [64]. Cold isostatic pressing (CIP) is isostatic pressing at lower temperatures, usually at room temperature. Nanocrystalline Cu consolidates produced via CIP are reported to have the same modulus of elasticity as microcrystalline Cu produced in a similar manner, but with a much higher strength [58]. In CIP, elastic-plastic deformation of the powder and can is the mechanism of deformation, since at this low a temperature creep in Cu is not activated [64]. The advantage of CIP is that relatively large samples can be consolidated, at room temperature, and the general shape of a sample can be dictated by the container shape. One disadvantage of CIP is that the can imparts deformation onto the powder in conjunction with the applied external forces, which causes shrinkage of the powder. The main disadvantage is that CIP cannot achieve full density.

Hot isostatic pressing (HIP) is isostatic pressing at elevated temperatures. Hot isostatic pressing of nc sized powders can produce bulk nc samples [27, 28, 52, 64, 65]. HIP requires the sample to be heated under load. Samples produced via HIP deform in an inhomogeneous manner [52]. Al bulk alloy was produced by HIP [27], and resulted in full density with increasing pressing temperature of amorphous Al. However, high

consolidation temperatures can result in grain growth. Kawamura, Mano, and Inoue [27] found that for Al alloy consolidated via HIP, nanoscale Al was dispersed within an amorphous matrix, but if no amorphous matrix was present, only UFG Al alloy existed in the compacted powder. HIP produces a sample without texture, which is fully dense [28]. However, the HIP microstructure of an aluminum alloy found by Billard *et al.* [28] contains mc grains embedded in a UFG matrix, which does not make the material strictly an UFG material. SEM images by Billard, et al [28] show that the mc regions help to stop the propagation of cracks. However, this study started with nanosized powder, but HIP resulted in a mc and UFG microstructure, which may be due to grain growth because of the required high processing temperatures. The disadvantage of HIP is that high temperatures and extremely high pressures (~1-2 GPa) are required for successful consolidation.

2.3 Equal Channel Angular Extrusion (ECAE)

2.3.1 Introduction to ECAE

Equal Channel Angular Extrusion (ECAE) was invented by VM Segal in 1972 in Russia, and was first described in [66]. ECAE is a processing method in which a material is forced through a die of equal channel sizes, which imparts large plastic strains on the material thru simple shear. The simple shear applied may be due to a wide range of angles, but the most common angle is 90° [15-17, 21-23, 29-31, 33, 60, 67-74] since this angle provides the optimal extrusion characteristics. Mathematically, the shear imparted on the material (γ) depends on the die angle (2θ).

$$\gamma = 2\cot\theta \qquad [79] \qquad \text{Equation 2.3}$$

ECAE presents a method of grain refinement that allows for large test samples to be produced, as compared with the small samples obtained from SPT. This method also allows for repetitive and alternating extrusions to be performed on the same material, since the cross section is only nominally changed after extrusion. Extruding coarse grained samples produces sub micrometer sized grains. As mentioned earlier, the use of nanoparticles can produce UFG and nm sized materials by using ECAE as a method of powder consolidation. The advantage of this method, as compared with conventional consolidation, is that consolidation can be achieved at room temperature, for many materials [11, 32, 75-77]. Of course, there are some materials in which elevated extrusion temperatures are necessary [15, 16, 29, 60, 69, 70]. Processing materials via ECAE can result in an increase in material strength, but may result in a decrease in ductility.

2.3.2 Basics of ECAE

Several parameters of the ECAE process can be varied. This section will discuss the different processing parameters, and their influence on the behavior of materials. This section will also discuss the reasons behind the present study's use of certain parameters.

2.3.2.1 Die Angle

Several studies examined the effect of different die angles [78-84]. Figure 2.1 shows what is meant by die angle, and a cross section view of the ECAE die. According to Segal [79], to impart the largest uniform shear, the die angle should be as small as possible, but for $2\theta<90$ degrees, a dead metal zone is formed at the channel corner. A

study by Nagasekhar *et al.* [80] explored the stress and strain histories in ECAE processing using Finite Element Analysis (FEA) to predict the behavior of a material extruded through die angles between 60-160°. Nagasekhar *et al.* concluded that the differences between effective strain values at two different points are lowest at a die angle of 90° [80]. The maximum principle stress values at two different points are lowest at die angles equal to or less than 120° [80]. Banghong [78] performed numerical research on the effect of die angle, and concluded that a die angle of 90° produces the most effective strain, which agrees with the conclusions of Segal and Nagasekhar *et al.* Wu and Baker [81] studied the strain imparted on plastic layers of two different colors by die angles of 90° and 120°. Wu and Baker found that the 90° die imparted a larger shear deformation than the 120° die, which agrees with the previous studies. Thus, for this study, a die cross section angle of 90° was used, to impart the largest shear strain on the material.

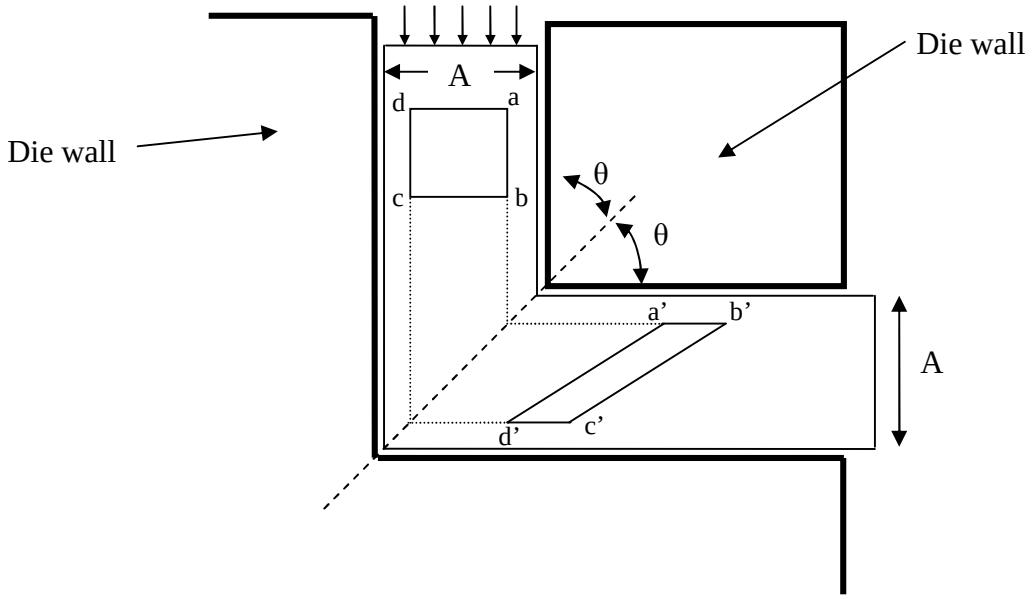

Figure 2.1: Schematic cross-section of an ECAE pass of a solid material [22]. A square element (a, b, c, d) is shown after its pass through the die (a', b', c', d').

2.3.2.2 Routes in ECAE

Different strain paths can be applied during ECAE thru changing the rotation of the billet around its axis after subsequent passes. Different ordering of rotations between the successive passes is called the route. Each route can be used for multiple passes. The descriptions are given in the Table 2.1.

Table 2.1: ECAE routes currently used in research

ECAE route		A	B	C	C'	E
Number of passes		1, 2, 4, 8	2, 4	2, 4	4	4, 8, 16
Rotation before	Odd passes	0º	+90º	+180º	+90º	+180º
	Even passes	0º	-90º	+180º	+90º	+90º
Microstructures		Lamellar	Filamentary	Equiaxed	Equiaxed	Equiaxed
Deformation analogy		Rolling	Drawing	Shear	Shear	Shear

Route choice is important in tailoring the texture of the extruded material. Ferrasse *et al.* [30] studied the effect of routes on texture evolution. Routes A, B, and C, and D (equivalent to C' in the current study) were performed, with two to eight passes. They found that route A produced a texture evolution similar to rolling, route D showed no significant changes in the pole figures, route B produced a cyclical texture evolution in which the odd number passes are a mirror symmetry of the even numbered passes. Thus, for the present study, extrusions using route B were performed for only even number of passes. Route C produces new type of textures [30]. This study suggests that route D and B would be best to decrease strong textural development, along with route C after 5 passes. Route A appears to develop the strongest textural development.

Furukawa, *et al.* [67] studied the shearing characteristics for different processing routes and number of passes. Table 2.2 shows the results of this study.

Table 2.2: Shearing characteristics of a cubic element, with three orthogonal planes (X, Y, and Z) for different ECAE processing routes [67]

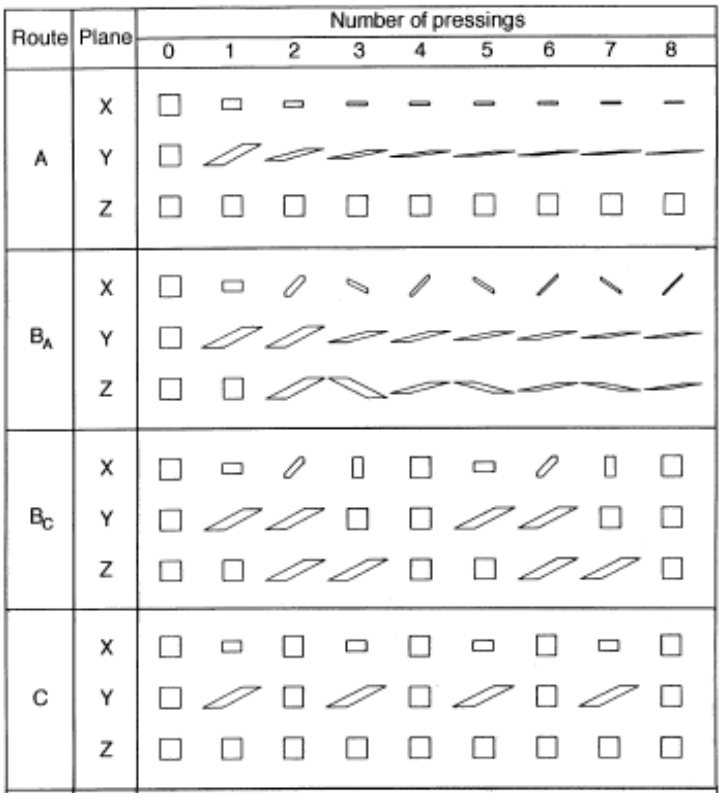

The results of the study by Furukawa *et al.* show that for routes B_c(called C' in the present study) and C, after 8 passes, the shearing characteristics returns back to the original shape in the X, Y, and Z planes of an originally cubic element. Route B_c(C') shows a cycle back to the original strain after every four passes, where route C shows cycles after every two passes.

Haouaoui *et al.* [18] studied the effects of ECAE to consolidate micro and nanopowders. The consolidated micro-powder exhibited near-elasto-plastic response under tension tests, and certain ECAE routes (2A and 2B) resulted in less dislocation density than that in the ECAE-processed bulk Cu [18]. Consolidated nanopowder was found to have a bimodal distribution of grain sizes, which resulted in a very high

strength and relatively high ductility in compression. Robertson *et al.* [61] used a similar method as Haouaoui *et al.*, to achieve bulk amorphous Cu. The micron-sized Cu alloy was subjected to consolidation via ECAE, and was successfully warm extruded.

2.3.2.3 ECAE and Back Pressure

Back pressure (BP) is a system in which pressure is applied opposite to the punch pressure, which combines the high hydrostatic pressure and the uniform shear over large volumes during ECAE. Figure 2.2 shows the back pressure set up for the current study.

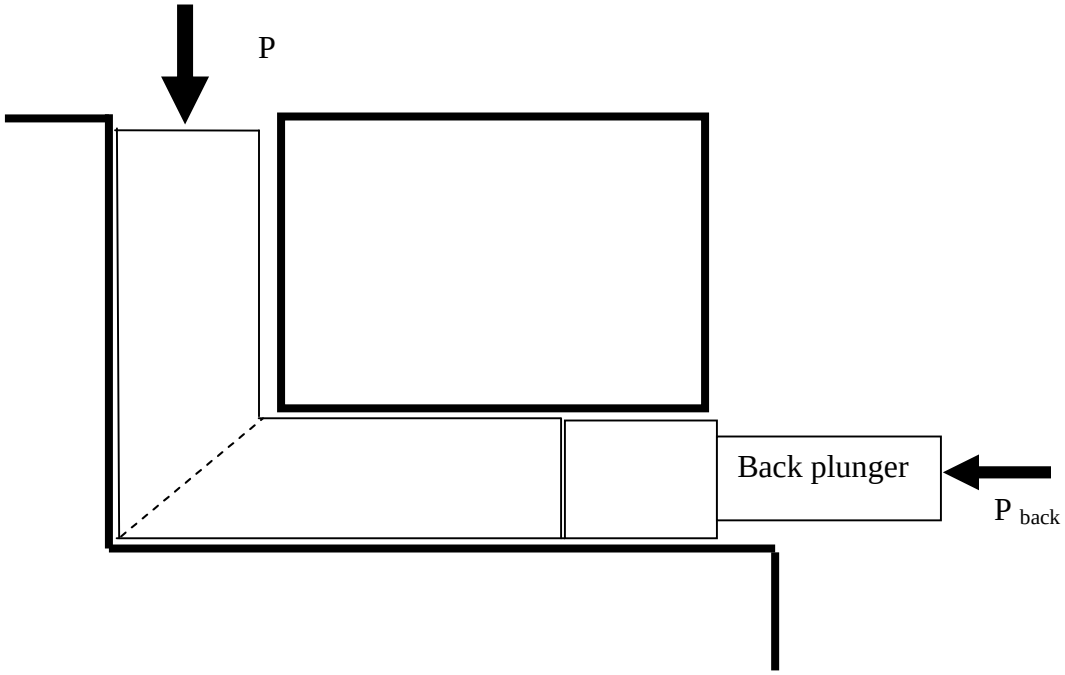

Figure 2.2: Current back pressure schematic, showing application of back pressure to the ECAE press.

Back pressure was used to successfully consolidate pure Al micron sized particles by Xia and Wu [17]. Full density of compacts was achieved using back pressure, extruded at 100°C, and had strength of 160 MPa and ductility of 11% strain to fracture, as compared with bulk ECAE Al with a stress of 64 MPa and a ductility of 23%

strain to fracture. In a similar study, Xia and Wu [33] were able to consolidate micro and nanosized Al powders into fully dense bulk material using ECAE with back pressure. Fully dense samples were obtained from the micron sized powder up to an extrusion temperature of 300°C, but fully dense nanopowders were obtained only at 400°C, with back pressure. The consolidated microcrystalline powder had strength of 170 MPa after four passes with a ductility of above 10%. Compressive strength of the ECAEd nanopowder was 270 MPa after two passes, with a ductility of 2%. These studies indicate that the use of back pressure with ECAE can enable the consolidation of micro and nanopowders into full density, at relatively low temperatures.

2.3.2.4 Can Material

Differences in can materials can cause changes in transmitted forces to the powder by imparting different hydrostatic pressures. Haouaoui *et al.* found that nickel canning and a minimum of two passes produced a good Cu nanopowder consolidates [8].

Kim *et al.* [32] found that consolidating powders via ECAE without a can, or with a can made out of low ductility metals (such as Al alloys) results in cracks in the canning material and internally, in the consolidate. Therefore, proper can selection is important in the consolidation of powder. In this study, nickel and Cu cans were used to consolidate the powders, both of which are ductile cans. Nickel is used because it has a higher strength, and can impart greater hydrostatic pressures, which is especially useful in consolidating nanopowders. As a rule of thumb, can material with similar flow

characteristics as the powder inside the can is selected for ECAE [21]. In the current study, Cu 101 was selected for the mc Cu, and Ni was selected for the nc Cu.

2.3.3 ECAE of Copper

Grain refinement of bulk Cu via ECAE resulted in significantly higher strength material, with relatively good ductility, compared to conventional sized grain Cu [11, 71, 85-88]. Bulk ECAEd Cu exhibited an increase in strength and ductility [8] for microstructures 300 nm to 500 nm. The study by Haouaoui *et al.* [8], which precedes the present study, explored the use of ECAE on bulk Cu. F. Dalla Torre *et al.* [71] found that 4 passes (in route B_c, with back pressure) on bulk Cu produced the highest UTS. Also, grain size was the smallest, with the least amount of variation in samples subjected to 4 passes. Eight passes produced the second highest UTS.

Powder behaves differently than bulk material during ECAE. Consolidation of Cu powders, micron and nanometer sized, via ECAE resulted in stronger material than the ECAEd bulk Cu [61], but much lower ductility than the ECAE bulk or coarse-grained Cu [18]. Powder consolidation occurs during the shear zone, as shown in Figure 2.3. The particles orient along the shear angle, but agglomerates (especially for nanopowder) can cause the sample to have residual porosity. Haouaoui *et al.* concluded that nanopowder Cu was sensitive to the parameters chosen for extrusion, and that to obtain good consolidation, a minimum of two passes are necessary for nanopowder Cu [18].

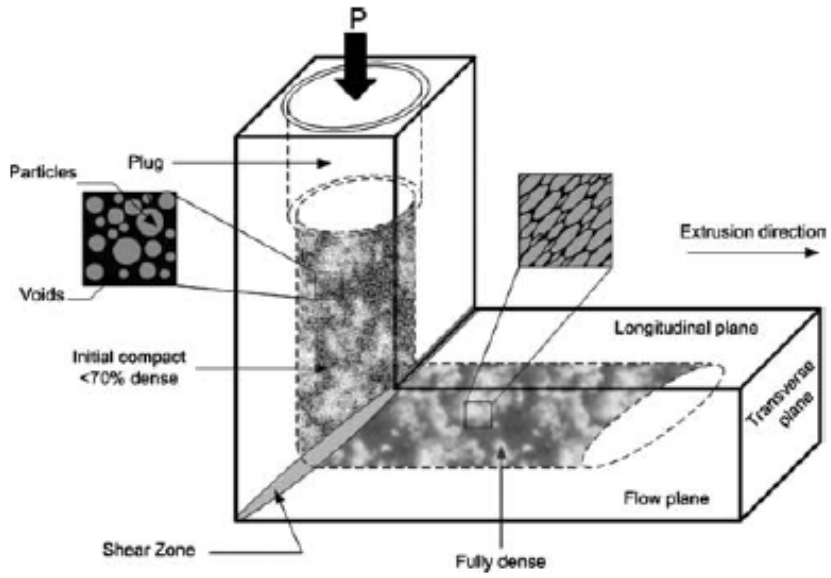

Figure 2.3: Schematic of the ECAE powder consolidation process [21].

Haouaoui *et al.* found that ECAE of micro and nanosized powder yielded significant increases in yield strength, compared to coarse-grained annealed Cu [18]. However, the nm Cu had very little ductility, which Haouaoui *et al.* attributed to remnant porosity and premature debonding between agglomerates. Thus, for the present study, room temperature swaging was performed after ECAE of billets in attempt to remove remnant porosity. Swaging was selected because it is relatively simple, fast, and can be performed at room temperature, as opposed to conventional extrusion, which takes much more time, is difficult, and requires elevated temperatures, which can cause grain growth in the consolidated powders.

2.3.4 ECAE of Aluminum Alloys

Bulk aluminum alloy extruded via ECAE was stronger than its respective coarse grained alloy, but exhibited lower ductility [34, 35, 85]. Current research on ECAE consolidation of Al powder includes the use of back pressure [17, 33]. Aluminum

powder consolidated using ECAE with back pressure resulted in significantly higher strengths (~2.5 times that of bulk ECAE Al, and ~4 times bulk Al as cast), but with a much lower ductility (~5 times less than bulk Al as cast) [17]. As mentioned previously, back pressure helps to consolidate the Al powders effectively. The present study examined the effect of ECAE on Al alloy powders with and without back pressure.

ECAE of Al alloys produced fine grain structures, which are stable at temperatures less than 240 °C (which is ~0.35 T_m), depending on the type of Al alloy, but this grain structure was completely lost at super plastic temperature regions [89]. The microstructure contained a large volume fraction of low-angle grain boundaries, with a bimodal distribution of grains in [89]. The study by Zhilyaev *et al.* [37] found that increasing number of ECAE passes lead to an increase in high-angle grain boundaries, which are attributed to high strength and low ductility [90]. Al studied in [89] had a microstructure with large regions of subgrains within fine micron range grains, and grain refinement was not affected by die channel geometry and backpressure [37].

One of the concerns in nanoparticle consolidation is the oxide build up on powder surfaces, which limits the material's ductility. A study by Lin and Lavernia [63], which modeled the oxide break up of Al powders during ECAE, found that it is possible to significantly refine oxides in powders during ECAE, such that the oxide particles are 1 to 10 nm in size. Increasing number of passes, decreasing processing temperature, and decreasing tool angle are predicted to minimize oxides in the powder surface.

III. EXPERIMENTAL PROCEDURES

3.1 Materials

The materials of interest were Cu in different size powder forms provided by the US Department of Energy Ames Laboratory (Ames, IA) and Argonide Corporation (Sanford, FL), and on aluminum alloy powder (Al-10.5 Mg) provided by University of California, Davis (Davis, CA)

3.1.1 Copper Powder

High purity Cu powder was obtained in two different sizes; 20 to 45 μm provided by the DOE Ames laboratory (denoted as mc Cu), and nanoparticles with an average particle size of 100 nm provided by the Argonide Corporation (denoted as nc Cu). The mc Cu was produced by gas atomization, and was sealed in Ar gas when it was recieved. The nc Cu was produced using the electro-explosion of wire process (EEW). In EEW, wire is fed into an argon-filled reactor, and then a high current and high voltage is applied to the wire in a microsecond pulse, which causes the wire to explode. The nc Cu powder was received in vacuum sealed glass tubes.

3.1.2 Aluminum Alloy Powder

Al-10.5 Mg powder, provided by UC Davis, having an average particle size of 50 μm, was produced using cryomilling. Cryomilling is the mechanical attrition technique in which powder is ball milled in slurry formed with milling balls and a cryogenic medium [57]. Al-10.5 Mg powders were mechanically milled at cryogenic temperatures (approximately -190 °C) for 8 hours [57]. Stearic acid was used during the production of the Al powder to minimize cold welding during milling, a process called passivation.

Residual amounts of stearic acid are removed by degassing the can under high temperature, as described in the next section.

3.2 Sample Preparation for Processing

Two types of metal cans were used (nickel and Oxygen Free High Conductivity Copper (OFHC)), and fabricated at either four inches or seven inches lengths. OFHC Cu and nickel cans were chosen because they can produce desired hydrostatic forces on the powder, which decreases the number and size of porosity [21]. A general rule of thumb is to select the can material such that it has similar flow characteristics as the powder inside the can [21]. Karaman *et al.* [21] found, thru trial and error, that using nickel cans to consolidate nc Cu powder showed better integrity than steel cans. The dimensions are in Figures 3.1 and 3.2 for four and seven inch cans, respectively.

The 4” cans were used to compare cross sections of the Cu powder consolidates processed using different extrusion conditions. Powder was filled into the cylindrical cavity of the can, with 0.75” diameter and 2” in length.

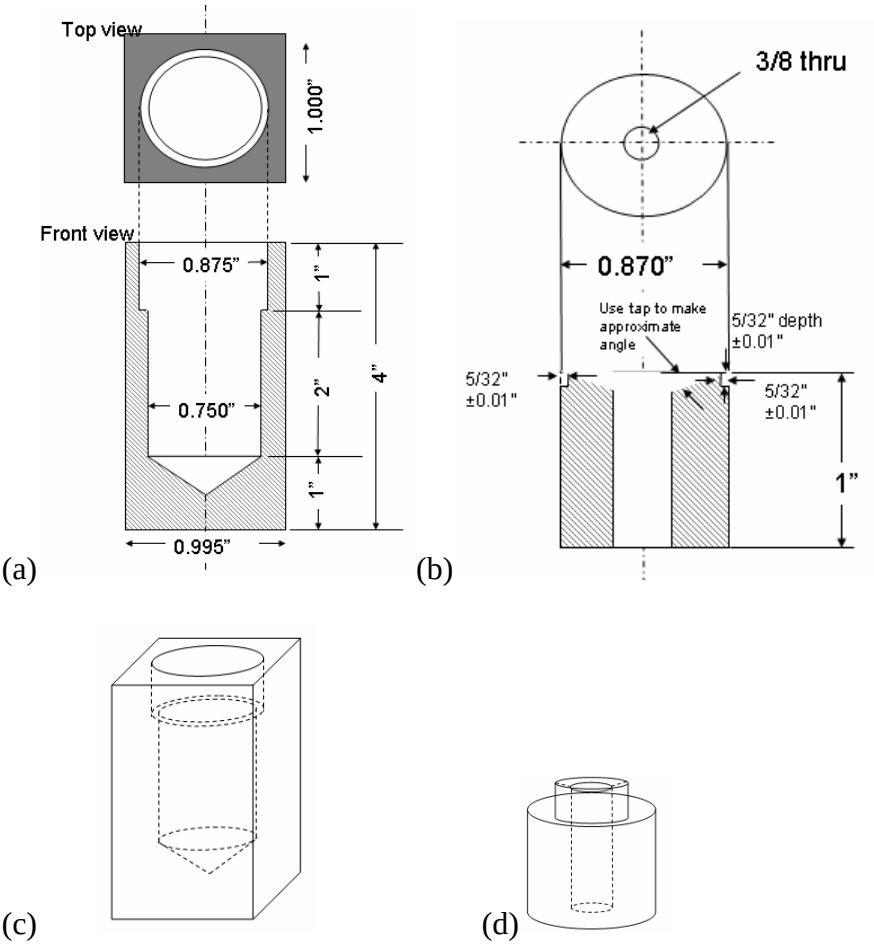

Figure 3.1: 4" Can with cap for powder filling, for mc Cu powder (a) dimensions of the can, (b) dimensions of the plug, (c) isometric view of can, (d) isometric view of plug.

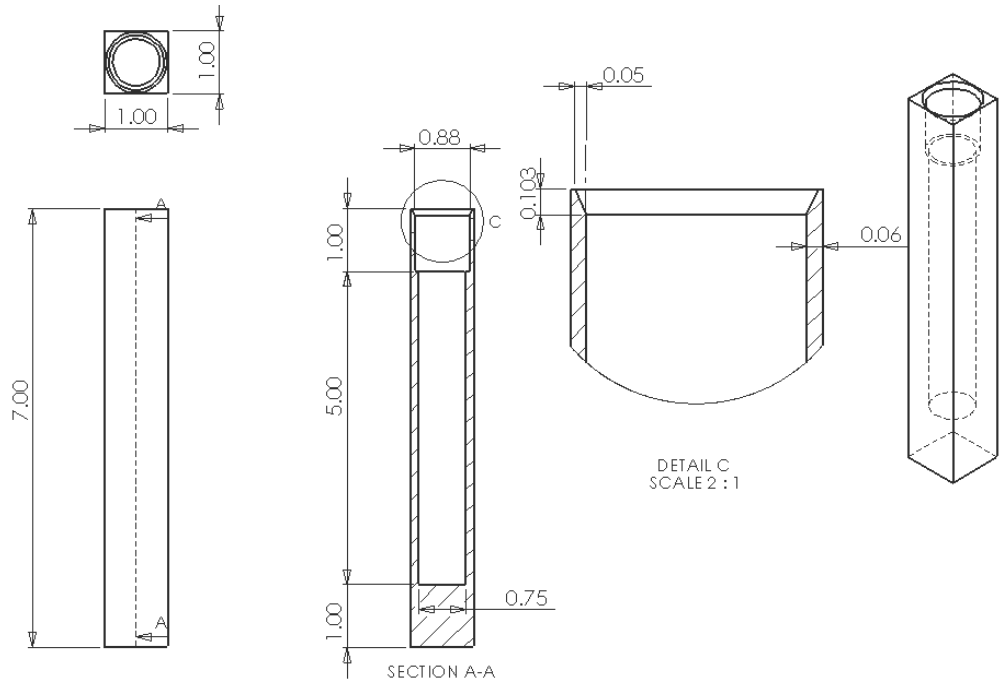

(a)

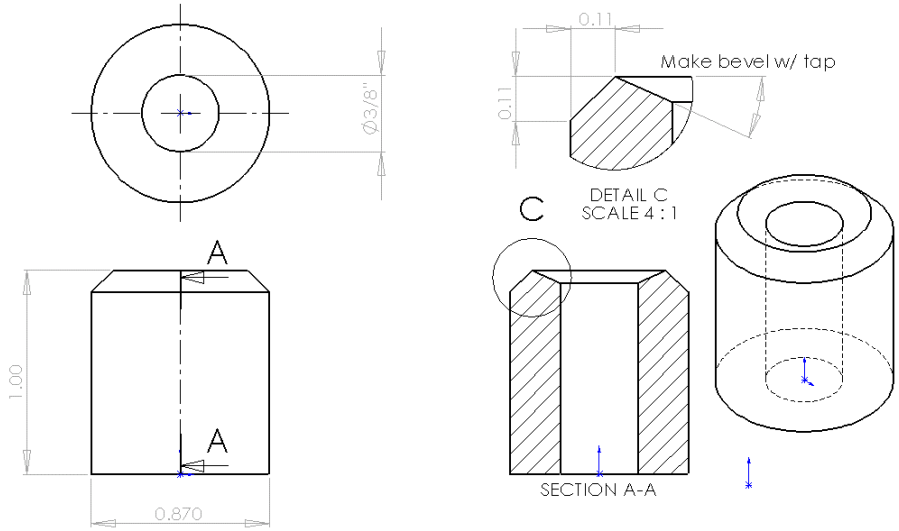

(b)

Figure 3.2: (a) 7” cans made out of Cu 101, (b) cap, made out of Cu 101 for filling of microcrystalline Cu powder.

The 7” cans were used to consolidate powder to obtain large enough billets to extract tension and compression samples from. Powder is filled into the cylindrical cavity of the can, with 0.75” diameter and 5” in length.

Nickel cans were designed as shown in Figure 3.3, to be used with nc CU and AL-10.5 Mg powders. A 0.875” diameter Cu tube was cut to 1” in length, to fit into the 0.880” hole in the can, and a Cu cap was made to fit into the tube. This was done because the solder used did not adhere well to Ni, but adhered well to Cu. The Cu tube was brazed onto the empty nickel can at 800 °C in a heat treating oven, using shaped 56% silver brazing alloy (Safety-Silv 56, JW Harris Co, inc, Mason, OH), cadmium free, 1/16” diameter and brushed with Stay-Silv white brazing flux(JW Harris Co, inc, Mason, OH). The brazing alloy was kept in place by using super glue. The can was then cleaned with an acid solution of 2.5% HNO_3 and 2.5% Nitric acid (remainder distilled water) to remove flux residue inside the can.

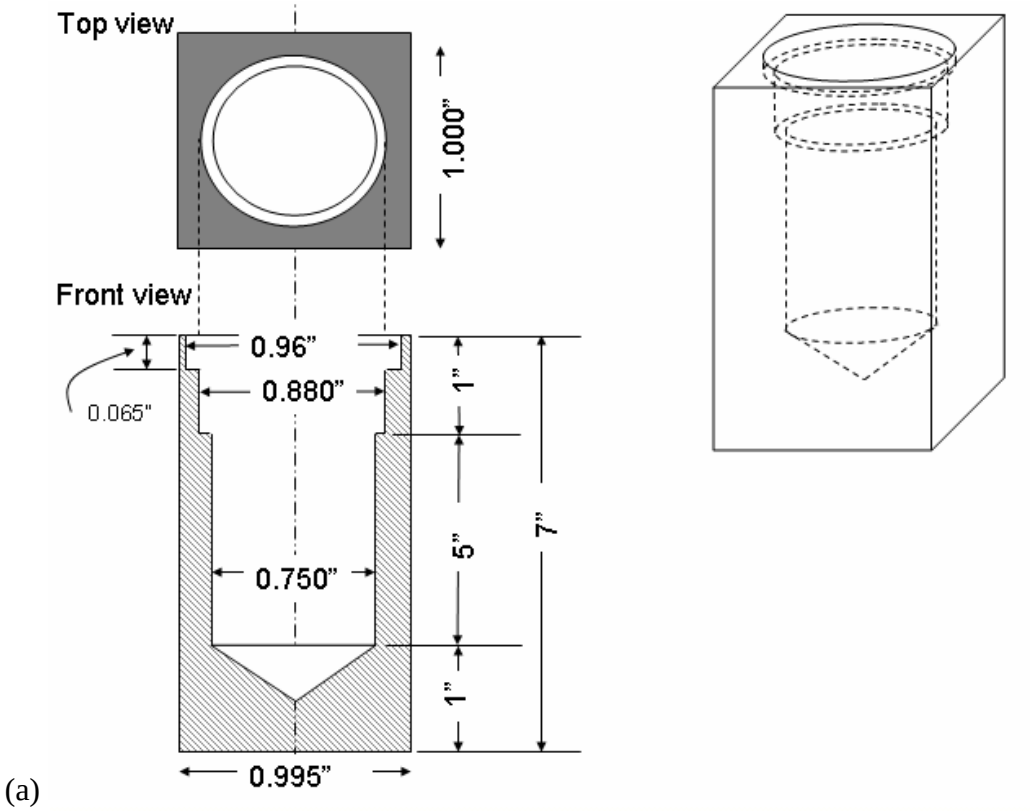

(a)

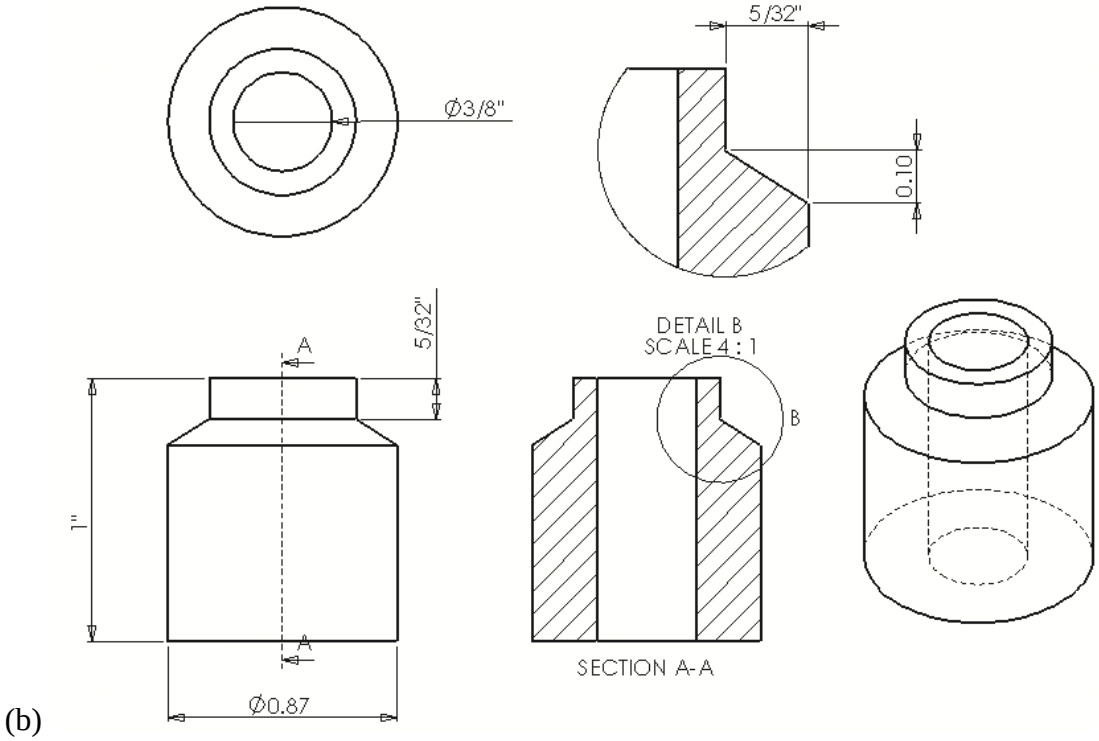

(b)

Figure 3.3: (a) 7” can design for filling with nc Cu and Al-10.5 Mg powder, Material: Ni, and (b) associated plug geometry, Material: Cu 101 OFHC.

Can, cap, and tube were sanded in contact areas, and then cleaned in an ultrasonic cleaner for approximately 1 minute in an acetone bath, to remove grease and particles from machining. Solder was shaped for cans to be used with Cu powder. A ring of solder was formed to fit the can-plug interface (which is circular, Figure 3.4a), and a spiral of solder was formed, as shown in Figure 3.4b, to fit into the plug's 3/8" inner cavity. The spiral diameter was made such that it would cover the plug's inner diameter.

(a) (b)

Figure 3.4: Solder shaping for (a) inside cavity of the plug, (b) and can-plug interface for melting after degassing, to seal the filled can under vacuum.

The parts were then soaked in acetone for another minute to remove residual grease from contact with skin. This was done to eliminate surface oxidation and contamination to ensure soldering and brazing could take place.

The powder was then pressed into the cans in a high purity Argon atmosphere. The atmosphere was regulated in an Omni-Lab double wide glove box system, supplied by Vacuum Atmospheres Company (Hawthorne, CA) with less than one ppm of oxygen and moisture. Two types of powder filling methodologies are followed: tapping and

hydraulic cold pressing. The goal was to investigate the initial tap density (also called the green density) on the final consolidate performance. Hand tapping produces a lower green density, since it does not compress the powder, which forces the powder to fill into porous areas. Hydraulic cold pressing forces the powder to compress, and fill in porous areas, and thus increases the green density of the packed powders.

The powder was poured into a can using a funnel. The can was then agitated by tapping it on the work surface, to settle some of the powder. This produced useful consolidates only for the microcrystalline powders. Nanopowder agglomerates became too large to fit thru the funnel, and very low green density was obtained due to inter-agglomerate porosity. Experience has shown that nc Cu filled by tapping, in which the powder was settled by tapping, produced little usable powder. The sizes of the consolidates from these low green density cases were too small to produce any mechanical testing samples.

For the cans filled using the hydraulic hand press, the powder was filled incrementally, by approximately 10 to 15 grams an increment, then the hydraulic press was used to compact the powder. The press had a punch that could fit into the can, and was made out of tool steel. The powder was compacted under the maximum pressure (~17 kips) that the press could exert.

To determine the powder weight filled into the cans, the cans were weight before and after the filling. An average volume of the powder cavity was determined by weighing the amount of distilled water needed to fill the can up to the plug line. The green density of each filled can was determined by:

$$\frac{W_{powder}(g)}{V_{powder\_cavity}(cm^{3})} = green\_density(g/cm^{3}) \qquad \text{Equation 3.1}$$

Where W_{powder} is the weight of the powder in the can, and $V_{powder\ cavity}$ is the volume of the powder cavity– measured to be approximately 36.5 cm^3.

The can was then capped. Some clean high temperature fiberglass cluster was put in the 3/8" diameter hole in the plug. This was found to be necessary, because the vacuum would cause powder to react to the solder, and bubble up, so the can could not be sealed. In addition, powder could be sucked up by the vacuum pump, when the vacuum is initialized. Two types of soldering alloys were used, depending on whether the filled material was Cu powder or Al powder.

The solder used for Cu powder was Silvabrite ^{TM}, 0.119" diameter, 96% Tin 4% Silver, lead and cadmium free solder made by Engelhard (Plainville, MA). This is a medium melting temperature solder, typically used by the plumbing industry. The melting temperature is 220 °C. Shaped solder wire was placed into the grooves at the top of the cap, and spiraled solder was placed into the 3/8" ID of the plug. This was done so that solder could be used to seal the cap to the can, at low temperatures after degassing, to prevent recrystallization of the powder.

For the Al alloy powder, a Zn- 27% Al (in weight) brazing alloy produced via rolling at Texas A&M University's MESAM laboratory (College station, TX) was used to braze the cans, due to the high temperature degassing requirement of the Al alloy powder. High temperature was required to remove the stearic acid used during the production of the cryomilled Al-10.5 Mg powders. The melting temperature for Zn-27

Al is approximately 450 °C. Melting temperatures can be varied depending on the concentration of Zn and Al in the alloy. The design of the brazing alloy components are shown below. Figure 3.5 shows the approximate dimensions of the brazing alloy.

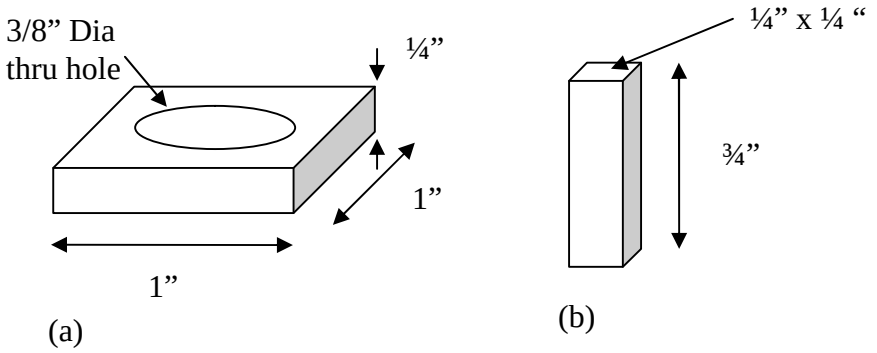

Figure 3.5: The dimensions of the Zn-27% Al brazing alloy parts used for sealing cans filled with Al-10.5 Mg powder (a) for the can top, (b) for the plug inner hole.

The cans were then degassed according to Table 3.1. Degassing is necessary to remove gasses and moisture that can hinder powder cohesion during ECAE. Sealing temperature is the temperature at which the solder melts, in order to seal a vacuum in the filled cans.

One main concern that is prevalent for nc materials is grain growth due to elevated temperatures. Gleiter [46] claims that grain growth is primarily driven by excess energy stored in the grain boundaries. Thus, during this study, lower degassing temperature was selected for nc powder degassing, to limit the amount of grain growth. Nanocrystalline Cu experiences grain growth at annealing temperatures greater than 100 ºC [54]. Thus, extrusions performed in this study were conducted at temperatures less than or equal to 100 ºC, for Cu powder, to prevent grain growth. The powders were

subjected to a degassing temperature of 130 ºC to eliminate trace moisture and gases which would produce flaws in the consolidates, which are detrimental to the strength of the material.

Table 3.1: Degassing times and temperatures before sealing the powder filled cans

Powder	Size	Degas Temp (°C)	Time(hrs)	Sealing temp (°C)
Cu	25 to 45 μm	150	8	220
Cu	100 nm	130	8	220
Al 10.5 Mg (UC Davis)	50 μm	250	3	n/a-used crimping
Al 10.5 Mg (Texas A&M)	50 μm	400	3	450

A schematic of the set up of the vacuum system is shown in Figure 3.6, and a picture of the actual vacuum system is shown in Figure 3.7. Additional equipment used in the degassing and sealing of the cans is shown in Figure 3.8.

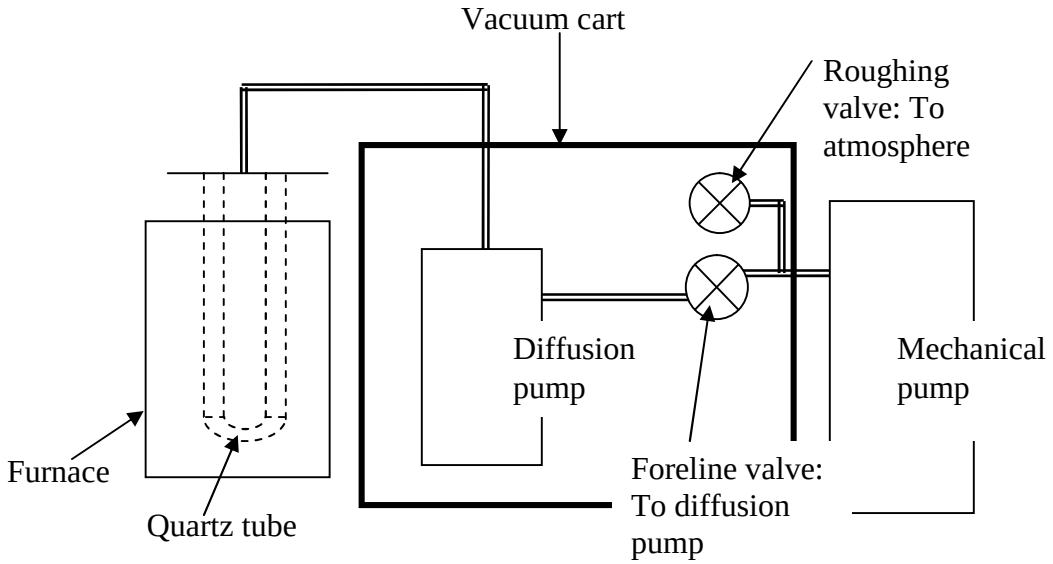

Figure 3.6: Schematic of vacuum set up for the degassing and sealing of cans filled with powder prior to ECAE, designed and set up at Texas A&M University.

(a)

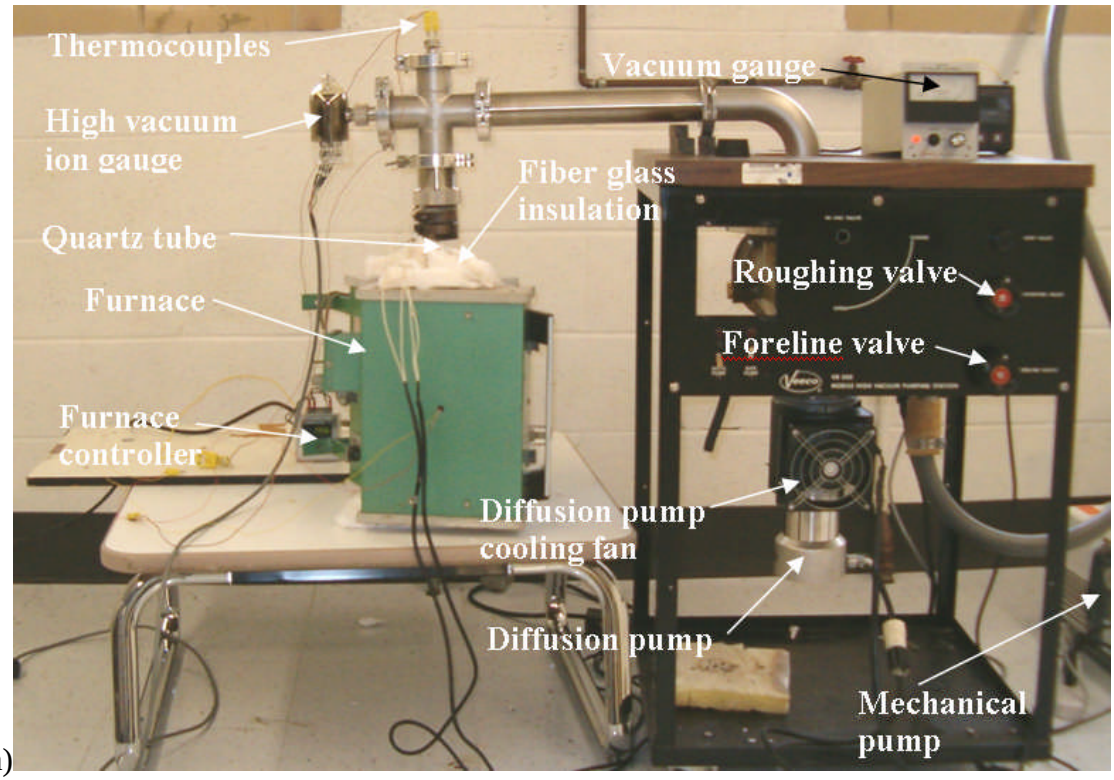

(b)

Figure 3.7: The set up of (a) degassing vacuum system, (b) Mechanical vacuum pump, used for degassing and sealing of cans filled with powder, prior to ECAE.

The high vacuum ion gauge measures lower pressures, and can be attached to a vacuum meter capable of measuring less than 1 millitorr of pressure. The vacuum system is operated using a vacuum gauge, and measures down to 1 millitorr of pressure. It is attached to a DV-1M thermocouple gauge tube, which is inserted into the vacuum system after the foreline valve. A thermocouple gauge tube works for between 3 to 6 months, and high pressure (or low vacuum levels) when there is no leak are indicators that the gauge needs to be replaced.

Experiments revealed that the K-type thermocouple used to control furnace temperature did not work well in vacuum, especially when it was not in full contact with a surface, since heat convection does not occur well under the reduced pressure. A thermocouple holder was designed as shown in Figure 3.8, to ensure the proper positioning of the two thermocouples used. One thermocouple is placed approximately at the middle of the can. Another thermocouple is placed at the top of the can, to monitor melting of the solder. The holder was designed to fit into the quartz tube, and sit atop the aluminum sleeve (shown in Figure 3.9). This ensured that the thermocouples were touching can surface and reduced the time the can is exposed to air.

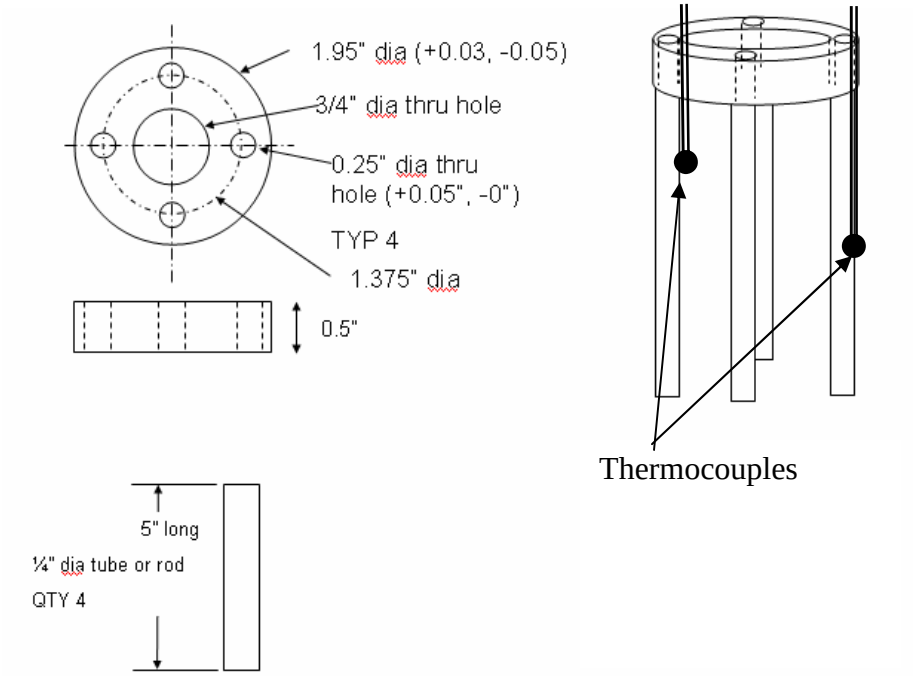

Figure 3.8: Thermocouple holder design. Thermocouples are attached to the holder, and placed such that the tips of the thermocouples will be in contact with the side of the can and the top of the can.

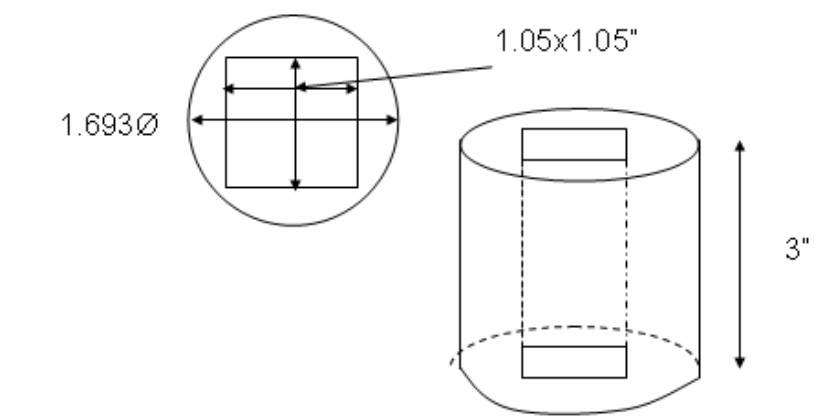

Figure 3.9: Aluminum sleeve to hold can upright inside quartz tube during degassing and sealing.

Flow charts for powder filling and degassing and sealing procedures are shown in Figures 3.10 and 3.11, respectively. These flow charts include the details for all three types of powders.

Figure 3.10: Process chart for the powder filling procedure into metallic cans.

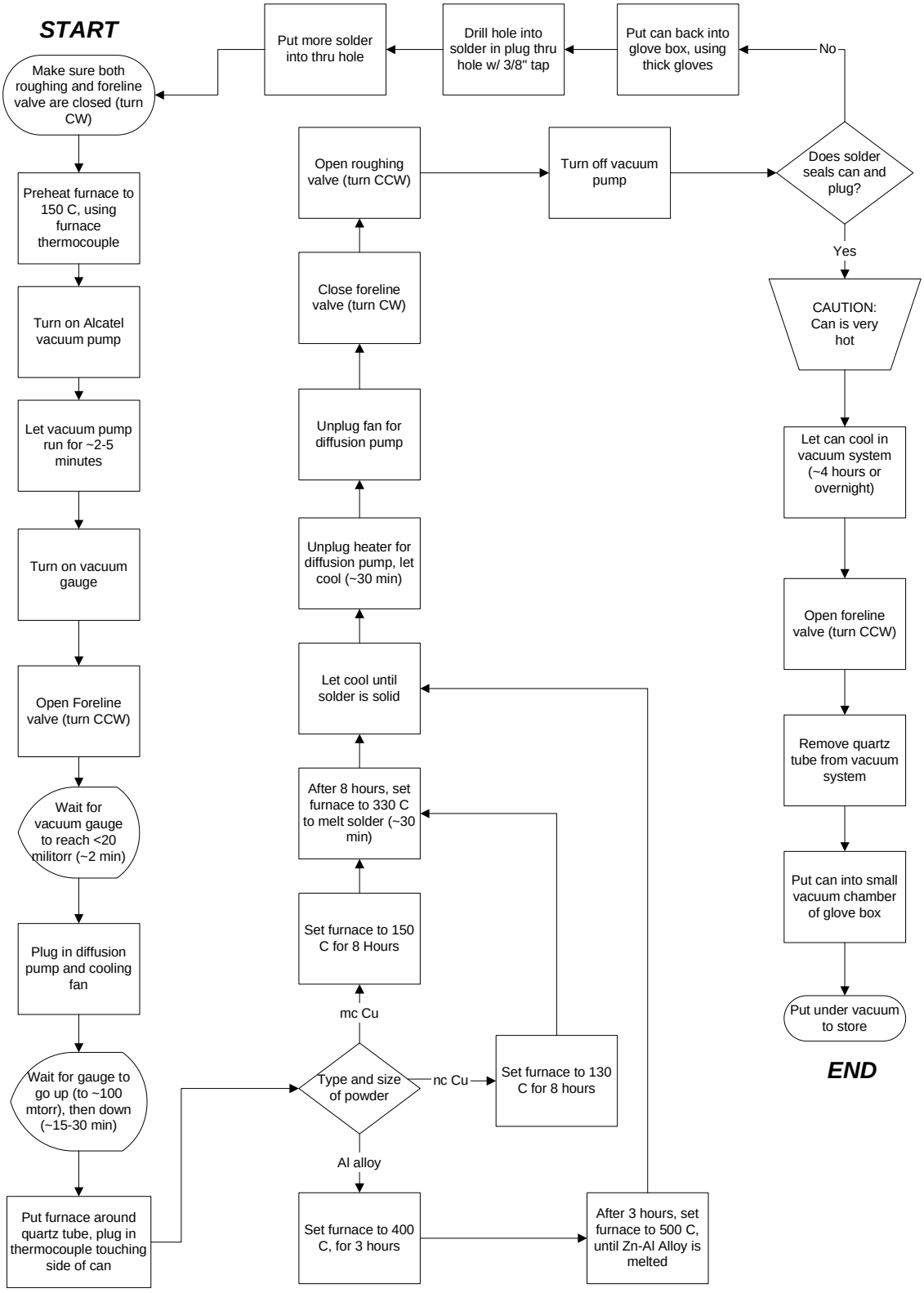

Figure 3.11: Process chart for the vacuum degassing and sealing procedure.

After degassing is completed, the temperature of the furnace was increased to melt the solder, sealing the cans in order to prevent oxidation or absorption of moisture during extrusion. Degassing temperatures needed are shown in Table 3.1.

Cans were then ready to be extruded via ECAE.

3.3 Equal Channel Angular Extrusion Procedure:

3.3.1 Processing Schedule

The filled cans were extruded using different processing routes, temperatures, and the number of passes. Throughout this thesis, the extrusion will be shown by two characters, one number followed by a letter. The most common ECAE routes are listed in Table 3.2. The number shows the number of ECAE passes and the letter represents the ECAE route used. For example, route 5A indicates that the can was extruded 5 times, using route A, in which the can was not rotated between passes.

Table 3.2: The most well-known ECAE processing routes [22].

ECAE route		A	B	C	C'	E
number of passes						
Rotation before	Odd passes	0°	+90°	+180°	+90°	+180
	Even passes	0°	-90°	+180°	+90°	+90
Microstructures		Lamellar	Filamentary	Equiaxed	Equiaxed	Equiaxed
Deformation analogy		Rolling	Drawing	Shear	Shear	Shear

The routes used for this experiment were A, B, and C’ (also known as B_c)

3.3.2 Experimental Schedule

Table 3.3 shows the complete experimental matrix including the can material, number of ECAE passes, ECAE route, extrusion temperature, powder material, and powder size that was extruded via ECAE. BP indicates the back pressure during extrusion. An extrusion rate of 0.01 inches/ second was used for all extrusions. The

effects of ECAE route for two, four, and eight passes, along with the effects of back pressure, and the effects of post processing swaging on micro and nanopowder were examined in this study.

Cans that were extruded at an elevated temperature were held in a heated die for 15 minutes prior to extrusion, and extruded in the heated die. The cans were then water quenched after extrusion.

For all extrusions, a force-displacement graph (inches versus pounds-force) was generated during extrusions. Significant drops in force over short displacements would indicate that shear localization occurred, or large porosity existed in the powder. Shear localization occurs due to failure in the material, and is undesirable. It leads to poor consolidation, and causes defects in the material.

Between extrusions, minor machining was necessary to ensure that the cross section of the cans were less than 1.00 inches, to fit into the die. Faces of the can were milled off such that the loss of can material was minimized. Machining coolant was used to keep the temperature on the specimen low, to avoid recrystallization of the material.

Table 3.3: Details of experimental plans

Case	*can mat'l*	*powder mat'l*	*powder size*	*Route*	*ECAE temp*	*ECAE rate (in/sec)*	*prep conditions*	*post processing*
A1	Ni	Al 10.5 Mg	50 micron	4B	RT	0.01	degas 250 C, 3 hrs	
A2	Ni	Al 10.5 Mg	50 micron	4B	150 C	0.01	degas 400 C, 3 hrs	none
A3	Ni	Al 10.5 Mg	50 micron	4B+BP	150 C		degas 400 C, 3 hrs	none
3	Cu	Cu	20-45 µm	1A	RT	0.01	RT, Ar, Degas 150 C 8 hrs	none
4	Cu	Cu	20-45 µm	1A	RT	0.01	RT, Ar, Degas 150 C 8 hrs	none
9	Ni	Cu	20-45 µm	1A	RT	0.01	RT, Ar, Degas 150 C 8 hrs	none
11	Cu	Cu	20-45 µm	8C'	RT	0.01	RT, Ar, Degas 150 C 8 hrs	none
12	Cu	Cu	20-45 µm	8B	RT	0.01	RT, Ar, degas 150 C, 8 hrs	none
13	Cu	Cu	20-45 µm	4B	RT	0.01	RT, Ar, degas 150C, 8 hrs	Swagging 3.2:1
19	Cu	Cu	20-45 µm	2B+ BP	RT	0.01	RT, Ar, degas 150C, 8 hrs	none
20	Cu	Cu	20-45 µm	4B+BP	RT	0.01	RT, Ar, degas 150 C, 8 hrs	none
24a	Cu	Cu	20-45 µm	2B	RT	0.01	RT, Ar, degas 150 C, 8 hrs	Swagging 3.2:1
24b	Cu	Cu	20-45 µm	2B	RT	0.01	RT, Ar, degas 150C, 8 hrs	none
27	Cu	Cu	20-45 µm	4B	RT	0.01	RT, Ar, degas 150 C, 8 hrs	none
10	Ni	Cu	nano	8B	RT	0.01	RT, Ar, degas 130 C, 8 hrs	none

Table 3.3 Continued

Case	*can mat'l*	*powder mat'l*	*powder size*	*Route*	*ECAE temp*	*ECAE rate (in/sec)*	*prep conditions*	*post processing*
14	Ni	Cu	nano	8C'	RT	0.01	RT, Ar, degas 130 C, 8 hrs	none
15	Ni	Cu	nano	4B	RT	0.01	RT, Ar, degas 130 C, 5 hrs	Swagging 3.2:1
16	Ni	Cu	nano	4B	RT	0.01	Heated to approximately 220 C, for less than 2 hours. Degased for 5 hrs @130 C	none
17	Ni	Cu	nano	4B	100 C	0.01	RT, Ar, degas 220 C, 8 hrs	none
18	Ni	Cu	nano	4B	1, 2 100 C 2,3 RT	0.01	RT, Ar, degas 130 C, 8 hrs	none
21	Ni	Cu	nano	4B+ BP	100	0.01	RT, Ar, degas 130 C, 8 hrs	none
22	Ni	Cu	nano	2B+BP	100	0.01	RT, Ar, degas 130 C, 8 hrs	none
23	Ni	Cu	nano	2B+BP	RT	0.01	RT, Ar, degas 130 C, 8 hrs	none

3.3.3 Post- ECAE Swaging

Swaging was done at room temperature at the DOE Ames Laboratory (Ames, IA), to an area reduction of approximately 3.2:1, using a Fenn swaging die set. Swaging was selected to try to eliminate remnant porosity in the sample after ECAE to determine the effect of strain path changes on the consolidate performance, and to minimize the number of ECAE passes by combining abrupt strain path changes. Swaging was selected over conventional extrusion because swaging can be performed at room temperature, is more cost efficient, and is simple and easy to perform. Conventional extrusion requires elevated temperature, which we wanted to avoid since elevated temperatures can cause grain growth, and can cause the can to become bonded to the consolidated powder by diffusion.

Extruded cans were lathed down to a cylinder with the diameter of approximately 0.96”, for swaging. Swaging involves the reduction of a material’s diameter from compressive forces applied by radial hammering. Table 3.4 shows the die reduction calculations for a circular cross section, with diameters of the die set.

Table 3.4: Die sizes available at Ames Lab for Fenn die set, showing area reduction ratio of a cylinder 0.95" in diameter.

Die Ø (inches)	area (in^2)	reduction ratio (x:1)
	$=0.25*\pi(Ø^2)$	$=a_x/a_0$
1	0.79	
0.95	0.71	1.00
0.9	0.64	1.11
0.85	0.57	1.25
0.8	0.50	1.41
0.75	0.44	1.60
0.71	0.40	1.79
0.67	0.35	2.01
0.625	0.31	2.31
0.595	0.28	2.55
0.56	0.25	2.88
0.525	0.22	3.27
0.5	0.20	3.61
0.475	0.18	4.00
0.45	0.16	4.46
0.425	0.14	5.00
0.4	0.13	5.64
0.375	0.11	6.42
0.35	0.10	7.37
0.325	0.08	8.54
0.3	0.07	10.03
0.275	0.06	11.93
0.25	0.05	14.44
0.23	0.04	17.06

3.4 Powder Extraction

3.4.1 Radiographic Images

Radiographic images were taken at the Texas A&M University Department of Veterinary Large Animal Clinical Sciences (College Station, TX). Gamma-radiation

images were taken to determine the shape of the consolidated powder inside the can after ECAE, to improve the accuracy of powder extraction. Gamma-radiation was produced using a cobalt source. It worked best for high contrast materials- such as nickel cans and Al alloy powder.

Radiographic images are given in Appendix A.

3.4.2 Machining Techniques

The powder consolidate was extracted using a mill before cutting tension and compression samples. This was important so that tension and compression test samples could be cut only from the powder consolidate, not from the can material, especially when the can material and the powder material are the same.

For powders packed in Ni cans, extraction was relatively simple. The two ends of the can were cut off, to expose powder. The depth for each cut is approximately 1” from each end. The shape of the consolidated material can easily be determined from the x-ray images. Then, the can material was removed from the sides, until thick streaks of powder are exposed. Since the powder and can are different materials, it is easy to distinguish between the powder and can. Once all four sides are exposed the corners of the can are chiseled off, to remove all can material.

For Cu powder packed in Cu cans, X-ray does not differentiate between the powder and the can. Since the boundary between the consolidated powder and the can cannot be seen by visual inspection, extracting Cu powder from a Cu can is relatively challenging. The ends of the ECAEd can were cut off by approximately 1” from each end, and then ground, polished, and etched following the procedure introduced in section

3.5, to reveal the powder-can boundary. These boundaries were traced with permanent marker, to determine where to cut tension and compression samples.

3.4.3 Tension and Compression Specimens

Dimensions of tension and compression test samples are given in Figures 3.13 and 3.14, respectively. The samples were cut using a Mitsubishi Wire Electrical Discharge Machining (EDM). The surfaces of the samples were then polished up to 1200 grit to remove any wire EDM residues and surface roughness.

Mechanical behavior of the mc Cu powder consolidate was compared to the results obtained in a previous study by Haouaoui [22]. The major difference is that Haouaoui used ~325 mesh powder, which contains powder 45 μm or smaller particles. Powder is sieved thru known sizes, until the larger particles are removed from the powder, and only the smaller particles (<45 microns) remain. The present study examines the behavior of extruded powders with in a tighter range: 20-45 μm. The effect of the range of powder size on mechanical behavior will also be explored. Also, the effect of a higher number of passes, strain path changes via ECAE and swaging, and the use of back pressure was explored.

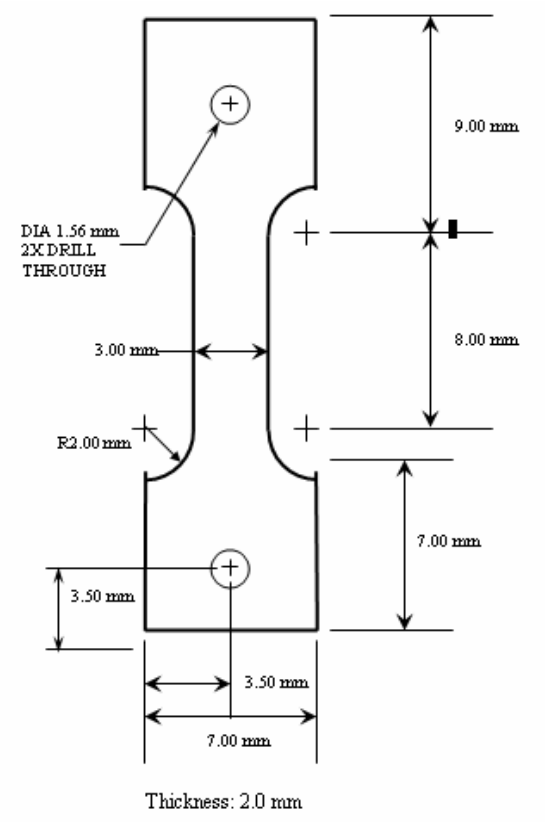

Figure 3.12: Schematic of tension test samples, cut from extracted ECAE consolidated powder via wire EDM.

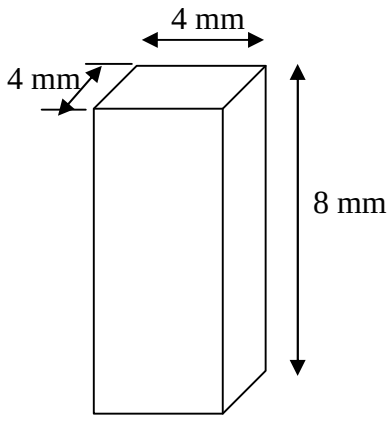

Figure 3.13: Schematic of compression test samples, cut from extracted ECAE consolidated powder via wire EDM.

3.5 Microstructural Analysis

3.5.1 Optical Microscopy

3.5.1.1 Section Cutting

Samples for macroscopic imaging and microscopy were obtained by cutting the extruded billets by Wire EDM or with a Buehler Isomet 1000 diamond saw.

3.5.1.2 Grinding and Polishing Procedure

Cross sections of powder were polished using a Buehler Ecomet 3 Variable Speed Grinder and Polisher (Lake Bluff, IL), and using an automatic polisher for mounted specimens. Grinding and polishing followed the schedule shown in Table 3.5, for Cu samples. Table 3.6 shows the grinding and polishing schedule for the aluminum alloy samples. Samples were ground and polished in two steps. First, the sample was placed along the rotation direction of the paper, which is perpendicular to the grinding marks from the previous grit size. Then, the sample was rotated by 90°, to be perpendicular to the rotation of the paper. This is done until the grinding marks from the first orientation are eliminated. Polishing with the polishing cloths was performed in a similar manner, until all scratches could not be seen under a 20x magnification. Samples were rinsed with distilled water after each grit size, to prevent contamination from larger grit sizes. Samples were cleaned in the ultrasonic cleaner after using each diamond suspension size, to remove diamond particles. After the final step, the polished samples were cleaned in an ultrasonic water bath, for approximately 1 minute, to eliminate residual colloidal silica.

Table 3.5: Grinding and polishing schedule for Cu samples.

Grit	Paper type	Lubricant	Speed (rpm)	Load (lb/ specimen)	Time (minutes)
150	SiC waterproof	Distilled Water	220	5-6	Until plane (~10)
320	SiC waterproof	Distilled Water	220	5-6	10
400	SiC waterproof	Distilled Water	220	5-6	10
600	SiC waterproof	Distilled Water	220	5-6	10
800	SiC waterproof	Distilled Water	220	5-6	10
1000	SiC waterproof	Distilled Water	220	5-6	10
1200	SiC waterproof	Distilled Water	220	5-6	10
Pellon cloth	n/a	3 μm diamond suspension	150	4-5	5
Pellon cloth	n/a	1 μm diamond suspension	150	4-5	5
Final polishing cloth (psa pack)	n/a	0.04 μm colloidal silica, distilled water	150	4-5	5-10

Table 3.6: Grinding and polishing schedule for aluminum samples.

Grit	Paper type	Lubricant	Speed (rpm)	Time (min)
600	SiC waterproof	Distilled Water	200	Until plane
1000	SiC waterproof	Distilled Water	200	10
1200	SiC waterproof	Distilled Water	200	10
Nylon cloth	n/a	3 μm diamond suspension	150	5
Nylon cloth	n/a	1 μm diamond paste	150	5
Final polishing cloth	n/a	0.04 μm colloidal silica	150	5

Samples were rinsed with distilled water, then isopropyl alcohol, and dried with a hot air blower, to eliminate water spots. Water spots are difficult to eliminate- and require re-polishing from 1200 grit or 3 micron diamond paste to remove, so it was important to ensure that the samples did not get water spots.

Optical images were taken from polished samples, to determine porosity content and particle deformation morphology.

3.5.1.3 Etching

The samples were then etched, to reveal grain/ prior particle boundaries and the powder consolidate-can boundary. Cu samples were dipped into etchant for 20 to 40 seconds at room temperature using a solution of distilled water and ammonium persulfate ($(NH_4)_2S_2O_8$), obtained by dissolving 10 g of ammonium persulfate with 100 ml of distilled water. Fresh etchant was needed for samples etched on separate days, since it was found that the etchant loses reactivity quickly.

The samples were then rinsed with distilled water to interrupt the etching, and then rinsed with isopropyl alcohol, then dried with hot air, to prevent water spots.

Aluminum alloy samples were etched using Keller's reagent, as defined in the ASM handbook, volume 2: Metallography and microstructures [91]. Keller's reagent was composed of 20 mL of distilled water, 20 mL of HNO_3 (70%), 20 mL of HCl (38%), and 5 mL of HF (40%). The samples were immersed in the etchant for 15 seconds, then promptly rinsed with water, and then dried with isopropyl alcohol and warm air.

Optical Microscopy images were taken up to a 150x magnification, to determine the morphology of the deformed powder, agglomerate size and deformation, and the porosity with in the powder.

A JEOL JSM-6400 scanning electron microscope (SEM) was used to view the microstructure of the powder consolidates. Since most of the consolidates had grain sizes in the nanometer range, optical microscopy is unable to resolve the grain boundaries. Thus, SEM images were taken, to provide a higher-resolution image of the consolidates.

3.6 Mechanical Testing

Dog-bone-shape flat tensile specimens were cut according to the schematic shown in Figure 3.13 using a wire electrical discharge machine (Wire EDM) from the consolidates. The surfaces were polished to a 1200 grit to remove stress concentrators and the EDM affected layer.

The samples were mounted onto the tension grips of a servo-hydraulic MTS test frame, and an 8 mm extensometer attached to the gauge section. Tension and compression tests were performed at room temperature with a controlled strain rate of $5x10^{-4}$ 1/s. The grips were machined from a 17-4 precipitation hardened stainless steel, annealed, and aged for 1 hour at 482 °C, then air cooled.

Data from the test frame is given in Newtons (N) for force, and mm/mm for axial strain, as well as in mm for axial displacement. The gauge cross section is measured with a micrometer, to determine the initial area to convert the force applied into stress.

True stress (σ_{true}) and engineering stress (σ_{eng}) are found as follows:

$$\sigma_{true} = \frac{P}{A} \text{ and } \sigma_{eng} = \frac{P}{A_o} \qquad \text{Equation 3.2}$$

where A is the instantaneous cross-sectional area, P is the instantaneous force applied, and A_0 is the initial cross sectional area. Assuming constancy of volume, we can use the following relationships between true stress (σ_{true}) and engineering stress (σ_{eng}), and between true strain (ε_{true}) and engineering strain (ε_{eng}):

$$\sigma_{true} = \sigma_{eng}(\varepsilon_{eng} + 1) \qquad \text{Equation 3.3}$$

$$\varepsilon_{true} = \ln(\varepsilon_{eng} + 1)$$

These equations are valid up to the ultimate tensile strength, and the onset of necking.

3.7 Model Validation

A powder compaction constitutive model was identified and incorporated into a commercial finite element software, ABAQUS, to simulate the powder consolidation using ECAE by our collaborators, Dr. Arun Srinivasa and his Ph.D student Anhul Kaushik. In the present study, we have performed experiments to evaluate the validity of the constitutive model and boundary conditions they are using. Validation experiments included an empty Cu can (Case 1), two Cu cans filled with 20-45 μm Cu powder (cases 3 and 4), a Ni can filled with mc Cu powder, and a solid billet (Solid #1), all 4” in length, with dimensions for a 1”x1” die, and extruded at room temperature using an extrusion rate of 0.01 in/sec for only one pass.

All samples were cut parallel to the flow plane, at approximately the midpoint of the transverse plane. This was performed to capture a view of the cross section of the

powder consolidate. The samples were ground, polished, and etched as described in Section 3.5.1. The porosity distribution and the orientation and location of the cavities were compared with the porosity distribution predicted in the model, assuming the can's has a Young's Modulus (E) of 124 GPa, and an initial yield strength (σ_y) of 80 MPa, with hardening to 300 MPa. Two surface interaction properties were considered in this model: 1. Outer can surface and die wall, 2. Inner can surface and powder. Two models were used, the Gurson model, and the Duva and Crow model. Figure 3.15 shows the density prediction from the model's simulation of a single ECAE pass.

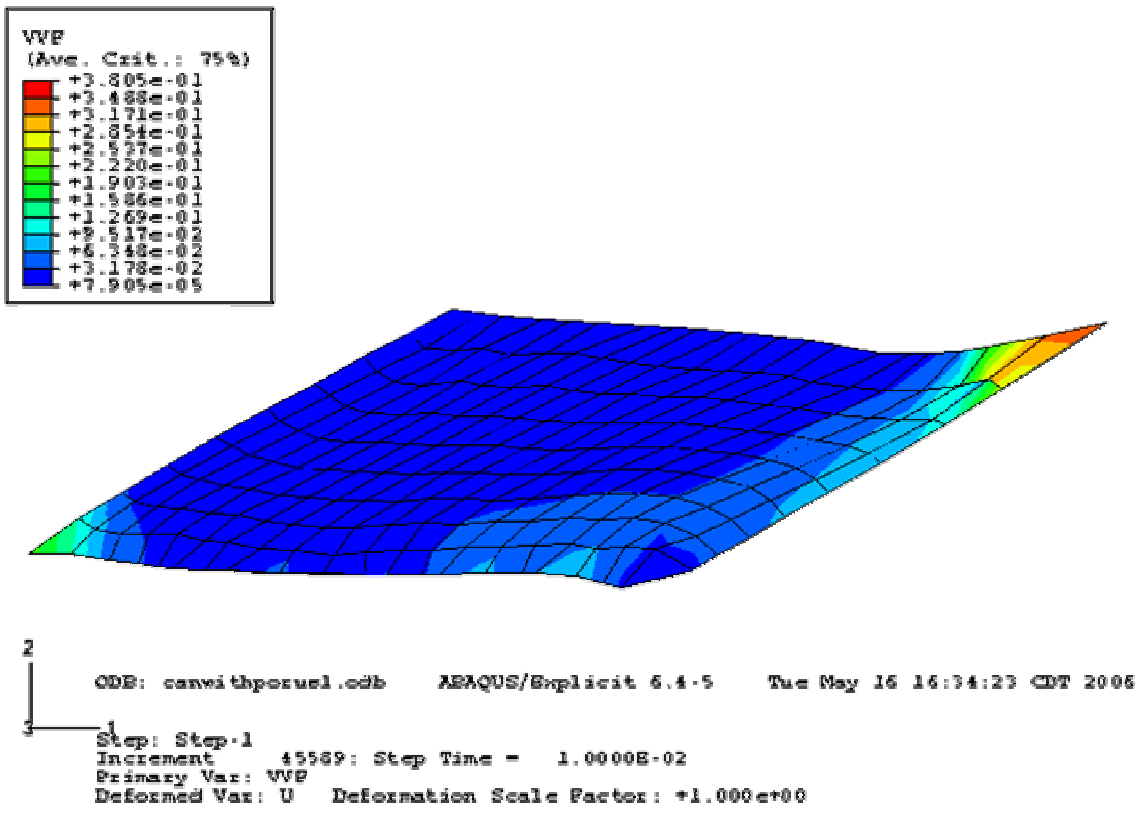

Figure 3.14: Shape and density prediction of mc Cu powder extruded via ECAE at 1 pass at RT.

IV. BEHAVIOR OF MICROCRYSTALLINE COPPER CONSOLIDATE

4.1 Experimental Results

4.1.1 Microstructure

Optical micrographs of various routes and number of passes were taken. Initially, three extrusions of microcrystalline Cu powder were performed, using route 1A. Two extrusions were performed in a Cu 101 can, and the other was performed in a Ni can. These three cases were performed to compare with the FEA model being created by Kaushik and Srinavasa [38].

Cross-sectional images reveals that the powders in both samples are oriented approximately 21 degrees from the horizontal plane. This is expected, since the shear plane during ECAE is expected to orient the powder during consolidation. Figure 4.1 shows the cross section views of (a) the microcrystalline powder packed in the Cu can (Case 3), and (c) the microcrystalline powder packed in the nickel can (Case 9). These cases follow the experimental plan outlined in Table 3.3.

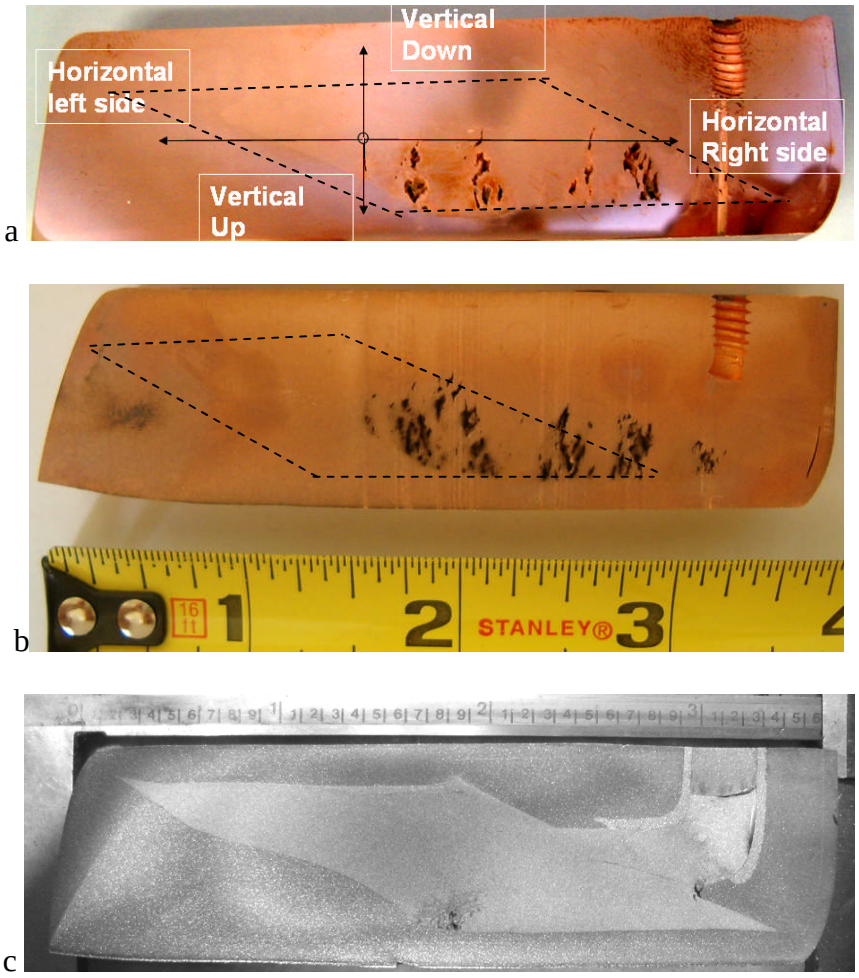

Figure 4.1: (a). Cross sections of mc Cu in Cu can (Case 3, with lubricant) (b) Cross sections of mc Cu in Cu can, with friction on top and bottom (Case 4), and (c) Cross sections of mc Cu in Ni can (Case 9). These images show the powder deformed shape and macroscopic cavities.

In Case 3, the consolidate has a much larger macroscopic cavity than in Case 9. An additional extrusion was performed on microcrystalline Cu in a Cu can, but with no lubricant, to increase the effect of friction. This indicates that selection of can material is an important part of finding optimal parameters for effective consolidation. A comparison between cross sections of case 3 and case 4 reveal that the macroscopic

cavity occurs at regular intervals, at almost the exact same positions at the bottom of the can. Kahsuik and Srinavasa predicted hydrostatic pressure drops at regular intervals, which may be the cause of the cavities.

Optical microscopy images were also taken from Case 3 and Case 9, to see the microscopic changes in the powder morphology. Figure 4.2 shows optical images of case 3, from a reference point, to the edge of the powder-can line. The dark lines indicate powder grains.

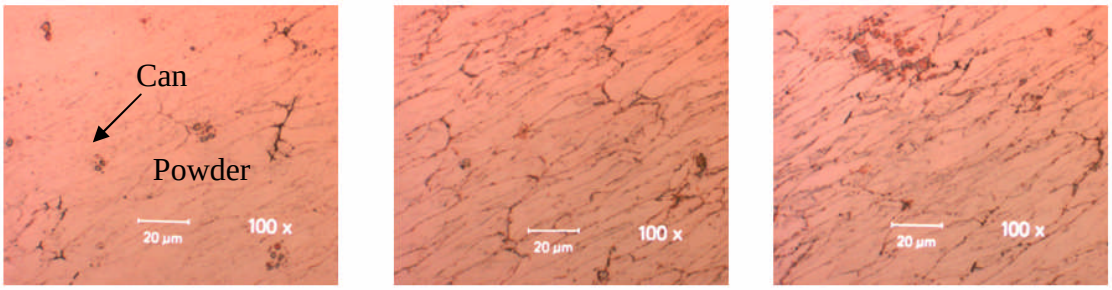

Figure 4.2: Optical images of Case 3 mc Cu 1A at RT, with no friction- middle of the powder to the powder edge which shows the can-powder boundary. These images were taken well away from the macroscopic cavity regions, and show prior particle boundaries elongated in the shear direction.

Particles appear to be elongated along the shear direction, and porosity between prior particles appears to occur at the upper and lower corners of the particles.

Images taken around the macroscopic cavities for Case 3 revealed particles which were not elongated along the shear direction. Unusual particle shapes are observed, as shown in Figure 4.3. Column a shows the 50x magnification of the powder near a pore, and column b shows the 100x magnification of the respective image.

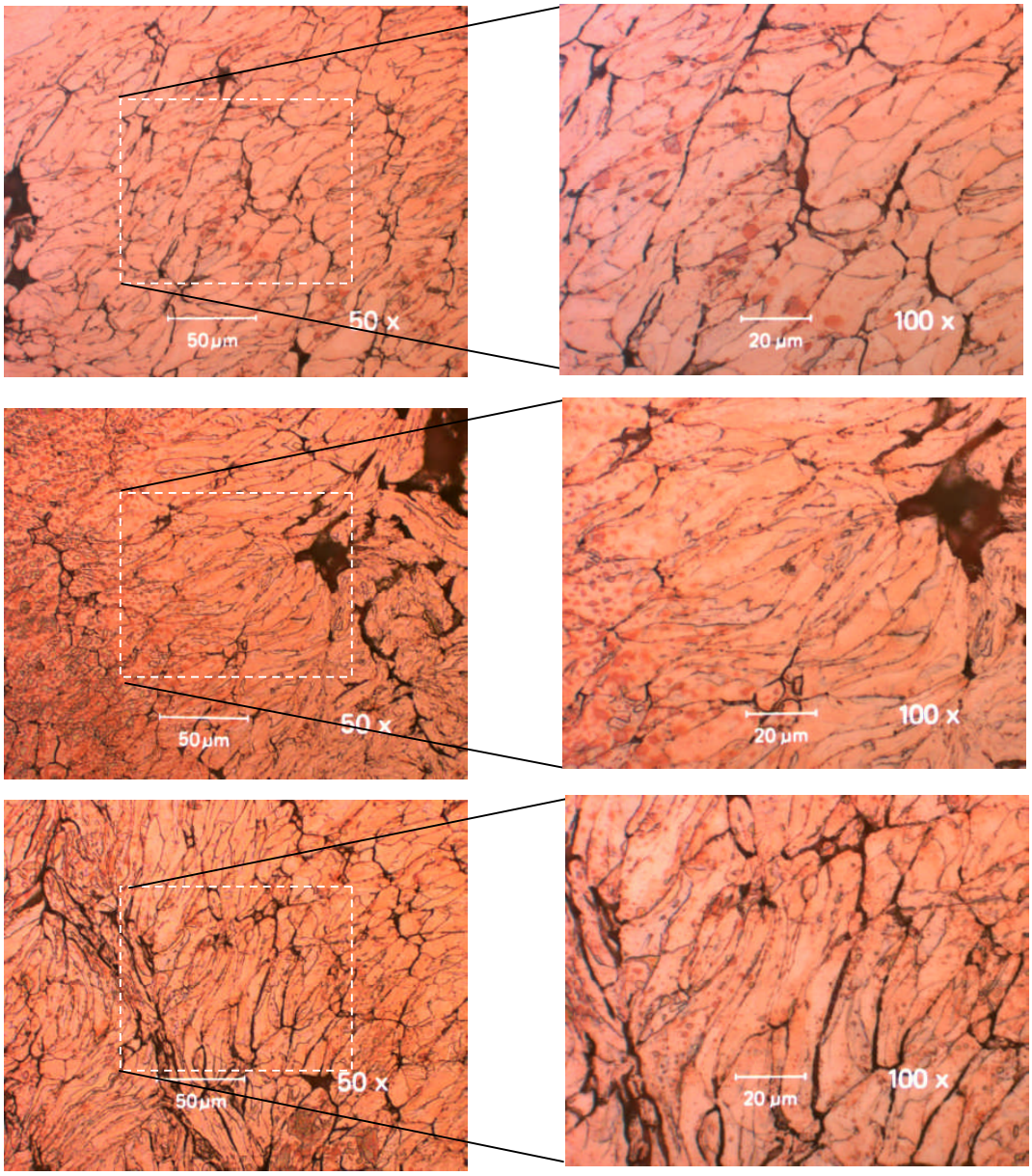

(a) (b)

Figure 4.3: Optical microscopy images of Case 3 mc Cu 1A at RT, with no friction at (a)50x, and (b) 100x, showing macroscopic cavities and microscopic porosity along prior particle grain boundaries.

Prior particles near the macroscopic cavities appear to flow around the cavity, which results in non-uniform distribution of deformed particles. These particles exhibit

microscopic porosity at various places, rather than only at the top or bottom corner. The odd shaped particles indicate that the stress state on these particles is more complex than just a simple shear deformation in this region.

Case 9 provided a much better consolidated powder, by using a nickel can. Nickel, as a stronger material than the powder, can provide higher hydrostatic pressures than a canning material of equal or lower strength than the powder. An optical image of Case 9 is shown in Figure 4.4.

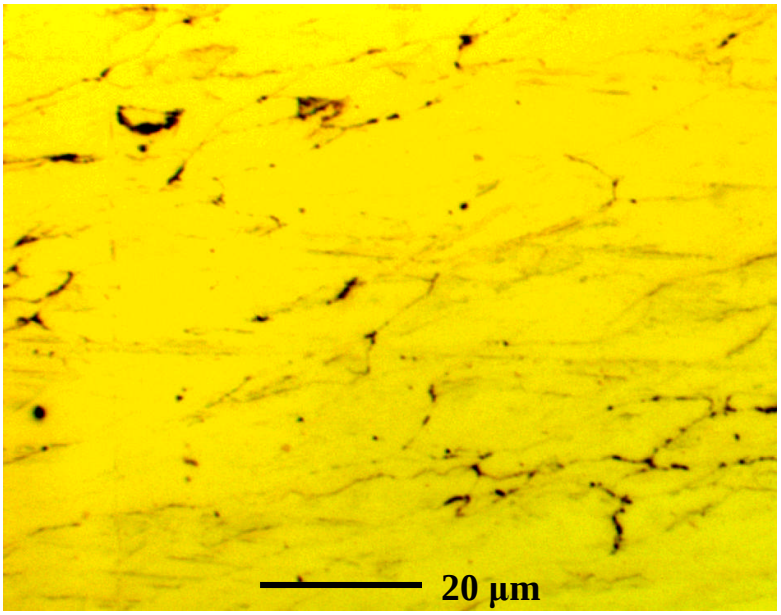

Figure 4.4: Optical image of mc Cu in a Ni can, showing prior particle boundaries elongated in the shear direction, with microscopic porosity occurring at the corners of the particle boundaries.

Microscopic porosity between grains in Case 9 appears to be significantly less than that found in Case 3. However, the location of the porosity is generally at the top and bottom corners of the prior particles, similar to what was observed for Case 3.

Microscopy images were taken of several other samples, which were extruded at different routes and number of passes. Case 13, mc Cu 4B with swaging at RT was the only other case of mc Cu in which prior particle boundaries could be seen with an optical microscope. An image of the consolidate after ECAE and swaging is shown in Figure 4.5.

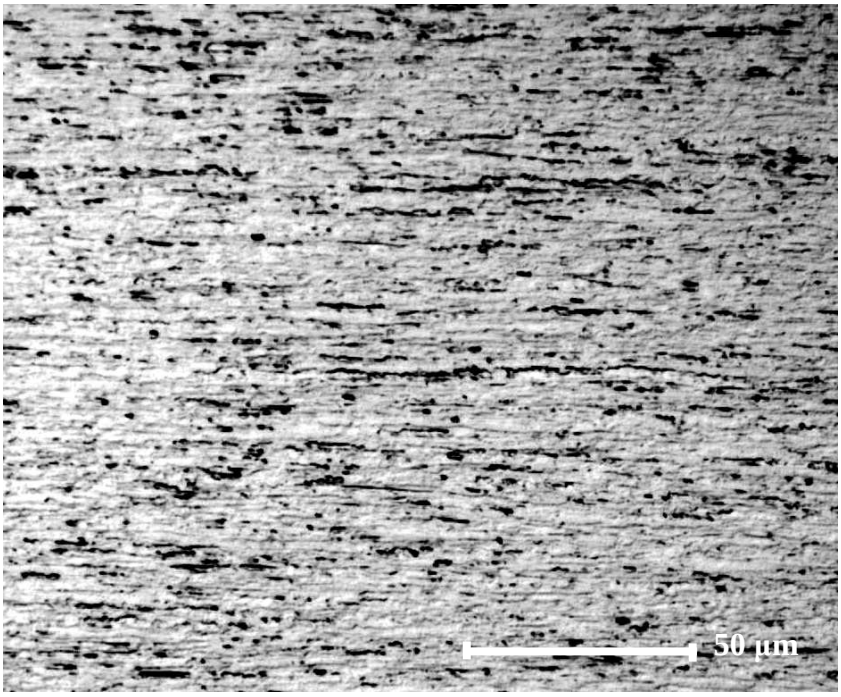

Figure 4.5 Optical image of mc Cu ECAE at 4B with swaging at room temperature, showing prior particle boundaries elongated and parallel to the swaging direction.

The grain boundaries for Case 13, 4B+ swaging at room temperature, are elongated, parallel to the swaging direction. The grains are long and thin, compared with the samples that are only ECAEd. Microscopic porosity is observed on some of the prior particles, at the tops and bottoms, rather than the corners as seen in Cases 3 and 4, of the prior particle boundaries.

4.1.2 Model Validation Experiments

An existing constitutive material model for the powder compaction process was used to simulate the powder compaction thru ECAE by Dr. Srinavasa and his student Anshul Kaushik. The results from the validation experiments closely matched the model. Validation experiments included an empty Cu can (Case 1), two Cu cans filled with 20-45 μm Cu powder (Case 3 and 4), and a solid billet (Solid 1), all 4" in length, and 1"x1" square cross section, and extruded at room temperature.

A solid billet of similar shape as the empty can and the two filled cans was extruded. The macroscopic deformation of the solid billet is well predicted by the model, as shown in Figure 4.6.

(a)

b)

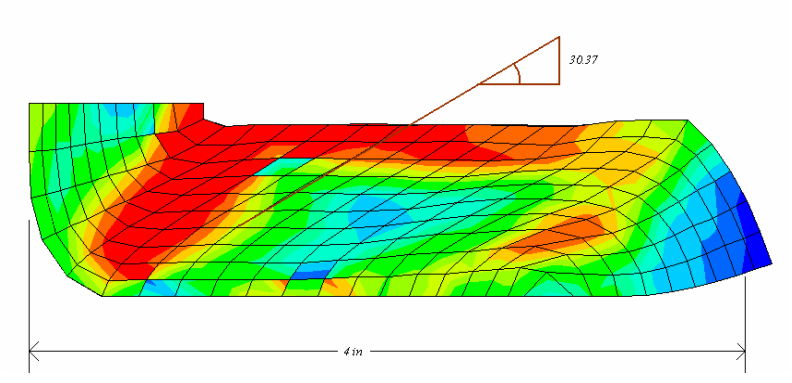

Figure 4.6: (a) Solid billet, side view, and (b) model prediction, side view, showing the predicted billet shape. The shearing of a single element in the model prediction closely matches the oriented markings on the solid billet.

The empty can was extruded at a rate of 0.1 in/sec, which was selected because the can was empty, and could be extruded at a faster rate than a can filled with powder. The two powder cans and the solid billet were extruded at a rate of 0.01 in/ sec. The powder cans were extruded using different lubrication conditions to evaluate the effect of friction on the consolidation. Case 3 was extruded with anti- seize lubricant, and Case 4 was extruded with no lubricant and a fixed bottom slider. This changed the friction acting on each can. The cans were cut with wire EDM, to obtain a cross-section for Optical Microscopy (OM) and Scanning Electron Microscopy (SEM) images. Initial macroscopic views are shown in Figures 4.7 and 4.8, for Case 3 and Case 4, respectively. Both cans show macroscopic cavities, which appears to follow a general pattern in the vertical direction (along the LD), regardless of the friction condition. The volume of the cavities in Case 4 is slightly more than Case 3, indicating that a low friction condition is better in consolidating powder. A comparison is shown in Figure 4.9.

Also included are the simulations using the Gurson model [38] for the powder cross section. The top surfaces of the models are irregular due to the coarse meshing, and can be corrected by refining the mesh. Case 3 and 4 both generally agree with the deformation of the powder- can interface predicted in the models.

The contours shown in the model results are for porosity. Dark colors indicate low porosity or more consolidation. Lighter colors indicate varying degrees of high porosity. The models predict porosity along the bottom of the powder after ECAE. In Figure 4.7 b, the prediction of the approximate location of the cavities is remarkable.

a)

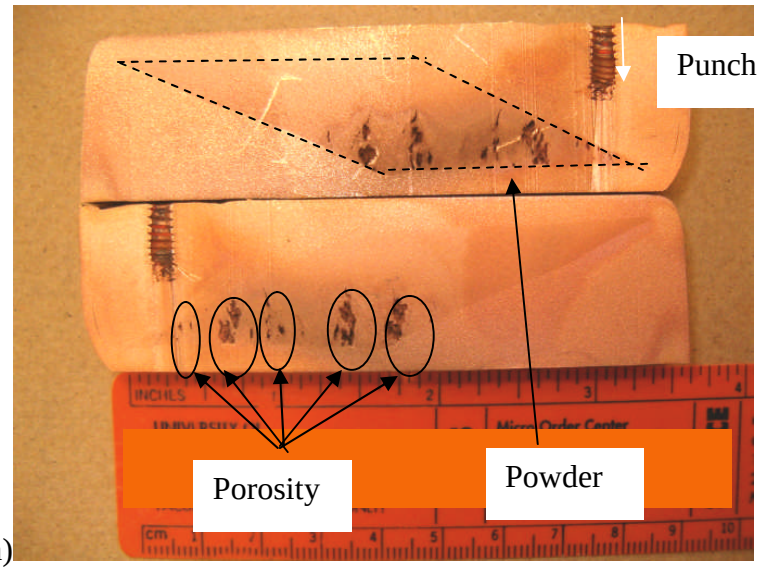

(b)

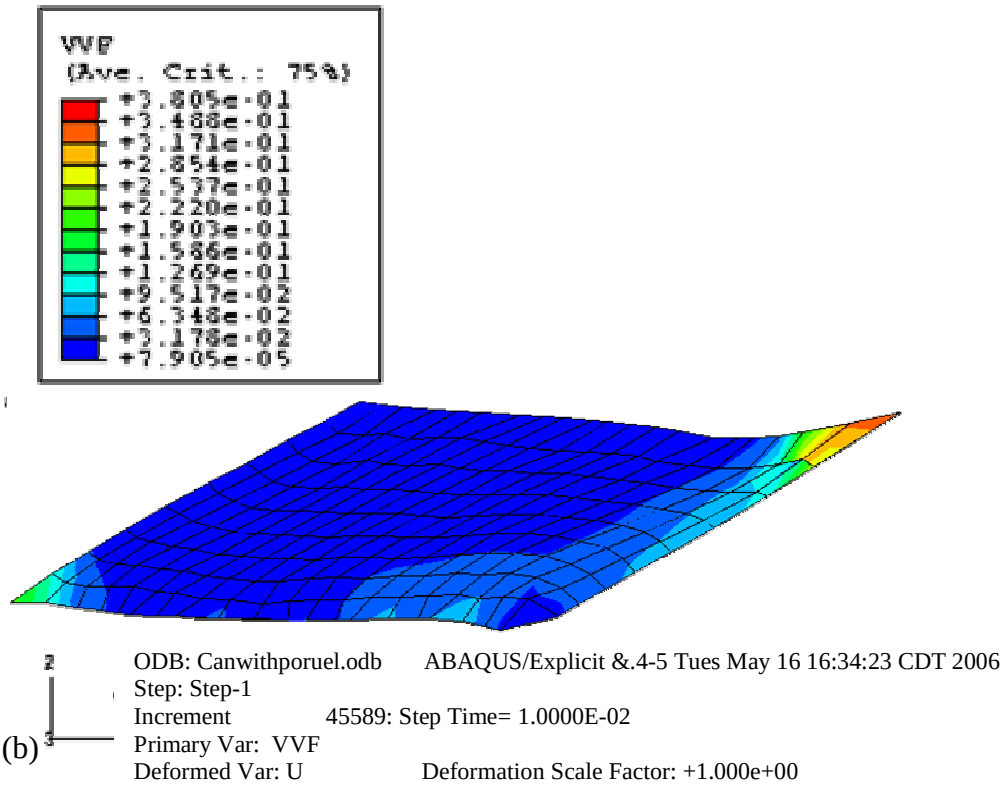

Figure 4.7: (a) Case 3 cross section after ECAE, (b) Model prediction of density for powder in case 3, showing expected cavities in the bottom corner of the consolidated powder. Darker colors are higher density areas, and lighter colors are lower density areas.

(a)

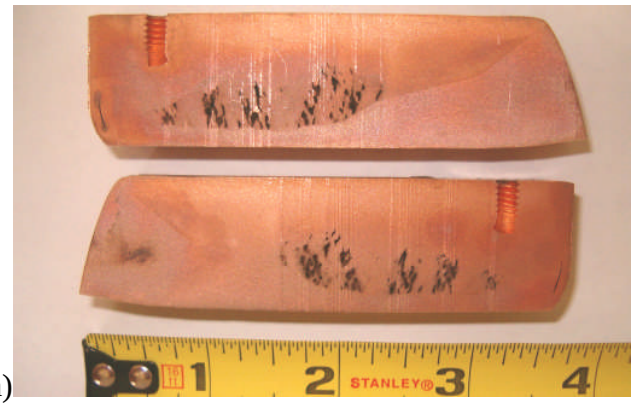

(b)

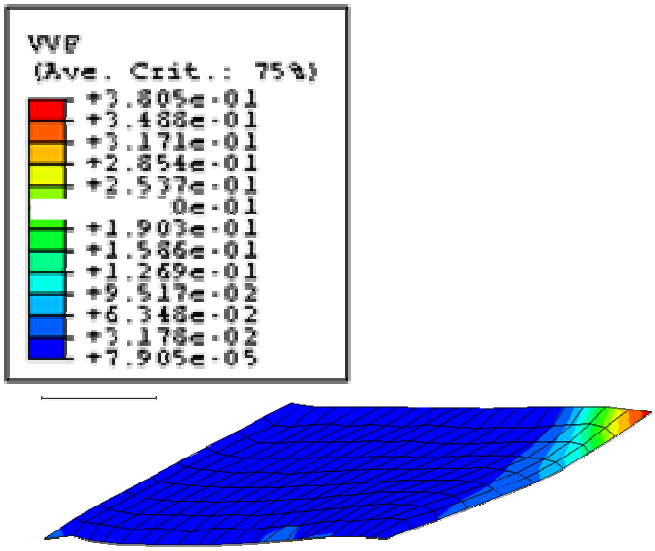

Figure 4.8 : (a)Case 4 Cross section after ECAE 1 Pass, (b) Model of powder density distribution in Case 4, showing a predicted powder shape which matches well with the actual powder shape obtained via ECAE.

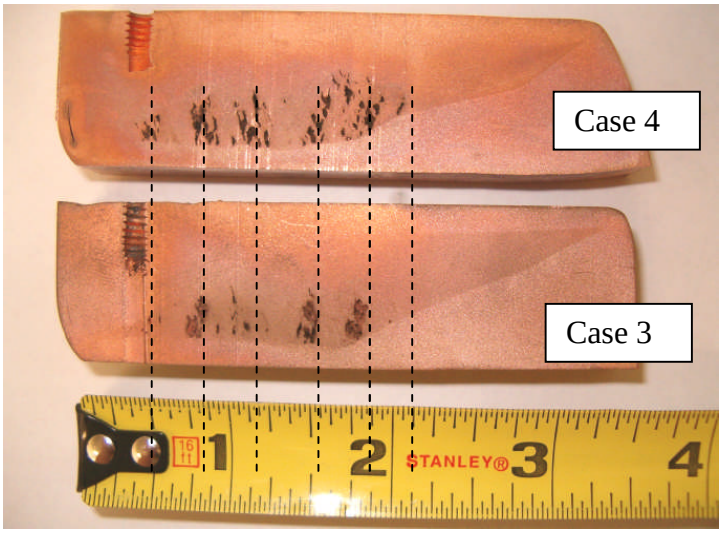

Figure 4.9: Case 3 (bottom) versus Case 4 (top) after ECAE 1 pass at room temperature. The macroscopic cavities occur at regular intervals, in the same locations on both friction conditions.

The cavities in both cans are generally evenly spaced from each other, with similar locations between the two cans regardless of the friction conditions.

The experiments proved that the constitutive model selected fit closely with the macroscopic features of the consolidated material. Figure 4.10 a shows the cross-section of the empty can after one ECAE pass at room temperature. Figure 4.11 shows the model prediction of the empty can. The model predicts the collapse of the can, and the slight indentation at the bottom as shown in Figures 4.10 a and b.

(a)

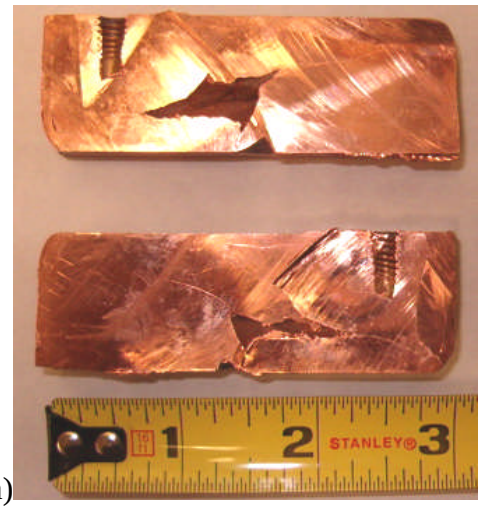

(b)

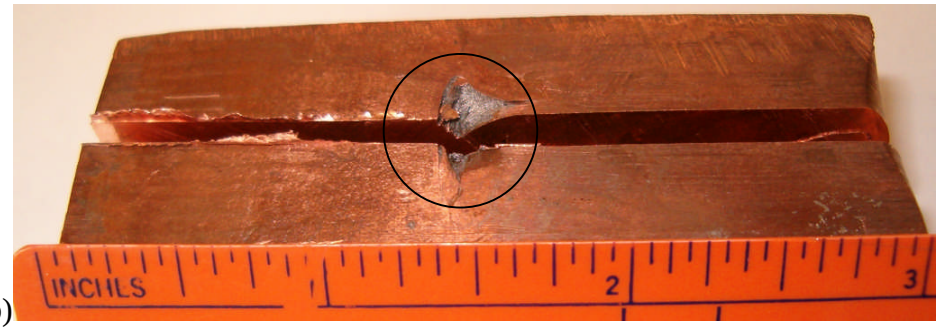

Figure 4.10: (a) Cross section of empty Cu can ECAEd 1 pass at room temperature, and (b) bottom of empty can extruded at ECAE 1 pass at room temperature, showing the bottom indentation.

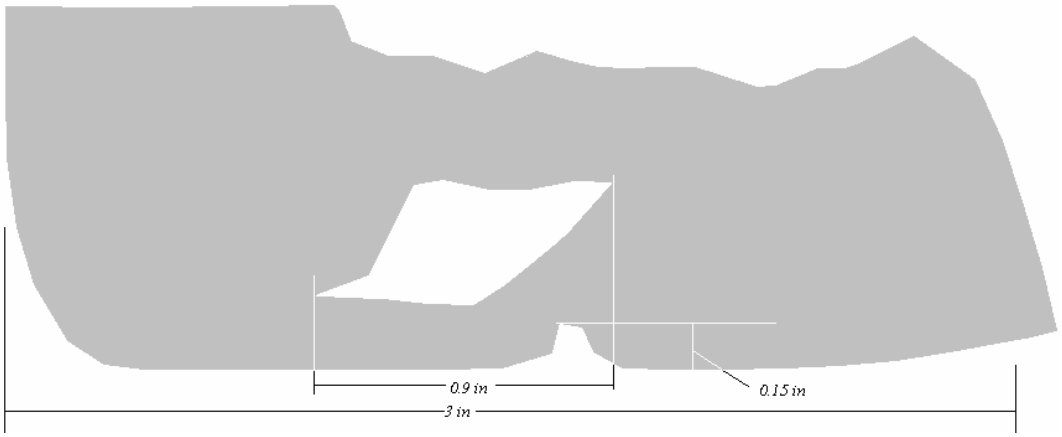

Figure 4.11: Predicted shape of the empty Cu can ECAEd one pass, at room temperature, from the constitutive model. Compared with the previous figure, the predicted cavities are similar to the experimental cavities.

Optical microscopy images were taken from Case 3, ECAE at 1 pass at room temperature, with a no-friction condition. Powder in regions significantly away from the cavity regions have been deformed in along a common direction due to the shear strain induced during ECAE, as shown in Figure 4.12. Porosity occurs in the upper and lower corners of the prior particle boundaries. Figure 4.13 shows grain boundaries within a prior particle boundary of ECAEd mc Cu powder.

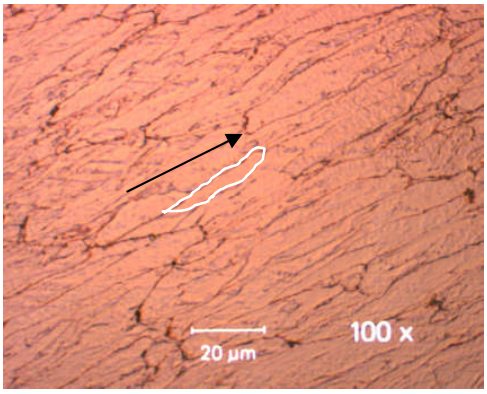

Figure 4.12: Powder in continuous region after ECAE, Case 3 extruded 1 pass at room temperature with lubricant to eliminate friction.

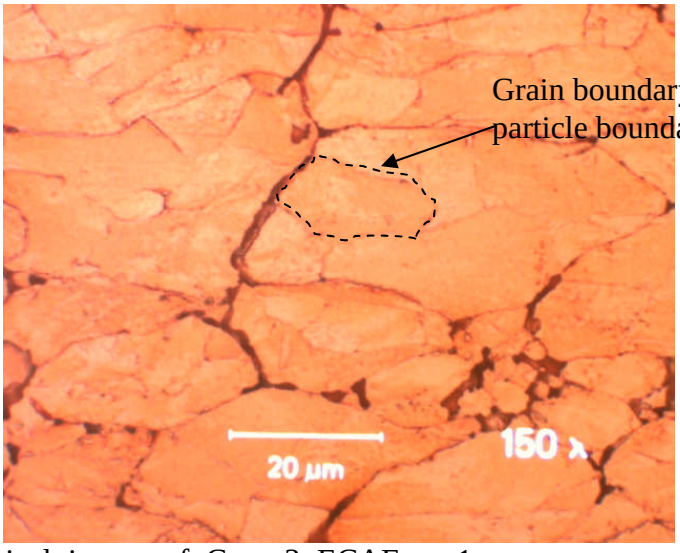

Figure 4.13: Optical image of Case 3 ECAE at 1 pass at room temperature with lubricant, taken from a region near a macroscopic cavity, showing prior particle boundaries with grain boundaries within the prior particle boundaries.

Powder has deformed non-uniformly in areas near the macroscopic cavity. The particles do not all elongate along the macroscopic shear direction. Figure 4.14 shows images of different cavities. The powder particles appear to bend around the cavity. Higher magnification images reveal that many of the darker lines that appear as particle boundaries are actually smaller porosity.

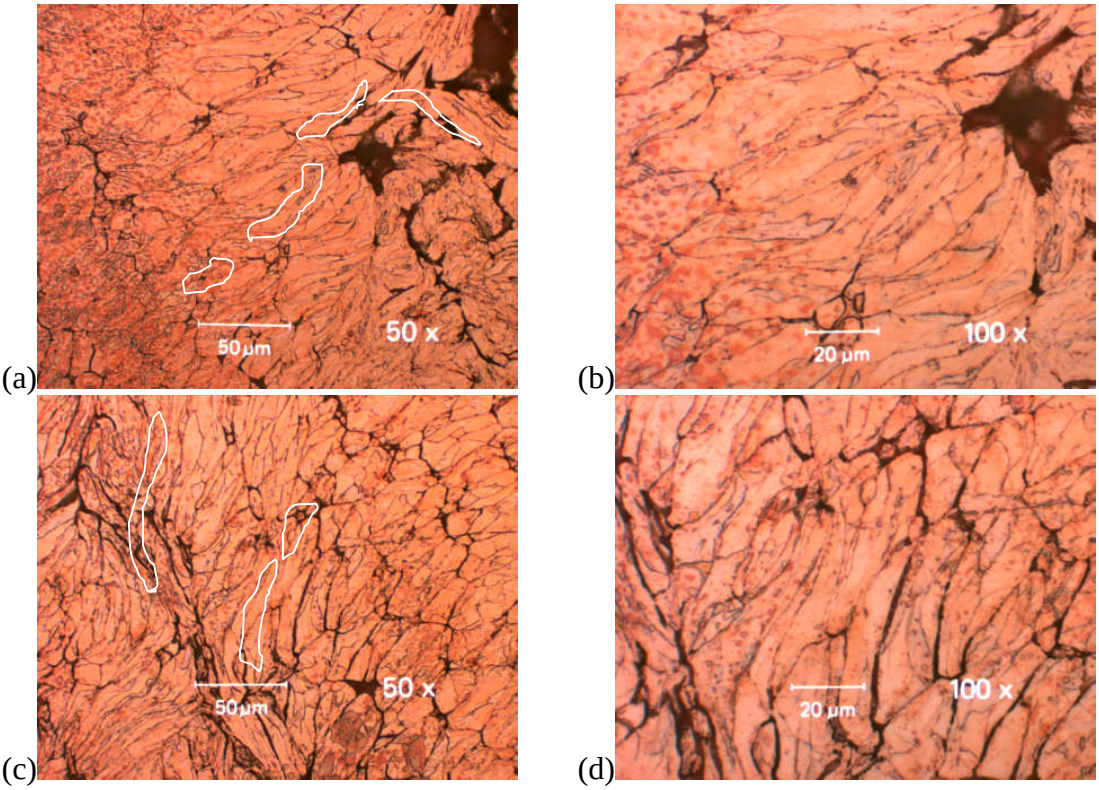

Figure 4.14: Powder near two macroscopic cavities of Case 3, ECAE at 1 pass with lubrication, of (a) the first cavity at 50x, (b)the first cavity at 100x, (c) of the second cavity at 50x, and (d) the second cavity at 100x magnification.

Porosity may be due to the lack of consolidation of the particles in those regions. Then, when the samples are cut open, the particles which were not consolidated may just

fall out, leaving porosities in the bulk. However, another possibility might be that the porosity existed before cutting the sample.

Eliminating the macroscopic cavities has been the one of the goals of this study.

Lack of full consolidation in select regions can be eliminated by multiple ECAE passes using certain ECAE routes, and/or by abrupt strain path changes. Increasing initial green density by more effective packing could also help in achieving higher final density levels.

4.1.3 Green Density

Green density is the density of the powder after it is packed into the can, but before consolidation. Green density for mc Cu powder was, on the average, about 58.25% of the theoretical value. Packing of the mc Cu powder was performed the hand tapping. Table 4.1 lists the green densities of mc Cu powder compacts, calculated as a percent of the theoretical density of pure Cu.

Table 4.1: Green density of mc Cu powders after packing in the cans, given as a percentage of theoretical density.

Case	size, powder type, route, ECAE temp	Green Density (% of theoretical)
3	mc Cu, 1A RT	60.09
4	mc Cu, 1A RT	57.04
9	mc Cu, 1A RT	57.93
11	mc Cu, 8C' RT	59.86
12	mc Cu, 8B RT	56.32
19	mc Cu, 2B+BP RT	66.32
20	mc Cu , 4B+BP RT	60.63
24a	mc Cu, 2B+swaging RT	63.09
24b	mc Cu , 2B RT	63.09
27	mc Cu, 4B RT	66.01

4.1.4 Tensile Testing of mc Cu Consolidates

Tension tests on the mc Cu consolidated via ECAE using different routes were conducted. The results are compared with the results reported in a previous study [22]. Tension test for ECAE consolidated mc Cu powder results are given in Figure 4.15.

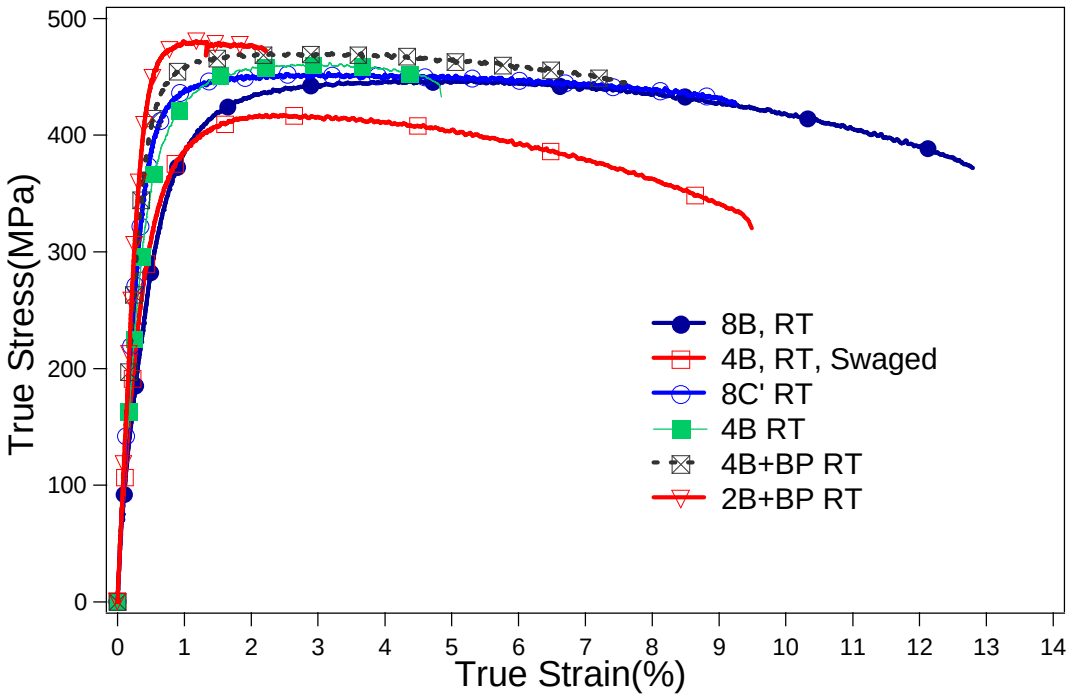

Figure 4.15: True stress-strain tension test of successful microcrystalline Cu consolidates. Route 8B has the highest ductility, and route 2B with back pressure has the highest strength.

Table 4.2 shows the mechanical properties for mc Cu, with the mean and standard deviation values shown for the cases in which multiple tensile tests were conducted.

Table 4.2: Selected mechanical properties of mc Cu consolidated via ECAE, showing UTS, and elongation to break.

Case	Route, temperature, post-ECAE processing	UTS (MPa)	Elongation to break (%)
Pure Cu bulk [22]	None	~250	~35
[22]	2A RT	420	1.9
19	2B+BP RT	480	2.22
13	4B+ swaging RT	405.25 ± 17	9.68 ± 1.9
27	4B RT	462.25 ± 2.5	3.12 ±0.72
20	4B+BP RT	474±7	5.92±2.0
12	8B RT	450.95 ±5.4	14.045 ±1.87
11	8C' RT	449.7±3.2	4.9±4.0

A comparison of the tensile behaviors of profiles from the middle and end of consolidates from Case 11 mc Cu 8C' RT and Case 27 mc Cu 4B RT are shown in Figures 4.16 and 4.17, respectively. These two figures shows that tension samples taken from profiles in the middle of the consolidate exhibit much greater ductility than those from the edge of the consolidated powder, but without a loss of strength. This may be due to higher consolidation achieved in the center samples.

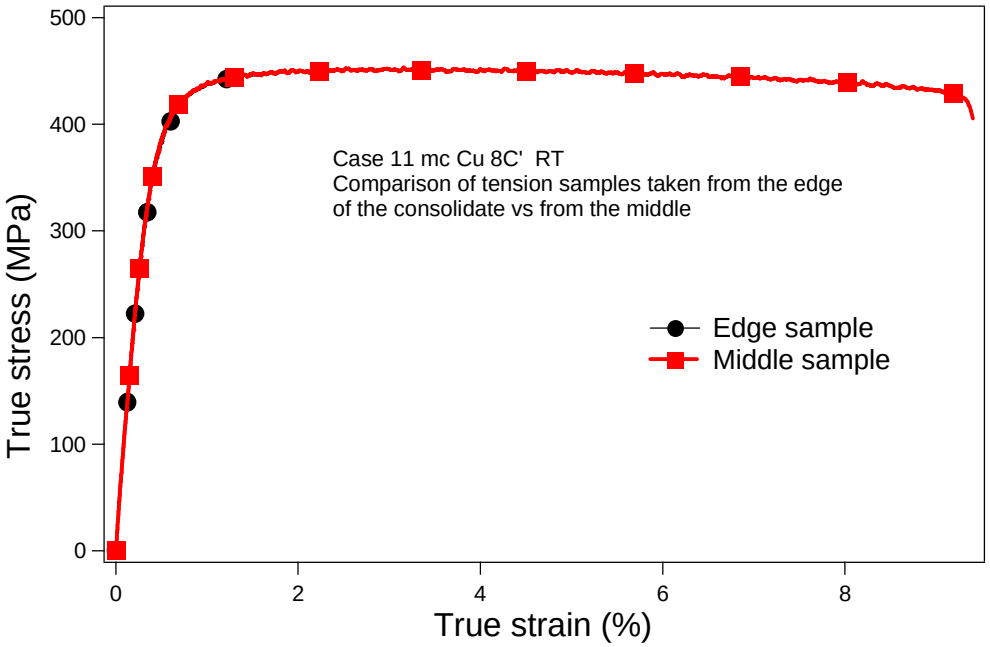

Figure 4.16: Case 11 mc Cu 8C' RT comparison of tension profiles from the edge versus from the middle of the consolidated powder. The tension sample from the middle has significantly more ductility than the sample from the edge of the consolidated powder.

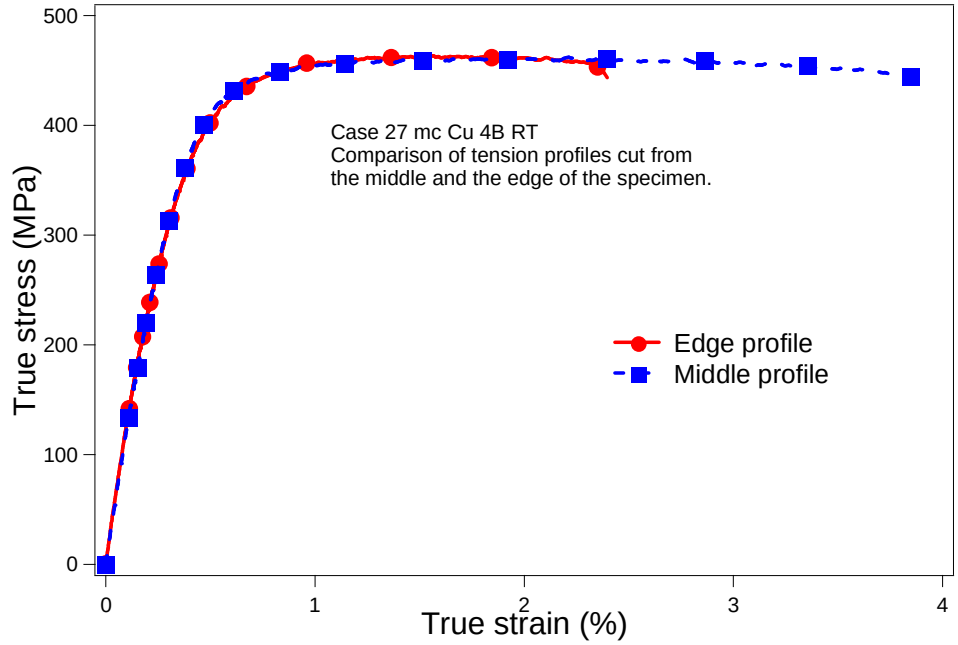

Figure 4.17: Case 27 mc Cu 4B RT comparison of tension profiles from the edge and from the middle of the consolidate. The profile from the middle of the consolidated powder has higher ductility than the profile from the edge.

A comparison of tension profiles cut parallel to the shear plane, and parallel to the extrusion direction plane is shown in Figure 4.18. Samples cut parallel to the shear plane have a higher ductility, without much decrease in the strength. This suggests that the powder is consolidated better in the shear plane, than in the extrusion direction.

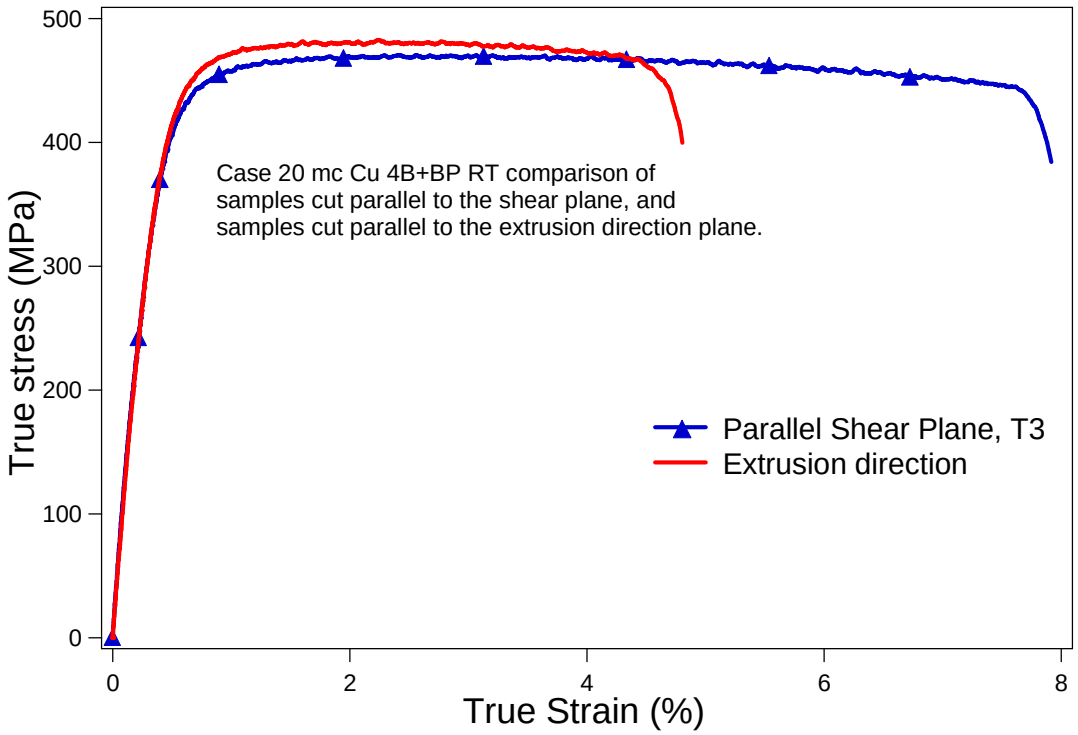

Figure 4.18: Comparison of 4B+BP RT tension profiles cut parallel to the shear plane and the extrusion direction plane. The tension profile cut from parallel to the shear plane has higher ductility, with minimal strength loss, than the profile cut parallel to the extrusion direction.

4.1.5 Compression Samples

Compression tests for the sample consolidated using route 4B at room temperature and then swaged exhibited an UTS of 410 MPa. The test was stopped at a true strain of approximately 35% strain, when the barreling started. Figure 4.19 shows

the compression test results for route 4B, compared with literature values for route 2B [22].

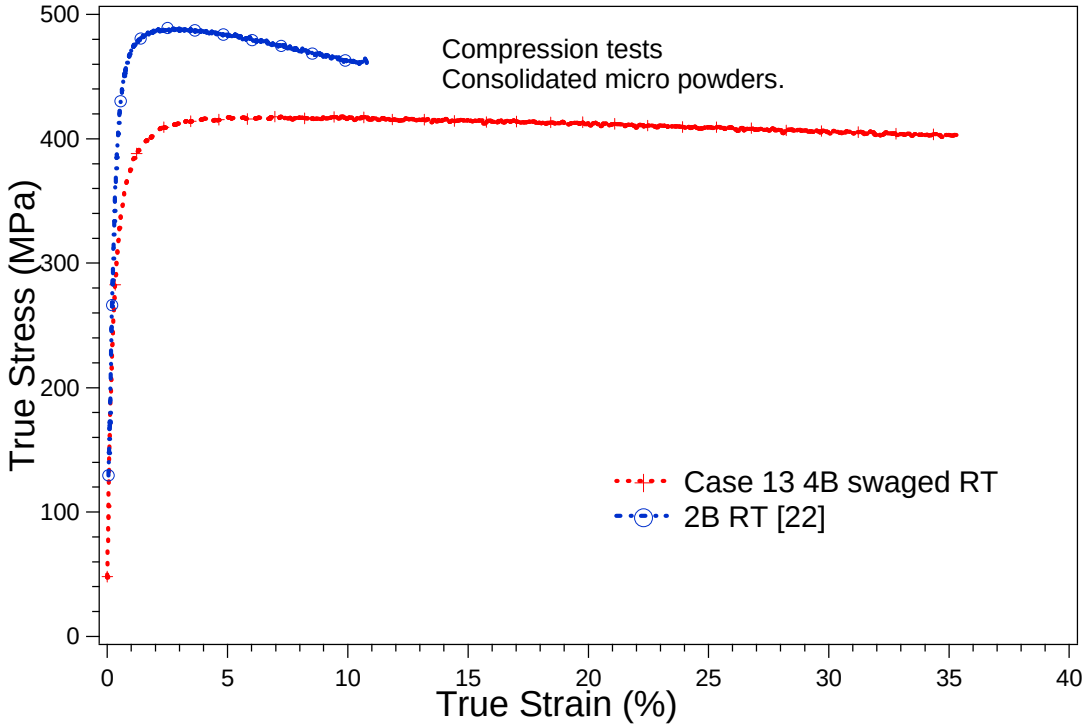

Figure 4.19: True stress- true strain compression test of mc Cu ECAE at 4B and swaged at room temperature compared with -325 Mesh ECAE at 2B.

A comparison between the tension and compression responses of the sample ECAE 4B processed and swaged at room temperature, shown in Figure 4.20, shows a notable difference in the strength levels and ductility of the material. The tension sample had a slightly lower ultimate tensile strength, and had a significantly lower percent elongation to break, than the compression sample, but the compression sample did not break.

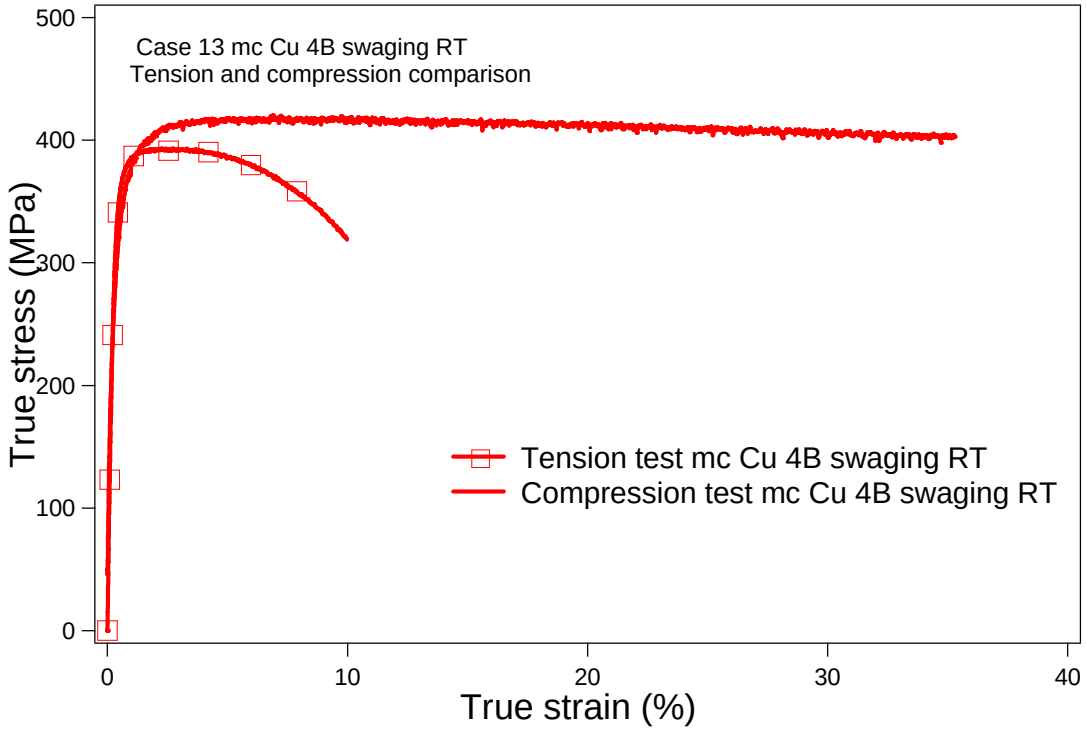

Figure 4.20: True stress- true strain comparison between tension and compression tests of mc Cu ECAE at 4B and swaged at room temperature.

Compression tests were run on only the mc Cu sample ECAEd at 4B with swaging because of its low tensile strength. Compression tests were run to determine if there were any advantages in using swaging after ECAE in compression, since tension tests did not result in any advantages.

4.2 Discussion

4.2.1 Effect of Strain Path Changes and Number of Passes

Prior particle boundaries can be clearly seen in ECAE 1A samples under optical microscopy. Similarly, it is possible to observe the prior particle boundaries, in the ECAE 4B samples in optical images. In particular, Case 13 which was ECAEd via 4B at

RT, then swaged at RT shows the grain boundaries are elongated. This is mainly due to the effects of swaging, which forces the powder to deform axially.

Prior particle boundaries can not be seen in optical images of Case 12 which is ECAE 8B sample consolidated at RT of mc Cu, which may be due to the multiple passes providing sufficient deformation to break the surface oxides and sufficient diffusion between the particles for good bonding. In addition, there is no visible porosity in the OM images up to 150x magnification. Thus, apparently, route 8B causes significant grain refinement, and the elimination of porosity and prior particle boundaries. A similar result was found by Dobatkin *et al.* [r160], during ECAE of bulk oxygen-free Cu. Neither prior grain boundaries nor the newly formed structures were revealed by etching and optical microscopy [r160].

The study by Haouaoui [22] on nc Cu fabricated using ECAE powder consolidation also observed that the powder deformed non-uniformly in the presence of porosity. The question is whether the porosity occurred because of agglomeration of the powder prior to ECAE, or due to particles which did not consolidate and were later removed during Wire EDM cutting. Either is possible, since Cases 3, 4, and 9 were extruded only once, and does not give pores or unconsolidated powders the opportunity to close or consolidate during subsequent passes. Optical images of additional passes did not result in the macroscopic cavities observed in the one pass samples.

In this study, a higher number of passes were studied than in [22]. Figure 4.21 shows a comparison of tensile tests for route B, with 2 (with BP), 4, and 8 passes at

room temperature. Route 2B has the highest strength, followed by route 4B, and then route 8B. Route 8B had the highest ductility, followed by 4B, and last, 2B (with BP).

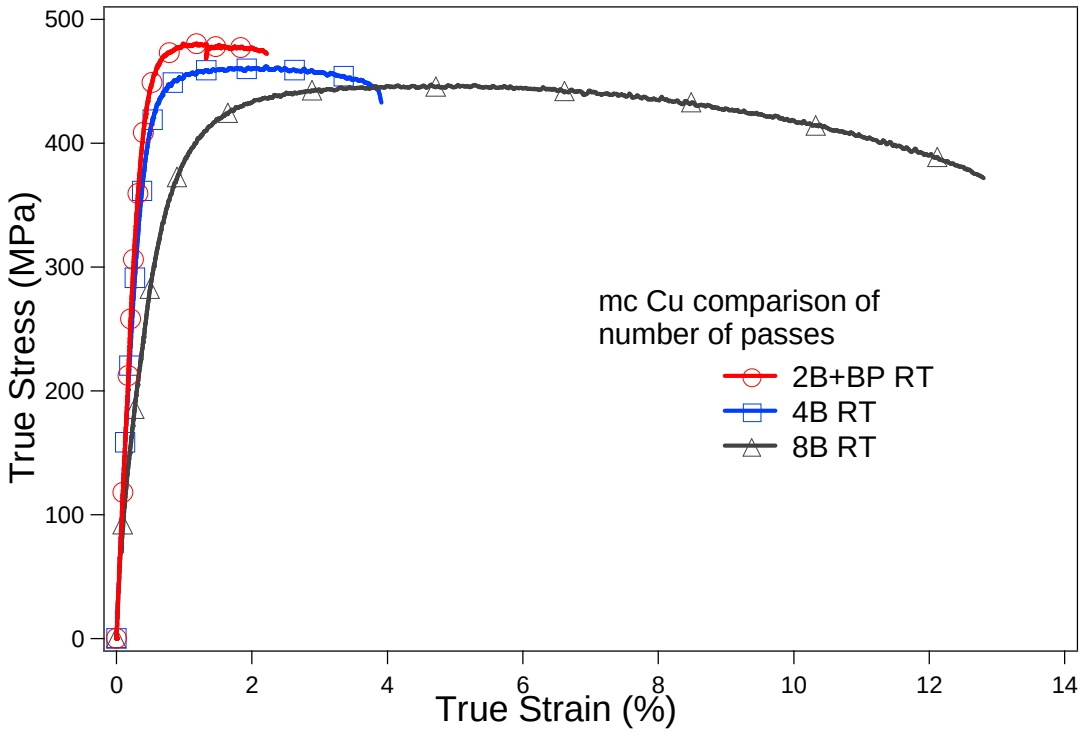

Figure 4.21: A true stress-true strain comparison between the number of passes for mc Cu ECAEd via route B at room temperature. Ductility increases with increasing number of passes, while strength decreases with increasing number of passes.

Figure 4.22 shows a comparison for two different routes, with 8 passes. Route B results in a more ductile material, but route C' resulted in a stronger sample. The differences in strength between route C' and route B are small, at a difference of 1.28 MPa in average UTS. By hypothesis testing, assuming two equal unknown variances, the average strengths of Case 11 and Case 12 are statistically the same, up to a confidence level of 99.9995%. Thus, we cannot conclude that the change in route actually increases the UTS of the material. However, we can conclude that the elongation to break of 8B is

larger than that of the 8C' sample, with a difference in averages of 9.145%, up to a confidence level of 75%.

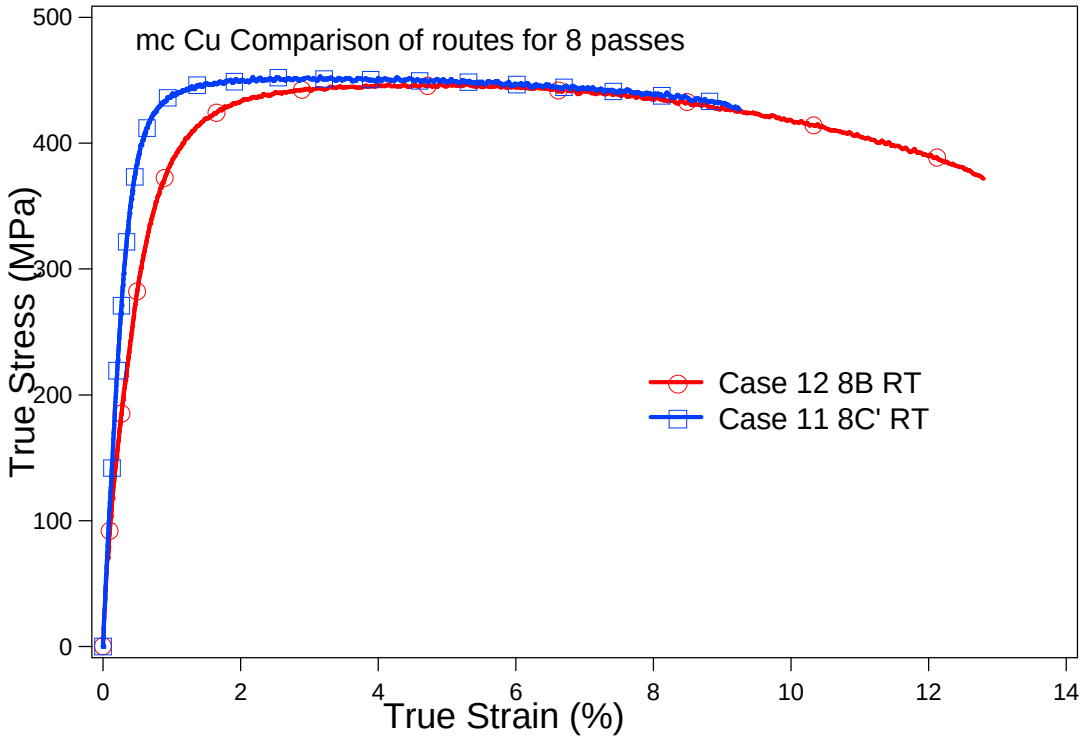

Figure 4.22: A tension true stress-true strain test, comparing the effect of route B versus route C' on an 8 pass mc Cu consolidated powder's mechanical behavior. Route C' produced a more ductile sample, and route B produced a stronger sample.

In general, increasing the number of passes will increase the ductility of mc Cu powder, as will using route B. However, increasing the number of ECAE passes will result in a decrease in strength of the material. These conclusions are made without considering the effect of swaging on the consolidated mc Cu powder's mechanical behavior. The effects of post-ECAE deformation from room temperature swaging are discussed in the next section.

4.2.2 Effect of Swaging

The ECAEd and swaged micron sized Cu particles consolidated via ECAE at 4B at RT demonstrate a higher ductility in compressive response of the only ECAE consolidated mc Cu (325 mesh powder), at route 2B. The compression test results were shown in Figure 4.11.

In tension, the swaged 4B mc Cu exhibited lower ductility and strength, as compared with previous mc Cu samples produced using route 2B. The ductility of the 4B swaged case is superior to the purely extruded cases. It appears that swaging is a viable option to increase the ductility of materials consolidated via ECAE. A comparison plot between the tensile behavior of 4B RT, 4B with BP, and the 4B with swaging is shown in Figure 4.23.

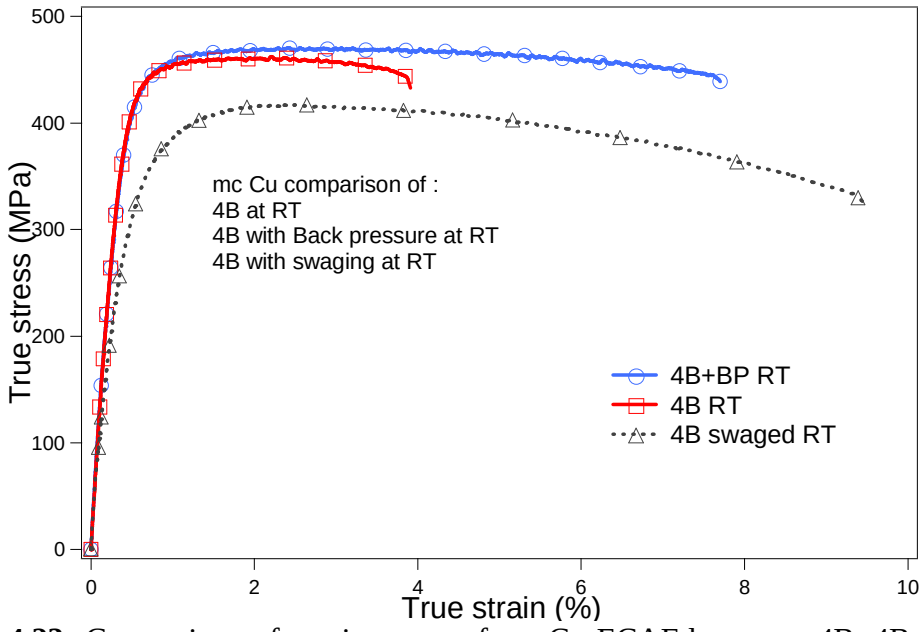

Figure 4.23: Comparison of tension tests of mc Cu ECAEd at route 4B, 4B with back pressure, and 4B with swaging, all at room temperature. Swaging causes the highest ductility and the lowest strength.

4.2.3 Effect of Back Pressure

The comparison plot of tensile behaviors of 4B RT, 4B with back pressure, and 4B with swaging, shown in Figure 4.24, shows the benefit of using back pressure. For route 4B, ductility and strength were both increased with the use of back pressure during ECAE, compared with the sample that was extruded without back pressure (4B at RT). However, the ductility in the case swaged after ECAE is greater than the case with back pressure, but the strength of the swaged case is lower than the 4B+BP case. This shows that back pressure can be used to maintain or increase strength, and provide moderate gains in the ductility of a consolidated powder.

Figure 4.24 shows the comparison between two and four passes at route B, with back pressure. Increasing the number of passes with back pressure increases the ductility, but decreases the strength. Comparing the 2B to the 2B+BP sample, the use of back pressure increases the strength of the material.

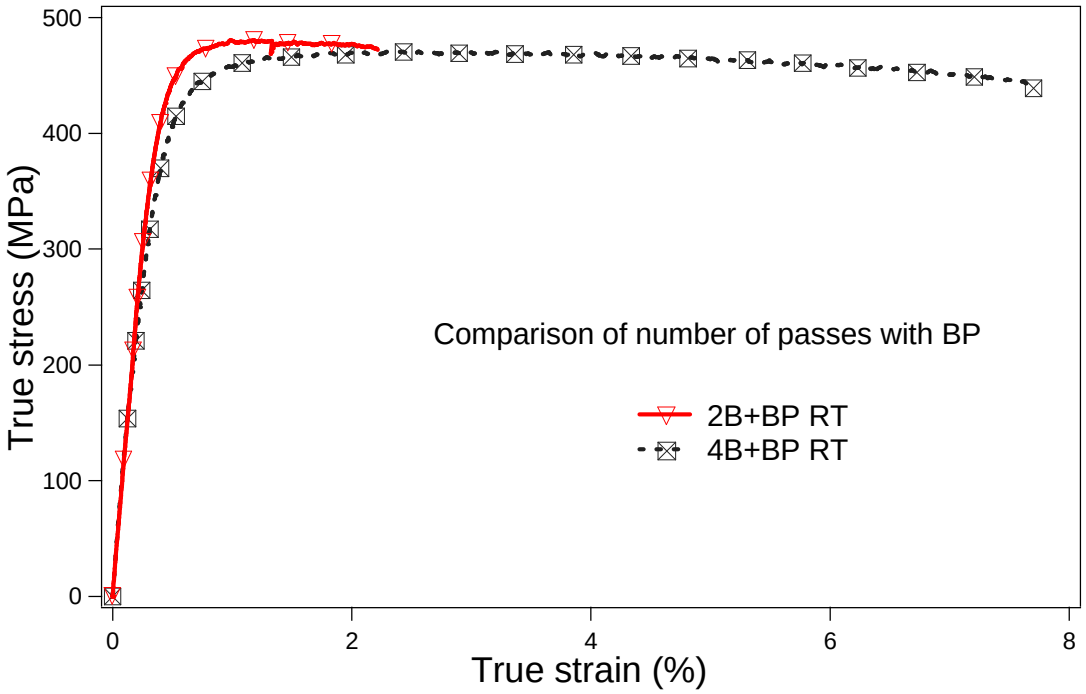

Figure 4.24: Tensile true stress-true strain comparison of 2B with back pressure and 4B with back pressure at RT. This shows back pressure results in higher tensile strengths, with lower ductility, and using route 4B+BP increases the ductility from route 2B+BP.

4.2.4 Effect of Can Material

Can material has a significant impact on the single pass consolidation of a microcrystalline powder. Comparing Case 9, 1A mc Cu in a Ni can, with Cases 3, 1A mc Cu in a Cu can with no friction, and 4, 1A mc Cu in a Cu can with friction, shows the marked difference in the formation of macroscopic cavities. A study performed by Xu and McMeeking [64] examined the effect of the can during isotatic pressing of Cu powder in a Cu can. They found that, for isostatic pressing, the powder behaves in three distinct stages in response to pressure. The can holds more axial than hoop stress. Xu and McMeeking also found that pressure on the powder was up to 20 MPa lower than

the applied pressure on the can, and that the powder does not experience isostatic pressure. It is logical to conclude that the consolidation achieved in the present study depends largely on how much stress is transmitted to the powder. However, the calculations peformed by Xu and McMeeking, to model the powder behavior, is for isostatic pressing, in which pressure is applied on all sides. ECAE applies pressure from the top, and forces the powder thru a shear zone, so the mathematical model developed by Xu and McMeeking cannot be used.

For samples extruded via route 1A, it seems that Ni cans provide the best consolidation, and eliminate porosity. However, as established by Haouaoui *et al.* [21], Cu cans should be used with mc Cu for a higher number of passes, because as a rule of thumb, selected can material should have similar flow characteristics as the powder inside the can.

V. BEHAVIOR OF NANOCRYSTALLINE COPPER

5.1 Experimental Results

5.1.1 Microstructure of nc Cu

The optical microscopy images of nc Cu powder consolidates reveals several large structural features, along with porosity. These features can be a consequence of agglomeration, since these are readily viewed without etching. Figures 5.1 show the optical microscopy images of an unetched Case 17 nc Cu 4B at 100 °C.

(a) 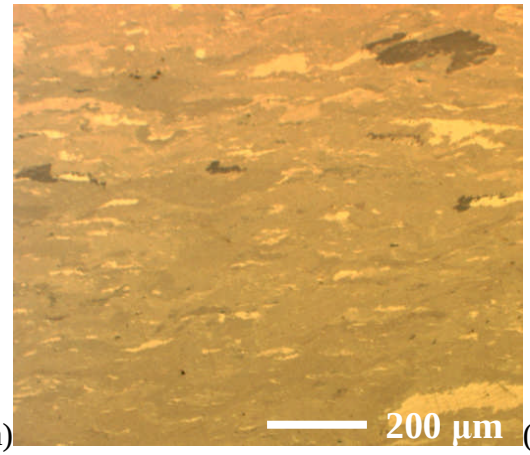

(b) 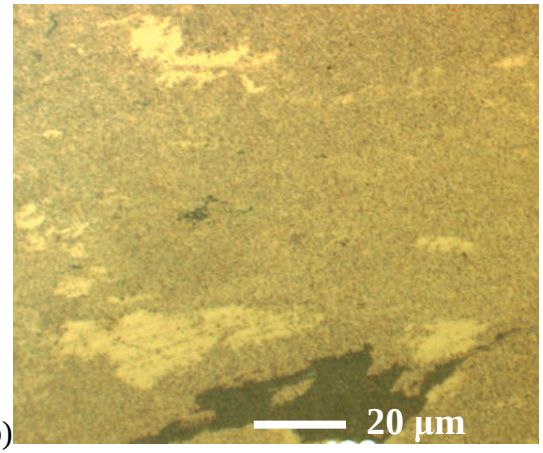

Figure 5.1: Optical image of Case 17 nc Cu 4B ECAEd at 100 °C, showing large features that may be a consequence of agglomeration of the nanopowders. Dark regions may be dark colored agglomerations, rather than porosity, as shown in (b) a magnification of a dark region.

Optical images reveal that small porosities exist in the samples, which are readily viewed prior to etching. Figure 5.2 shows an optical microscopy image of Case 17 ECAEd at 4B at 100 °C, with small porosities.

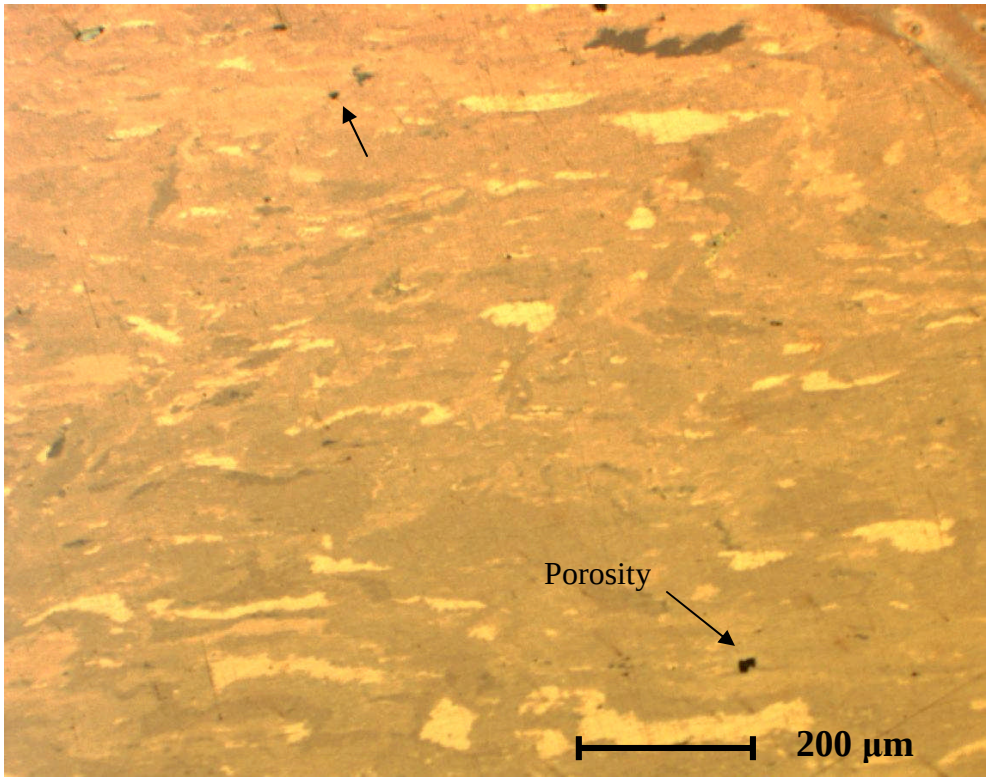

Figure 5.2: Case 17 nc Cu 4B at 100 C, 10x of broken tension sample, in gauge section, unetched sample, showing the location of potential porosity.

An examination of Figure 5.3, which shows the side surface perpendicular to the tensile fracture surface shows the orientation of the agglomeration boundaries parallel to the applied tensile force, which is also the direction of the extrusion. Also of note, the fracture line propagates thru the agglomeration boundaries, which indicates a strong inter-agglomerate bonding, and good consolidation.

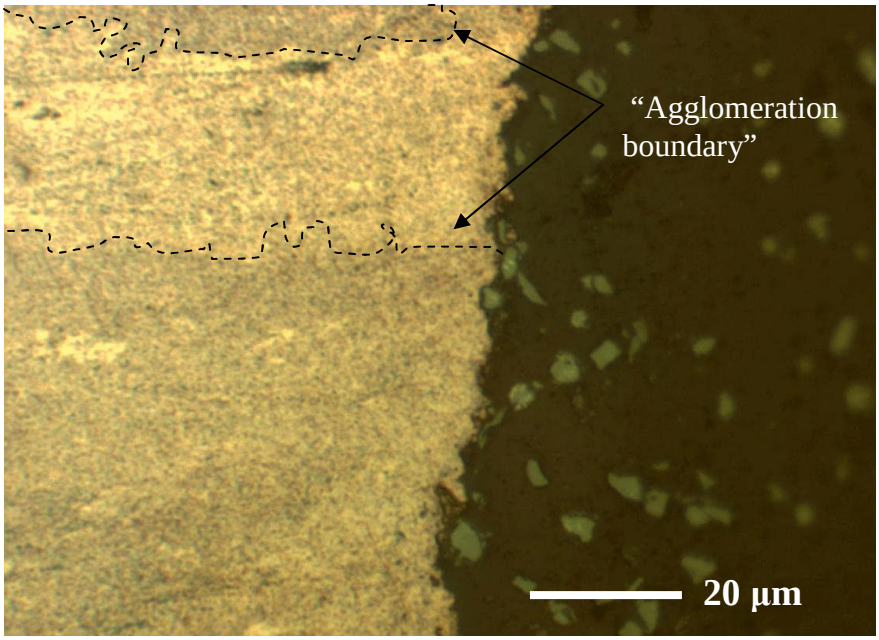

Figure 5.3: 100x Case 17 nc Cu 4B at 100 C, of broken tension sample, along fracture surface of an un-etched sample.

5.1.2 Tension Experiments

Tension tests were performed at room temperature on successfully consolidated nc Cu samples. Figure 5.4 shows the tensile true stress- true strain diagram of nc Cu consolidated using ECAE. A comparison with cold isostatically pressed (CIPed) Cu which was then ECAEd at route 4B is made to the present study.

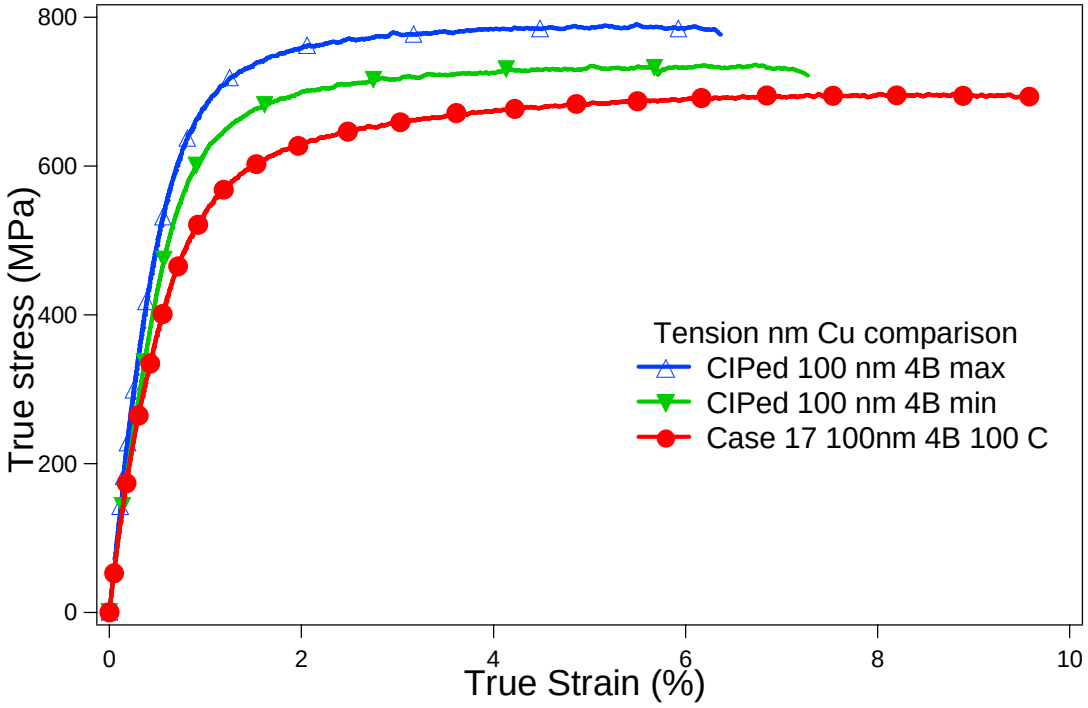

Figure 5.4: Tensile Stress-strain diagram of nm Cu, with a comparison with CIPed 100 nm Cu powder which was then extruded at 4B. Case 17, nc Cu 4B at 100 °C had the highest ductility, and the lowest strength.

A table of the mechanical properties of the nc Cu is given below, with averages and standard deviations given for cases in which multiple samples were taken.

Table 5.1 Mechanical properties of nc Cu consolidated via ECAE, with standard deviations.

Case	Route	UTS (MPa)	Elongation to break (%)
17	4B 100°C	659 ± 28.9	8.9275 ± 0.66
CIPed 100 nm sample 1	4B RT	787	6.34
CIPed 100 nm sample 2	4B RT	735	7.27

5.1.3 Green Density Measurements

The nc Cu of all cases had an average green density of 47.9% of theoretical before the consolidation, but this low value may be due to the fact that for the first few cans, powder was filled without the hydraulic hand press. In a previous study by Haouaoui [22], nc Cu powders were either hand-tapped into the can or compacted using the hydraulic hand press. The material packed using the hydraulic hand press was observed to provide better compaction of the powder before extrusion. The current study also found this to be the case. Nano-sized powder commonly forms into large and difficult to break agglomerates. Qualitatively, the powder often became stuck in the funnels that were used to transfer the powder into the cans, and it was difficult to dislodge the agglomerates such that additional powder could be applied. Quantitatively, there is a significant difference between the densities of the nanopowder packed without pressing and the cases in which the powders were packed with pressing, as shown in Table 5.2, showing the efficiency of hand pressing. Additional evidence of the formation of large agglomerates of nanoparticles is the disparity between the micro sized powder's green densities and that of the nanopowder.

In addition, if the green density of the powder is greater, then the product yield after ECAE will be larger. This is particularly useful for multiple passes, since the shape of the powder space is a function of the number of passes and routes. In some routes, the end regions of the consolidates may have a smaller cross section than the bulk of the consolidates and need to be discarded.

Table 5.2: Green density measurements of nc Cu.

Case	size, powder type, route, ECAE temp	Green Density (% of theoretical)
14	nc Cu 8C' RT	12.31
15	nc Cu, 8B RT	52.63
16	nc Cu, 4B RT	53.92
17	nc Cu, 4B 100 C	51.09
18	nc Cu, 4B (100 C & RT)	53.55
21	nc Cu, 2B+BP RT	52.63
22	nc Cu, 2B+ swaging RT	52.32
23	nc Cu, 4B+BP	54.78

5.2 Discussion

5.2.1 Effect of Swaging on nc Cu

Behavior of nc materials is very different from that of microcrystalline materials. The goal of applying swaging after ECAE of nanopowders is to try to eliminate porosity thru strain path changes. The idea is to remove these defects, which it thought to cause the significant decreases in ductility in nc Cu. Disappointingly, swaging appears to be detrimental to consolidation of nc Cu powders. Two experiments done, for 2B and 4B routes at RT were performed, in which swaging was performed in the same manner as for micro Cu powder. Swaging of nc Cu powder after ECAE resulted in failure of the material.

During extraction of both the 2B and 4B RT ECAE samples, a significant amount of agglomerated powder was dislodged. The consolidated regions were approximately 2 mm in diameter or less, and were too small to perform mechanical tests.

It is concluded that swaging of ECAE consolidated nano Cu particles catastrophically damage the consolidates instead of closing the porosity and increasing

the consolidate ductility. Higher number of passes were deemed to be unnecessary and are likely to produce similar results, since it is known [22] that the powders can be fully consolidated after 4 passes. Swaging of samples extruded under elevated temperatures, however, may need to be explored in the future.

5.2.2 Effect of Extrusion Temperature

Case 17 (nc Cu, 4B at 100°C) had higher elongation to break (around 9%) than a nc Cu sample that was extruded at route 4B at room temperature (around 7%). Also, it was observed that the force-displacement diagram obtained during extrusion was very smooth, and had no significant load drops in Case 17. A load drop in a force-displacement diagram usually indicates that the material has sheared, which is undesirable, because it causes damage in the powder consolidate. As mentioned in Section 2.1, defects in nanopowder consolidates can be a main contributor to diminished ductility.

The sample that was consolidated at elevated temperatures exhibited a lower UTS than the cases consolidated at room temperature. This may be due to grain growth beyond the nanometer scale. However, grain growth in Cu occurs at annealing temperatures usually above 100 °C [54], and the samples were held at 100 °C for 15 minutes before extrusion. The total time the powder was subjected to elevated temperature was less than 20 minutes. It is plausible, though, that the small deformation heat and deformation induced grain growth might be possible causes of grain growth. More probable is that this particular sample was degassed at a temperature higher than

120 °C for a long duration (more than 2 hours), since the thermocouple in the vacuum system was not properly working at the time.

Case 18, in which nc Cu was extruded at 100 °C for the first two passes, and then at room temperature for the last two passes, showed high loads in the two heated passes. Also, there were load drops during these two passes, though not as significant as the cases extruded at room temperature. This may indicate that a combination of higher degassing temperatures and elevated extrusion temperatures can lead to effective consolidation. A combination of these two parameters was not explored in this study.

Shear localization during ECAE is also indicated in the load-displacement curves taken during extrusion. Sharp drops in load during extrusion indicate that material failure has occurred, while smooth curves indicate that little or no material failure has occurred. A relatively smooth load displacement curve of a nc Cu being consolidated is shown in Figure 5.5, while a load-displacement curve with many load drops is shown in Figure 5.6.

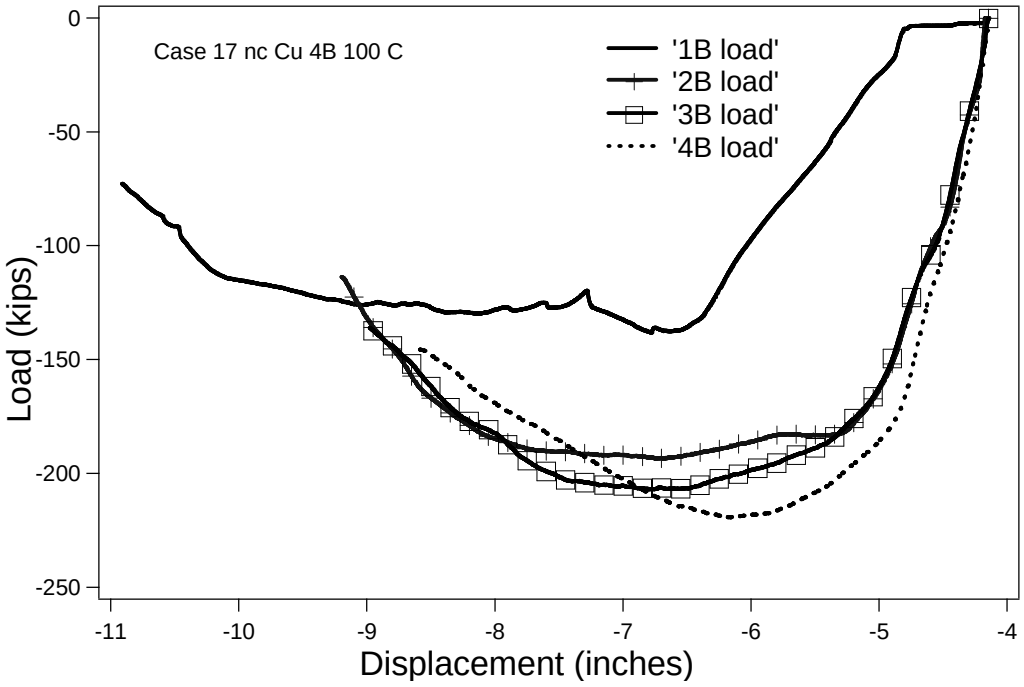

Figure 5.5: Case 17 nc Cu 4B 100 C Load displacement curves showing no load drops or shear localization, indicating that no damage to the powder occurred during ECAE.

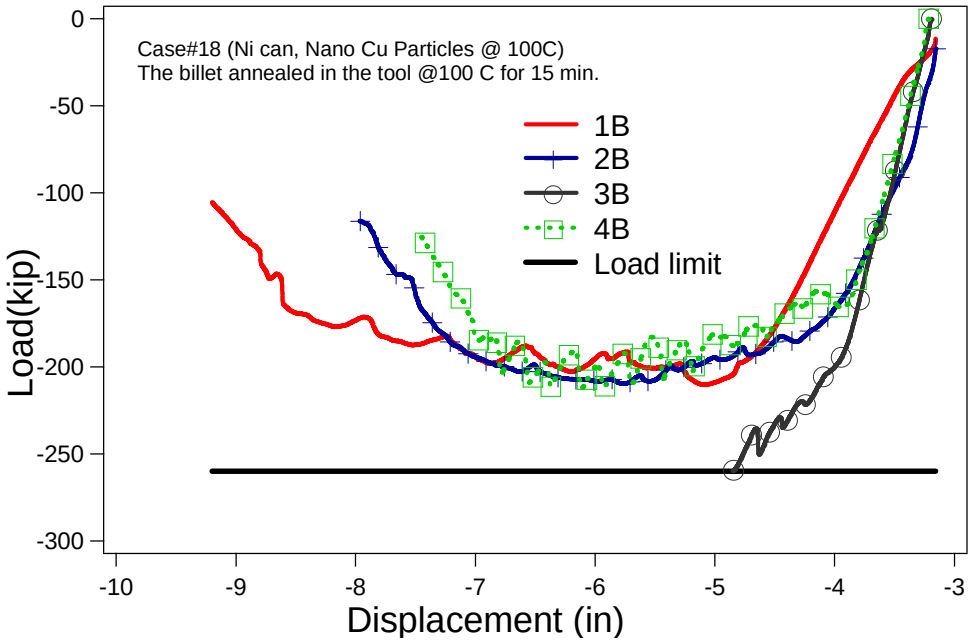

Figure 5.6: Case 18 nc Cu 4B at 2 passes at 100 C, 2 Passes at RT load displacement curves, showing significant load drops, which indicates damage occurred to the powder during ECAE.

One of the most significant achievements of this study is that the ductility of the nc Cu powder was improved. The average ε to break (%) of the Case 17 route 4B 100 °C is 8.9%. The average elongation to break for Cold Isostatically Pressed (CIPed) nc Cu ECAE route 4B at room temperature is 6.8%. This means that extruding nc Cu at an elevated temperature resulted in a 2.1% increase in the elongation to break. Assuming that the two different cases (17 and the CIPed case) have equal unknown variances, the mean elongation to break of Case 17 is statistically larger than the CIPed cases, with at least a 97.5% probability. This result indicates that the gain in ductility by extruding the nc Cu at an elevated temperature is a significant value, and due to a change in degassing or extrusion temperature.

Visual inspection of Case 18 shows that a combination of elevated temperatures at the first two passes and room temperature extrusions for the last two passes did not produce a useful consolidate. Figure 5.7 shows where the powder was mixed with the Ni can, and we can predict that it will be difficult to obtain mechanical test samples from the consolidate. Therefore, it is suggested that future consolidations of nc Cu be performed at 100 °C. This temperature was selected because it has been shown to improve the consolidation of the powder, but will not likely cause significant grain growth.

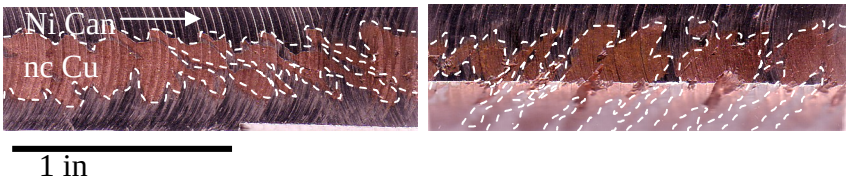

Figure 5.7: Case 18 nc Cu 4B at 100 C and RT consolidated powder showing Ni can be incorporated with Cu powder consolidate. The Ni can is outlined in white.

5.2.3 Effect of Back Pressure

Back pressure produced samples which were well consolidated, as shown in Figure 5.8. Nanocrystalline cases which were extruded with back pressure, in combination with elevated extrusion temperatures exhibited relatively smooth load-displacement curves during extrusion. This indicates that little material failure occurred during extrusion.

Figure 5.8: Case 22 nc Cu 2B+BP at 100 °C, with back pressure applied after half of the can was extruded. The top of the can half has shear localization, whereas the bottom part of the can is smooth, as a consequence of back pressure.

VI. BEHAVIOR OF ALUMINUM ALLOYS

6.1 Experimental Results

6.1.1 Microstructure of Al-10.5 Mg Alloy

The figures shown in this section exemplify the microstructure of the Al-10.5 Mg alloy powder consolidated via ECAE at 150°C extrusion temperature. Figure 6.1 shows the transverse plane cross section of the case A2, Al-10.5 Mg microcrystalline alloy extruded in a nickel can, using route 4B at 150 °C. The dark regions appear to be microscopic porosity in the consolidated material, and indicate that the consolidate is not completely dense.

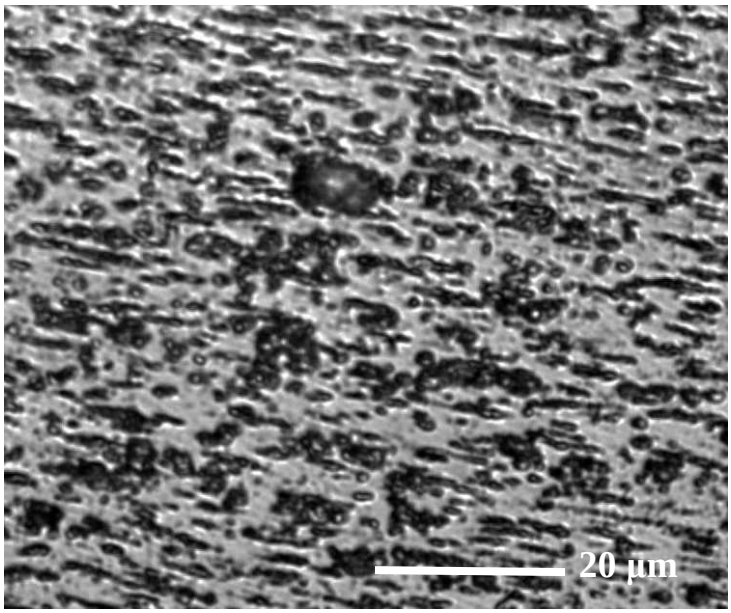

Figure 6.1 Al-10.5 Mg alloy Optical Image, 100x magnification of the transverse plane (TP) cross section, showing dark regions, which may be porosity. If the dark regions are porosity, this indicates that the consolidate is not completely dense.

Figures 6.2 and 6.3 show the Longitudinal Plane (LP) cross section of the successfully consolidated Al-10.5 Mg powder via 4B at 100 °C. High porosity exists in the powder, in this plane.

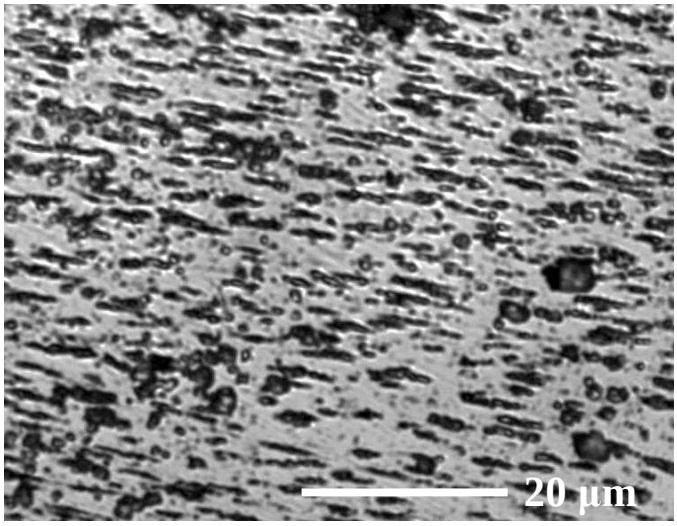

Figure 6.2 Case A2, ECAE at 4B at 150°C, showing the cross section parallel to the Longitudinal Plane (LP), at 100x magnification, with dark regions, which may be porosity. The dark regions in the LP direction appear to be elongated more than those from the Transverse plane.

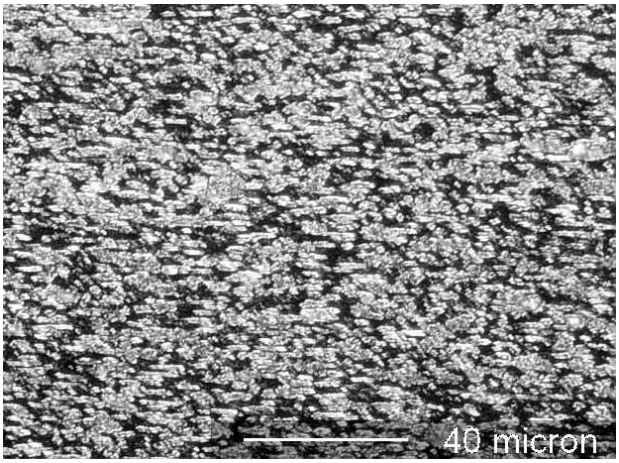

Figure 6.3 Optical Microscopy Case A2 ECAE at 4B at 150°C, showing a cross section in the Load Plane (LP), at 40x magnification, showing high porosity.

A higher magnification image captured using an SEM is shown in Figure 6.4, and 6.5. The image shows similar dark spots, arranged in oval patterns, which may be porosity. Further magnification shows rounded pores which are agglomerated, as well as thin, elongated pores. Dark spots in the appear to be along the shear direction of the last ECAE pass.

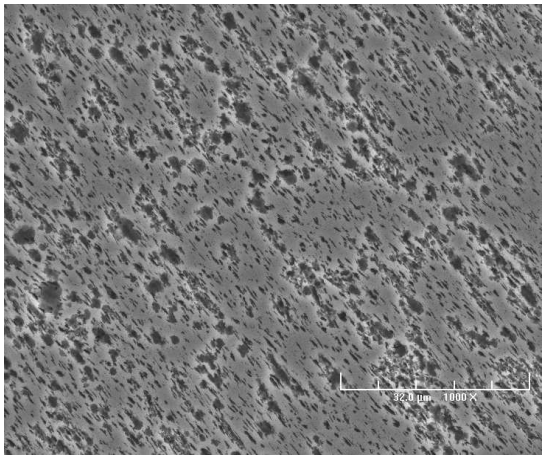

Figure 6.4: SEM image of Case A2 Al-10.5 Mg ECAEd at 4B 150 °C, at 1000X magnification. Dark spots, which may be porosity, arranged in approximately oval shapes.

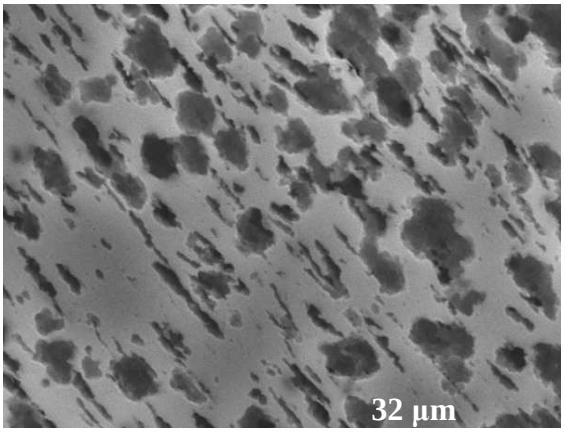

Figure 6.5: SEM image of Case A2 ECAEd 4B at 150 °C, at 4000X magnification, showing porosity in the matrix.

6.1.2 Tensile Tests of Al-10.5 Mg

Tension tests for the Al-10.5 Mg were performed on Case A3 ECAEd at 4B at 150°C in a Ni can, because this was the only aluminum consolidation case that resulted in a bulk consolidate large enough to cut tension samples out of. The tension results are shown in Figure 6.6. The ductility is extremely limited (at less than 0.3%). The sample broke above the gage section, so ductility and strength may be higher in a better consolidated sample

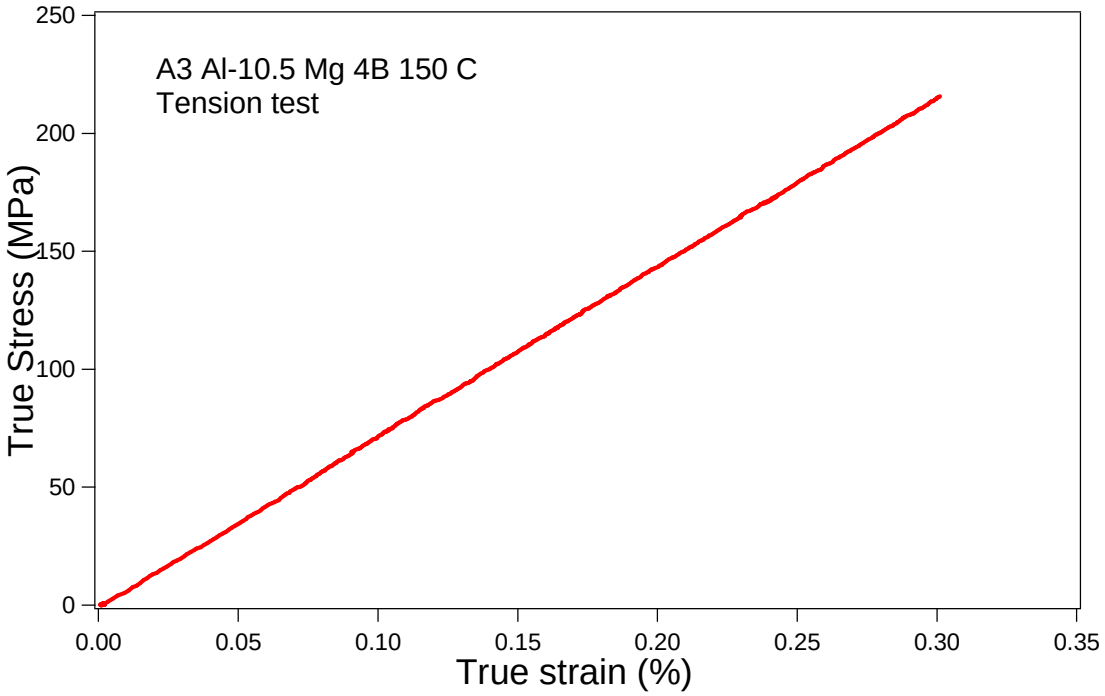

Figure 6.6: True stress-true strain tension test of Case A3 4B at 100°C in Ni can, showing very low ductility at 0.3%.

Han *et al.* [92] looked at the effect of Cold Isostatic Pressing and conventional extrusion on Al-5 Mg powder. One sample produced a tensile strength of 713 MPa,

which is much higher than what was obtained in the ECAEd Al-10.5 Mg powder, with a similar ductility of 0.3%. Tensile data on Al-10.5 Mg (called Al 520.0-T4) from the ASM Metals handbook [93] had a tensile strength of 330 MPa and ductility of 16%. The ECAEd Al-10.5 Mg sample has ductility and strength below those given in the ASM handbook. The comparisons of the tensile mechanical properties are made in Table 6.1.

Table 6.1: Tensile mechanical properties of consolidated Al alloy powders, from ECAE, CIPing and conventional extrusion, and of coarse grained material.

Material	Size	Consolidation method	UTS (MPa)	Elong.to failure (%)
Al-10.5 Mg	mc	ECAE 4B +BP 150°C	215	0.3
Al-7.5 Mg [92]	nc	CIP and conventional extrusion	713	0.3
Al-10.5 Mg [93]		None- coarse grained	330	16

6.1.3 Compressive Tests of Al-10.5 Mg

Compression experiments showed that the consolidated Al alloy powder is strong but brittle, as shown in Figure 6.7. The sample failed at less than 1% elongation, with no visible signs of plastic deformation. This case had a higher strength than Case 3, which was processed under the same ECAE conditions but with tensile tests performed on it. In a study on Al-7.5 Mg by Fan *et al.* [94], compressive strengths of cryomilled consolidated by Hot Isostatic Pressing and conventional hot extrusion were measured to be 611 MPa, with the test performed up to a true strain of approximately 0.4%. In a similar study, Wikin and Lavernia [57] examined the compressive behavior of cryomilled commercially pure nc Al powder which was consolidated via conventional

extrusion. They obtained a sample with an UTS of 410 MPa, and reached a ductility of 0.15% before stopping the test.

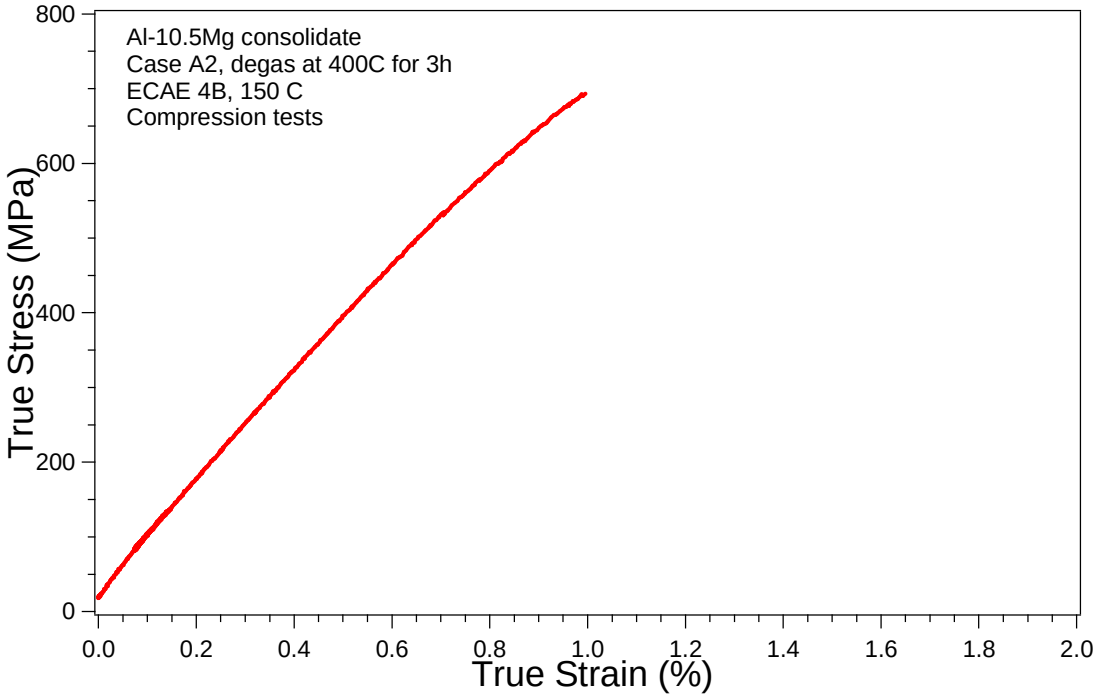

Figure 6.7 Case A2 Compression test: Al 10.5 Mg Consolidate, route 4B at 150 °C. The sample showed high strength and low ductility, before plastic deformation was observed.

The mechanical results of the Al-10.5 Mg are listed in Table 6.2, and are compared with literature data on Al-Mg alloys and pure Al, fabricated by cryomilling, and consolidated by different methods.

Table 6.2: Compressive mechanical properties of consolidated Al alloy powders, from ECAE, HIPing, CIPing, and conventional extrusion.

Material	Size	Consolidation method	Compressive failure strength (MPa)	Elongation to failure (%)
Al-10.5 Mg	mc	ECAE 4B 150°C	693	~1.0
Al-7.5 Mg [94]	nc	HIPing & hot conventional extrusion	611	~0.4
Commercially pure Al [57]	nc	Conventional extrusion	~410	~0.15

When compared with literature data, the mechanical behavior of the ECAE consolidated AL-10.5 Mg in compression appears to be superior to consolidation of similar Al alloys using different methods. The ECAEd case exhibits the higher strength and ductility than consolidated nc Al alloys.

6.1.4 Green Density of Al-10.5 Mg

The green density of Al-10.5 Mg was measured after packing, and prior to ECAE. The green densities are given in Table 6.3, in percent of the theoretical density of Al-10.5 Mg.

Table 6.3: Green density of Al powders after packing.

Case	size, powder type, route, ECAE temp	Green Density (% of theoretical)
A1	mc Al- 10.5 Mg, 4B RT	43.68
A2	mc Al- 10.5 Mg, 4B 100C	41.45
A3	mc Al- 10.5 Mg, 4B 100 C	43.68

6.2 Discussion

6.2.1 Effect of Back Pressure

Back pressure produced samples which were well consolidated, observed during visual inspection of the extracted samples. However, these samples exhibited low strength and ductility, when compared with coarse grained material and CIPed nc Al-7.5 Mg powder. It seems that either ECAE, the use of back pressure, or the combination of the two diminish the mechanical properties of mc Al-10.5 Mg powders during consolidation.

6.2.2 Effect of Can Material

Cu cans caused a loss of material during machining to extract the consolidated material. Parts of the Cu can were embedded within the Al consolidate, which made it difficult to obtain consolidated powder that was free from the canning material. Nickel cans, in combination with elevated extrusion temperatures, produced samples which were consolidated enough to obtain mechanical test specimens.

6.2.3 Effect of Extrusion Temperature

Increasing the temperature in which the Al-10.5 Mg powder was extruded from Room temperature to 150 °C resulted in a decrease in load drops during the extrusion, shown in Figure 6.8 which shows the load-displacement curve the Al-10.5 Mg powder ECAEd using route 4B at 150 °C. The load drops are an indication of shear localization and lack of full consolidation. The first pass in Case A2, extruded at 150 °C, had a smooth load drop (decrease in load over a long displacement), but the following three passes were smooth with very minor load drops. The Al sample extruded at room

temperature exhibited many large and abrupt load drops for all four passes, as shown in Figure 6.9. The sample produced was not consolidated into a usable sample. The sample from the elevated temperature extrusion produced a very well consolidated piece, in Case A1 (4B at room temperature).

The compressive failure strength of the ECAE Al-10.5 Mg is an average of approximately 692 MPa. This sample has strength and ductility above what CIPing or HIPing of cryomilled nc Al-Mg powder could achieve. The increase of consolidation temperature in the Al 10.5 Mg was advantageous in that it significantly decreased the number of load drops during extrusion, and consolidation was good such that usable pieces of consolidate were obtained.

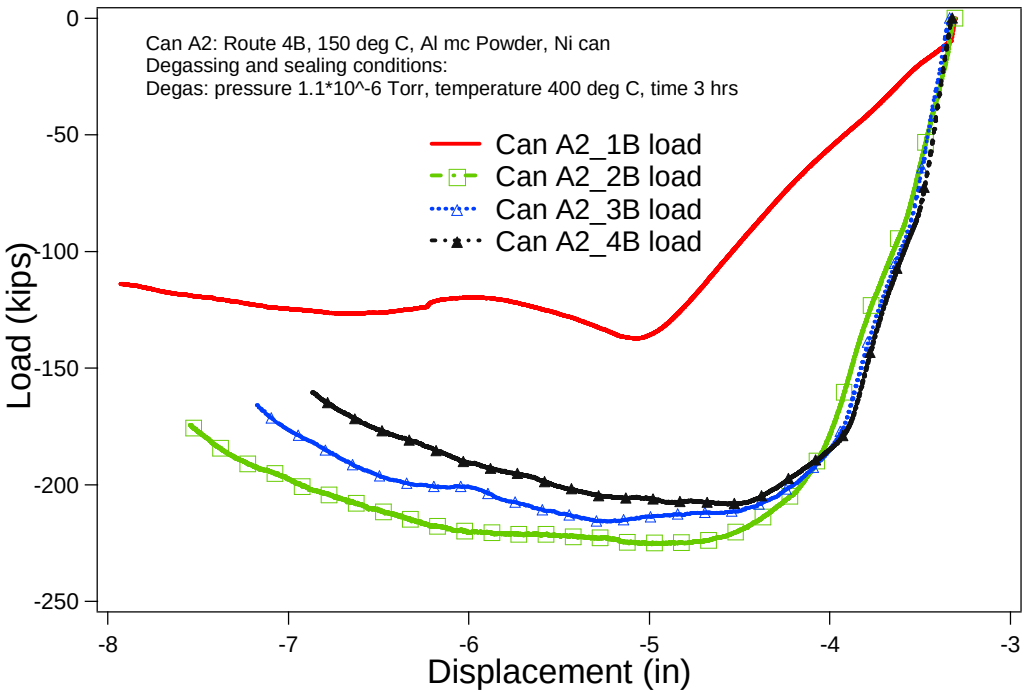

Figure 6.8: Load-Displacement graph, mc Al-10.5 Mg, Case A2 route 4B 150ºC, with smooth curves (except first pass). This indicates that little or no shear localization occurred during ECAE.

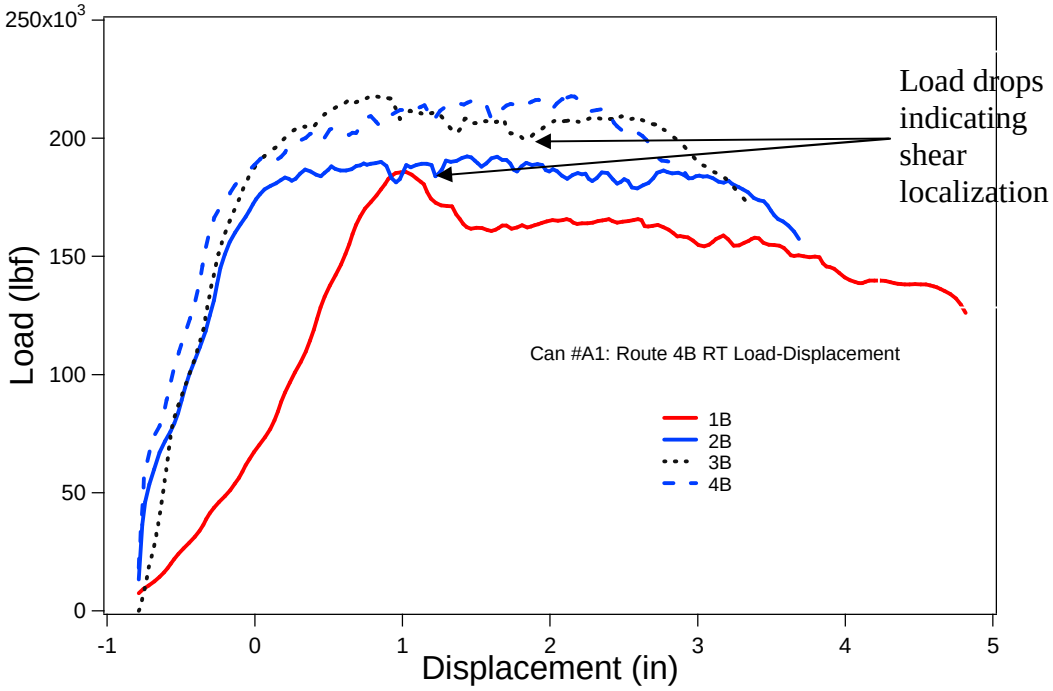

Figure 6.9: Load-displacement graph Aluminum, Case A1 route 4B RT, with significant load drops. This indicates that shear localization occurred during ECAE.

VII. COMPARISONS OF THE RESULTS

Comparisons of strength versus ductility from literature are shown in Figure 7.1. Comparisons of strength versus ductility of samples from the present study are shown in Figure 7.2, which includes mc Cu, and nc Cu. The literature data shows a decrease in strain, with an increase in yield strength, with the exception of the consolidated mc Al-10.5 Mg, which was weak in tension. The data from the present study also results in a decrease of ductility with an increase of UTS. This trend appears to be exponential. In Figure 7.2, in which the yield stress was compared with the strain of several studies, a similar behavior is observed.

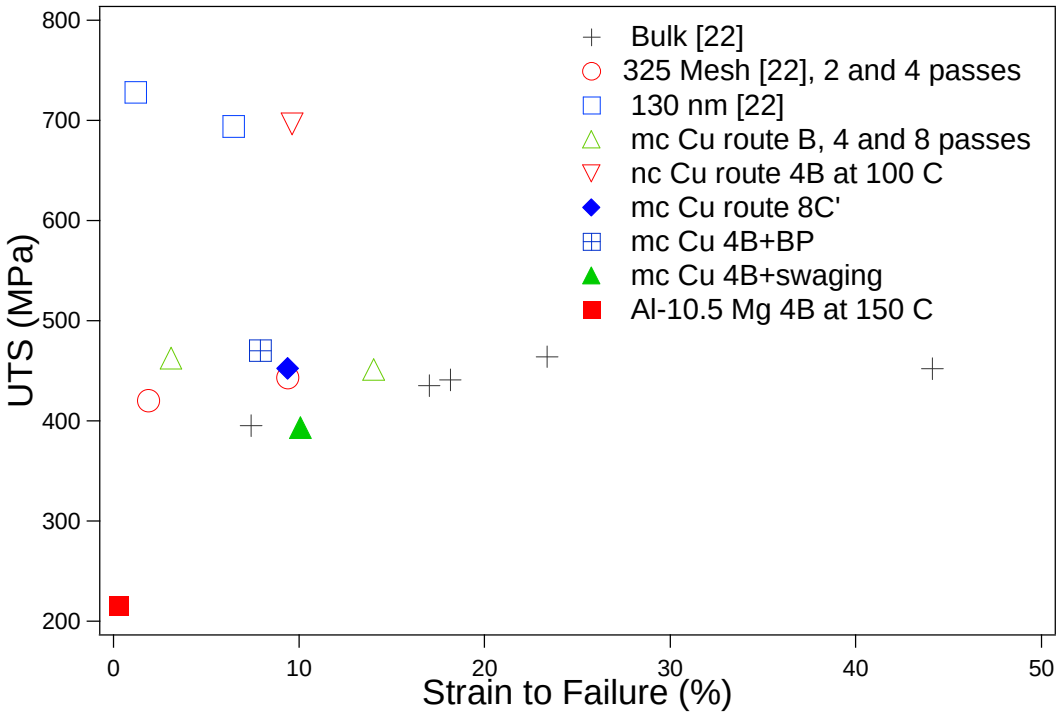

Figure 7.1: UTS vs Elongation to break of ECAEd samples, including nc and mc Cu samples, and results from [22]. The nc CU samples have the highest strength, with low ductility. Bulk Cu has the highest ductility, with relatively low strength. The nc Cu ECAE at 4B at 100 °C has strength equivalent to another nc Cu from [22], but with higher ductility.

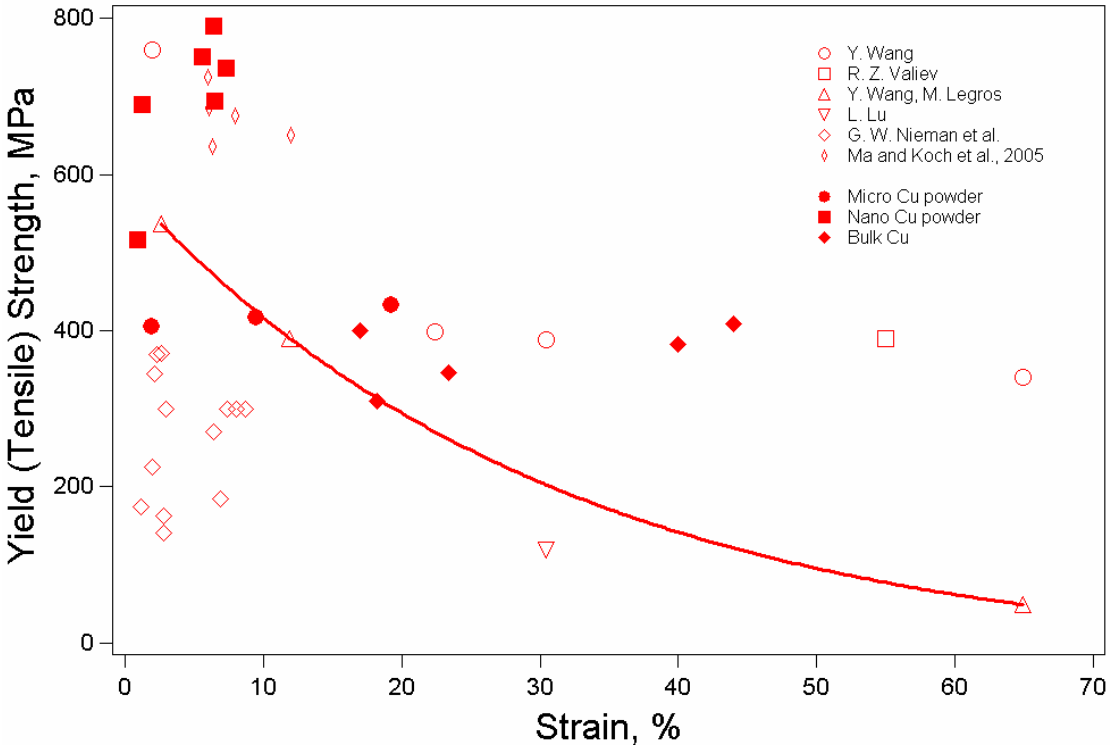

Figure 7.2: Tensile yield strength versus Strain of several experiments [22].

In addition to comparing the strength to the ductility of consolidated samples, the UTS was compared with the number of passes a sample was extruded at, to determine an optimal number of passes. The comparison of UTS to passes is shown in Figure 7.3, and includes data from a previous study [22]. Also, for both the UTS versus ductility and the UTS versus number of passes, the nc Cu are grouped together, with much higher strengths than the mc and bulk Cu. Tension test values of mc Al-10.5 Mg are included in the figures, but the strength and ductility of the Al-10.5 Mg samples are much lower than all of the other samples.

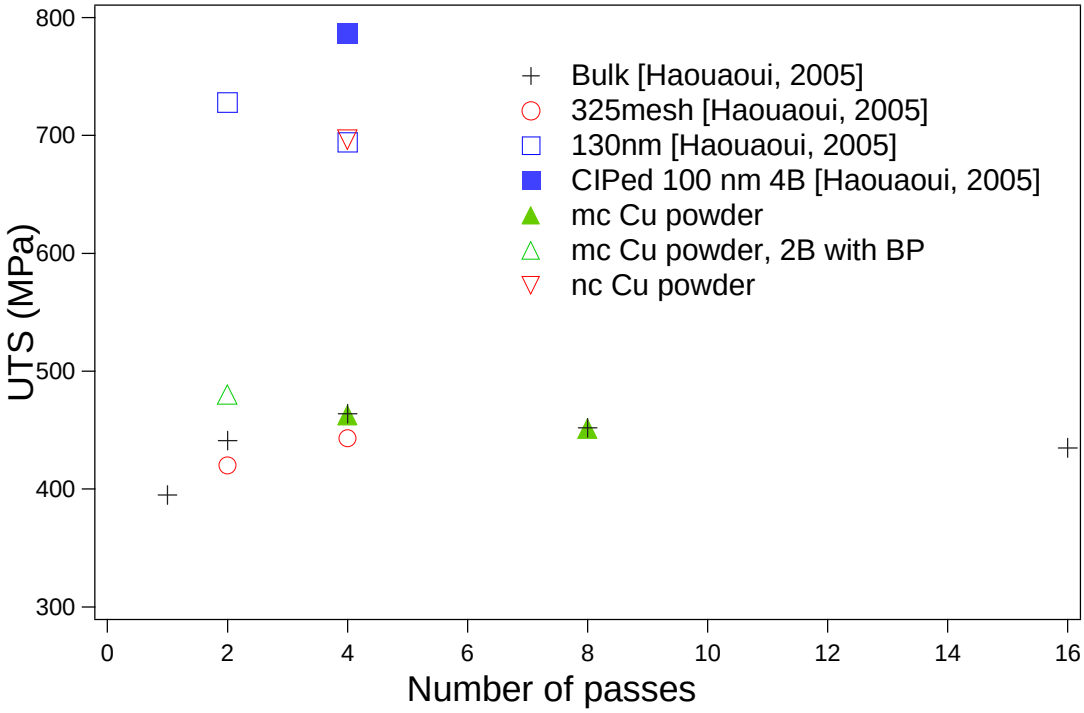

Figure 7.3: Comparison of UTS versus number of passes for route B, including nc and mc Cu samples. For nc Cu at 4 passes, strengths between samples from [22] and the current study are equivalent.

The effect of the number of passes was compared with the strain to failure for the consolidated powder, to determine an optimal number of passes for the best ductility. The comparison is shown in Figure 7.4, which combines data from [22], and the present study. For bulk Cu, the strain to fracture reaches a peak at 8 passes (for route B). For mc Cu consolidated powder, the ductility reaches a maximum at 8 passes (for route B), but we do not know if the ductility will decrease or increase with additional passes, since additional passes were not performed in this study.

For nc Cu, the ductility increased with increasing number of passes, up to four passes. The behavior of the nc Cu with a higher number of passes is not known, since the effect of additional passes were not evaluated. The nc Cu from the current study resulted

in higher ductility than the previous study, which may be due to the elevated extrusion temperature the powder was subjected to.

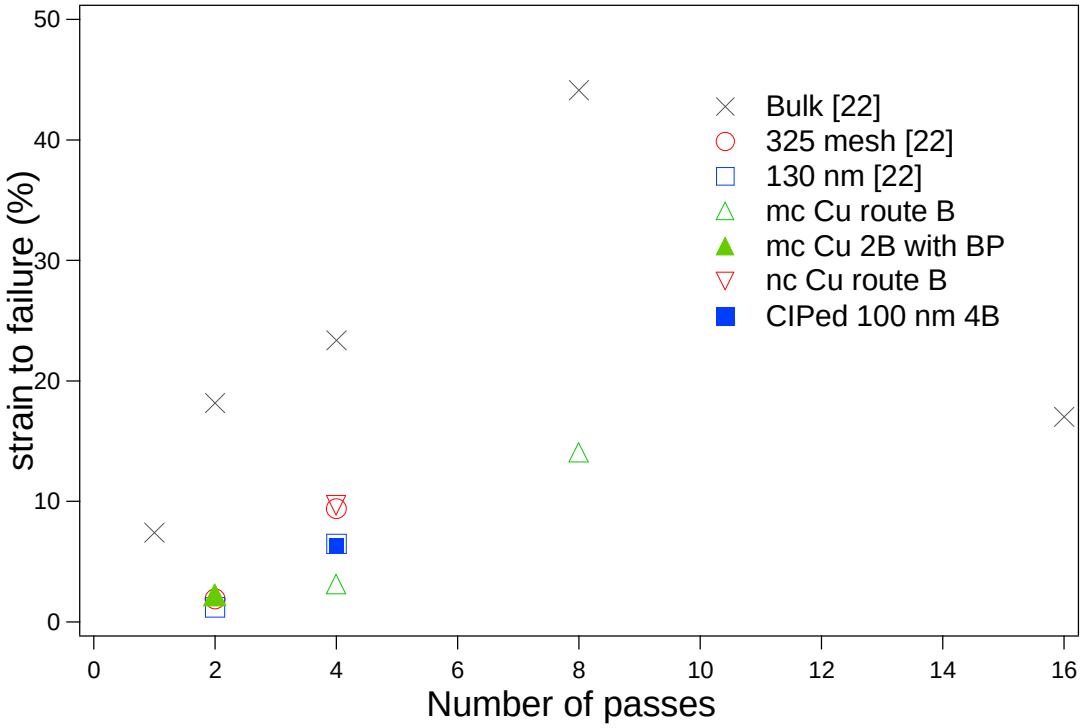

Figure 7.4: Comparison of strain to fracture and number of passes for route B from literature values [22], and for mc and nc Cu results. The nc Cu ECAE at 4B at 100 °C has higher ductility than 4 pass mc Cu. An increase in ductility with increasing number of passes is observed. However, samples from bulk ECAEd Cu indicate that the ductility of the consolidated Cu powder may reach a maximum at 8 passes, if further passes were performed.

VIII. CONCLUSIONS

Bulk ultrafine-grained and nc Cu and nc Al-10.5 Mg alloy were fabricated using ECAE to consolidate powders at relatively low temperatures. The effects of can material and friction conditions were compared with the density and specimen shape predictions from an FEA model. The effects of ECAE route, number of passes, processing temperature, and post-ECAE swaging on the mechanical behavior of microcrystalline and nc materials were explored. It was found that extrusion at elevated temperatures for nc Cu resulted in well compacted samples with higher ductility than nc Cu samples extruded at room temperature. The specific findings are summarized as follows.

1- The use of Ni cans for mc Cu extruded at 1 pass at room temperature resulted in the fewest macroscopic cavities, as compared with samples extruded in a Cu can. This was verified with an FEA using the Duva-Crow constitutive model for powder materials.

2- The microstructure of the consolidated microcrystalline Cu ECAEd at room temperature using one pass consists of large prior particle boundaries, which are elongated along the shear direction, and grain boundaries which exist within the prior particle boundaries. Particles around the cavities deform in an irregular manner, indicating complex deformation states in these regions. Prior particle boundaries and grain boundaries in the mc Cu extruded at room temperature following route 8B could not be revealed using optical microscopy due to the grain refinement, efficient break of surface layer, and sufficient diffusion of Cu leading to fully dense consolidates.

3- The use of back pressure (at 2000 psi) during the ECAE of microcrystalline Cu powder resulted in a strong consolidate, with minor increases (about a 2.5% gain) in ductility. Swaging of an ECAE 4B consolidate resulted in a more ductile sample than the ECAE 4B with BP sample, but with reduced strength of approximately 60 to 70 MPa.

4- Increasing the number of passes for either nc or mc Cu results in a decrease in strength of the material. However, ductility was increased with increasing number of ECAE passes. Additional processing parameters will need to be explored to obtain a combination of high ductility and high strength.

5- Route C' resulted in a stronger, but less ductile sample than route B in mc Cu after 8 passes. The differences in strength between routes B and C are relatively small at only about 5% of the measured values, so it may not be significant to conclude that route C' is stronger than route B. However, the differences in ductility of these routes are approximately 11% of the measured values, and it is probably more reasonable to conclude that route B will result in a more ductile sample.

6- For several mc Cu samples, two profiles were cut, one parallel to the shear plane direction, and one parallel to the extrusion direction. Samples cut parallel to the shear plane exhibited ductility at a strain of 1.5% higher than (a 60% increase of ductility) samples cut in the extrusion direction, with minor losses of strength, depending on the number of passes and route. Cutting tension samples from the shear plane direction is recommended to increase the ductility, while maintaining

comparable strengths, though additional tests will need to be run to determine if this behavior occurs in different routes and number of passes.

7- Tension and compression tests were conducted on the mc Cu samples which were ECAEd at 4B and then swaged. Compression samples resulted in higher strength (by approximately 6%) than the tension samples from the same consolidate ECAEd at 4B and then swaged.

8- The microstructure of nc Cu samples resulted in agglomerates which were easily discernable in optical microscopy, without etching. These agglomerates were elongated in the shear direction, but individual grain boundaries could not be seen in optical microscopy. This is expected, since the starting powder is an average size of 100 nm, which is too small for optical microscopy to resolve.

9- Nanocrystalline samples, which were swaged after 4B ECAE processing, did not yield any useful consolidate. Swaging of nc Cu at room temperature did appear to cause permanent damage in the ECAE consolidated billets.

10- Nanocrystalline Cu powders can be successfully consolidated at 100 °C via ECAE. Temperatures exceeding 100 °C are likely to cause significant grain growth. In addition to producing a well consolidated bulk nc Cu, the elevated extrusion temperature resulted in a more ductile specimen, with minor losses in strength. The ductility of the nc Cu (almost 10%) consolidated at 100 °C was comparable to, and in some cases better than, the mc Cu extruded using the same route and number of passes at room temperatures. However, the strength of the nc Cu (almost 700 MPa) is well above that of the equivalent mc Cu (less than 475

MPa). In fact, this sample has nearly the same strength as a similar sample from [22] extruded at room temperature. This result is promising, since many of the previous nc Cu consolidates exhibited high strength, but ductility lower than that of an equivalent mc Cu sample.

11- Elevated extrusion temperatures to consolidate Al-10.5 Mg powder resulted in a better consolidated sample than samples extruded at room temperature. Also, smoother load-displacement curves during ECAE shows that little or no shear localization occurred during extrusion, which indicates that material failure did not occur during ECAE, increasing the probability of a successful consolidation.

12- Consolidated Al-10.5 Mg samples, ECAEd without back pressure resulted in a high compressive strengths.

13- Al-10.5 Mg samples were extruded at elevated temperatures, and using back pressure. These resulted in low tensile ductility and strength, compared with other Al alloys.

IX. FUTURE RECOMMENDATIONS

9.1 Use of Ultrasonics and Pressing to Compact Powder

Future research to improve the green density of powder compacts should be done, to minimize or eliminate defects such as porosity and agglomeration. Current research in the pharmaceutical industry indicates that the use of ultrasound while pressing powder can increase the green density of a powder compact. Ultrasound is movement in the frequency above human hearing (>18 kHz). The research done in the pharmaceutical industry is driven by the difficulties of compaction of many organic powders into pills [95-98]. A few [99-103] studies have applied ultrasound to the compaction of non-organic powder, such as metals and ceramics. One particular study was made as early as 1967 [104], so the idea of applying ultrasound to compact powders is not a new concept.

The application of ultrasound allows for better compaction of powder because the ultrasonic waves reduce die wall and interparticulate, causing “jarring and vibrating” [95]. A study by Miyata and Oguma [105] found that vibration caused a significant increase in packing densities of several bi-modal size ratios. The most significant increase in relative packing density was achieved for a size ratio of 8. Research on ultrasonic compaction of ibuprofen, which is notoriously difficult to compact, by Levina and Rubinstein [95] found that using ultrasound and pressure at the same time produced the best compaction strength. Levina and Rubinstein [98] found that green density can be increased by as much as 14% by using ultrasound. Tsujino, Ueoka, and Aoki [101] found that increasing the amplitude of the ultrasonic wave increased the density

compaction, irregardless of the length of time spent under compression, for metallic powders. A study on the compaction of metal powders by Dragan and Protopopescu [103] found that the height/ diameter ratio played a significant part on the density gains that ultrasonic pressing can achieve. A height/diameter ratio of 3 is approximately 3 times higher than a h/d ratio of 1 (where the height is equal to the diameter). Also, Dragan and Protopopescu [103] found that the density variation along a compact's relative height was minimal when using ultrasound during compaction, but compaction without ultrasound produced a large decrease with increasing relative height.

9.2 Use of XRCT or XRD

The use of X-ray Computer Tomography (XRCT) in asphalt research provides an interesting insight into particle packing [106, 107]. Currently, XRCT is used for rather large particles (on the macroscopic order), but a new micro XRCT method is being developed. XRCT transmits an X-ray along a 180 degree rotation of a sample (usually round) composed of packed particles. This produces a cross-sectional view of that particular plane. Several cross sections can be taken by indexing the sample up or down by a specified distance.

Several research papers have been written about using XRCT to estimate porosity and powder behavior [105-110]. One particular study by Taud, et al. [108] evaluated the use of XRCT to estimate the porosity of porous media. Farber, et al. [110] used XRCT to study the porosity of granules, and was able to detect pores less than 1 micron in diameter. This technique would be particularly useful in evaluating the efficiency of the consolidation of powder, using non-destructive testing. This would be

particularly useful in determining the effectiveness of processing parameters in consolidating a material into a fully dense material. Additionally, the advantage of knowing the locations of pores in the consolidated material is to be able to extract samples with the lowest concentration of porosity.

9.3 Other Swaging Temperatures and Deformation Ratios

Swaging shows to be a promising method of further compacting powder, to eliminate porosity, and increase compressive ductility. Due to time constraints, higher temperature swaging, and different deformation ratios could not be performed. Future research should explore these two variables, once an optimal route is found for consolidating powders.

9.4 Other Post ECAE Deformation Techniques

Extracted powders can be subjected to further deformation techniques. One possibility is to use wire drawing, to create high strength wire. This can be used in combination with swaging and ECAE.

9.5 Move Degassing Set Up into Glove Box

One of the main issues in preparation of powder that this study has encountered is exposure to atmosphere. While we keep exposure to air minimal, it is necessary in the current set up to get the quartz tube into the vacuum. To eliminate the contact time with air, it is recommended that the vacuum system be routed into the glove box. The following design (Figure 9.1) is proposed to route essential vacuum and sealing equipment into the glove box.

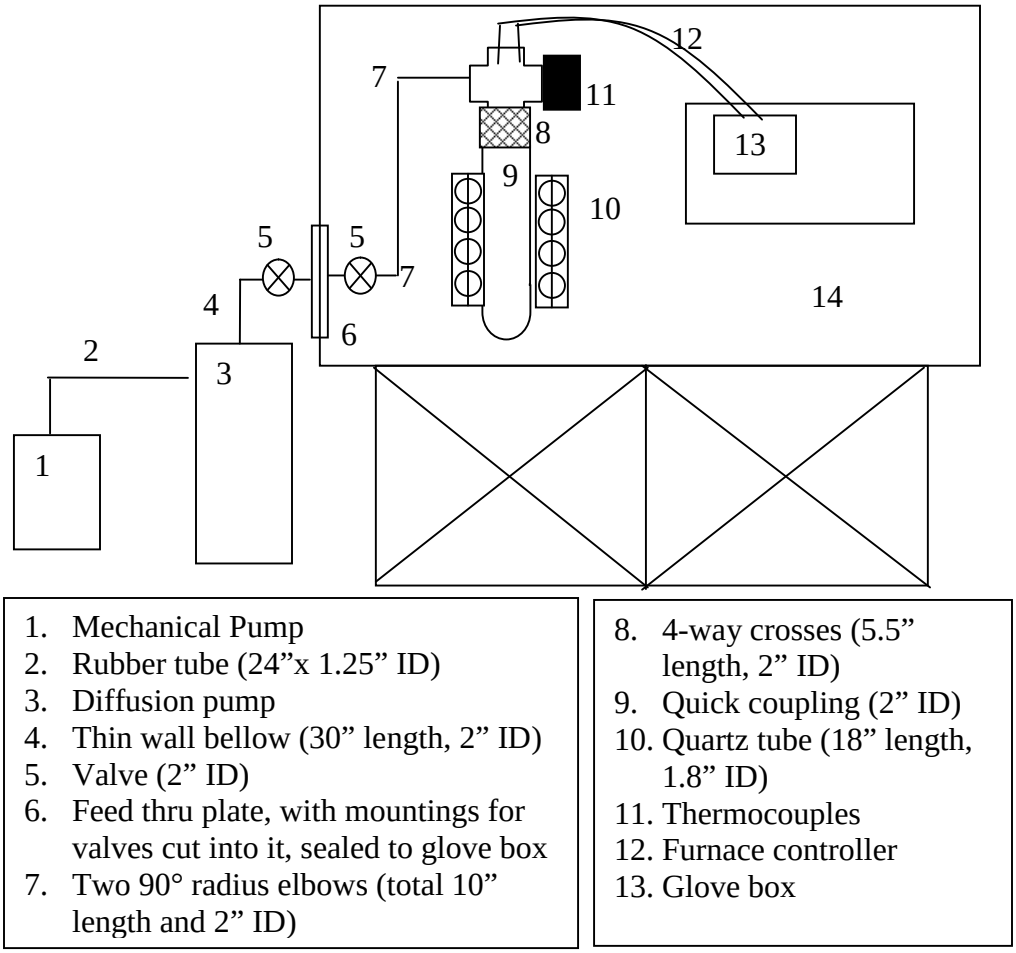

1. Mechanical Pump
2. Rubber tube (24”x 1.25” ID)
3. Diffusion pump
4. Thin wall bellow (30” length, 2” ID)
5. Valve (2” ID)
6. Feed thru plate, with mountings for valves cut into it, sealed to glove box
7. Two 90° radius elbows (total 10” length and 2” ID)
8. 4-way crosses (5.5” length, 2” ID)
9. Quick coupling (2” ID)
10. Quartz tube (18” length, 1.8” ID)
11. Thermocouples
12. Furnace controller
13. Glove box

Figure 9.1: Set up to transfer vacuum system into glove box.

9.6 Other Elevated Extrusion Temperatures for Nanocrystalline Cu

Promising results from elevated temperature nc Cu extrusions indicate that elevated temperatures may be beneficial when extruding nc Cu. Future research should include determining an optimal temperature to extrude nc Cu at to maintain strength, and further enhance ductility.

REFERENCES

[1] Li XW, Umakoshi Y, Wu SD, Wang ZG, Alexandrov IV, Valiev RZ. Phys. Stat. Sol(a), 2004; 201-15: R119

[2] Lukas P, Kunz L, Svoboda M. Mat Sci Eng A- Struct, 2005; 391: 337

[3] Vinogradov A, Miyamoto H, Mimaki T, Hashimoto S. Ann. Chim. Sci. Mat., 2002; 27-3: 65

[4] Hoppel HW, Valiev RZ. Z. Metallkd, 2002; 93: 641

[5] Li XW, Wu SD, Wu Y, Yasuda HY, Umakoshi Y. Mater Trans, 2005; 46-12: 3077

[6] Vinogradov A, Ishida T, Kitagawa K, Kopylov VI. Acta Mater , 2005; 53: 2181

[7] Mughrabi H, Hoppel HW, Kautz M. Scripta Mater, 2004; 51: 807

[8] Li XW, Wu SD, Wu Y, Yasuda HY, Umakoshi Y. Adv Eng Mater, 2005; 7-9: 829

[9] Wu SD, Wang ZG, Jiang CB, Li GY, Alexandrov IV, Valiev RZ. Scripta Mater, 2003; 48: 1605

[10] Furukawa M, Horita Z, Nemoto M, Langdon TG. J Mater Sci, 2001; 36: 2835

[11] Vinogradov A, Suzuki T, Hashimoto S, Kitagawa K, Kunzentsov A, Dobatkin S. Mater Sci Forum, 2006; 203-504: 971

[12] Huang CX, Wang SC, Wu SD, Jiang CB, Li GY, Li SX. Mater Sci Forum, 2005; 475-479: 4055

[13] Alexandrov IV, Zhu YT, Lowe TC, Islamgaliev RK, Valiev RZ. NanoStructured Materials, 1998; 10-1: 45

[14] Valiev RZ, Islamgaliev RK, Alexnadrov IV. Prog Mater Sci, 2000; 45: 103

[15] Yapici GG, Karaman I, Luo ZP, Maier HJ, Chumlyakov YI. J Mater Res, 2004, 19, 2268

[16] Yapici GG, Karaman I, Luo ZP, Rack H. Scripta Mater, 2003; 49: 1021

[17] Xia K, Wu X. Scripta Mater, 2005; 53: 1225

[18] Haouaoui M, Karaman I, Maier HJ, Hartwig KT. Metall Mater Trans A, 2004; 35A: 2935

[19] Zhu YT, Lowe TC, Langdon TG. Scripta Mater, 2004; 51: 825

[20] Agnew SR, Elliott BR, Youngdahl CJ, Hemker KJ, Weertman JR. Mat Sci Eng A-Struct, 2000; A285: 391

[21] Karaman I, Haouaoui M, Maier HJ. J Mater Sci, 2007, 42, 1561

[22] Haouaoui M. PhD thesis, Texas A&M University, 2005

[23] Furukawa M, Horita Z, Nemoto M, Langdon TG. Mat Sci Eng, 2002; A324: 82

[24] Botta Filho WJ, Fogagnolo JB, Rodriguez CAD, Kiminami CS, Bolfarini C, Yavari AR. Mat Sci Eng A- Struct, 2004; 375-377: 936

[25] Lee Z, Zhou F, Valiev RZ, Lavernia EJ, Nutt SR. Scripta Mater, 2004; 51: 209

[26] Yavari AR, Botta Filho WJ, Rodriguez CAD, Cardoso C, Valiev RZ. Scripta Mater, 2002; 46: 711

[27] Kawamura Y, Mano H, Inoue A. Scripta Mater, 2001; 44: 1599

[28] Billard S, Fondere JP, Bacroix B, Dirras GF. Acta Mater , 2006; 54: 411

[29] Purcek G, Altan BS, Miskioglu I, Patil A. Mater Sci Tech Ser, 2005; 2 1-9: 1044

[30] Ferrasse S, Segal VM, Kalidindi SR, Alford F. Mat Sci Eng A- Struct, 2004; A368: 28

[31] Yoon CY, Kim HS. Mater Sci Forum, 2006; 503-504: 221

[32] Kim HS, Seo MH, Oh CS, Kim SJ. Mater Sci Forum, 2003; 437-43 8: 89

[33] Wu X, Xia K. Mater Sci Forum, 2006; 519-521: 1215

[34] Horita Z, Fujinami T, Nemoto M, Langdon TG. J Mater Process Tech, 2001; 117: 288

[35] Vinogradov A, Washikita A, Kitagawa K, Kopylov VI. Mater Sci Eng, 2003; A349: 318

[36] Kusnierz J. Mater Sci Forum, 2003; 426-432: 2807

[37] Zhilyaev AP, Oh-ishi K, Raab GI, McNelley TR. Mat Sci Eng A- Struct, 2006; A441: 245

[38] Kaushig A, Srinivasa A. Int J Plasticity, 2007; (To be published)

[39] Segal VM. Mat Sci Eng A- Struct, 1995; A197: 157

[40] Maier HJ, Gabor P, Karaman I. Mat Sci Eng A- Struct, 2005; 410-411: 457

[41] Maier HJ, Gabor P, Gupta N, Karaman I, Haouaoui M. Int J Fatigue, 2006; 28: 243

[42] Agnew SR, Weertman JR. Mat Sci Eng A- Struct, 1998; 244: 145

[43] Gabor P, Maier HJ, Karaman I. Proceedings of the 16th European Conference on Fracture: Failure analysis of nano and engineering materials and structures, July 2006

[44] Kumar KS, Van Swygenhoven H, Suresh S. Acta Mater, 2003; 51: 5743

[45] Siow KS, Tay AAO, Oruganti P. Mater Sci Tech Ser, 2004; 20: 285

[46] Gleiter H. Acta Mater, 2000; 48: 1

[47] Chokshi AH, Rosen A, Karch J, Glieter H. Scripta Mater, 1989; 23: 1679

[48] Campion Y, Lanlois C, Guerin-Mailly S, Langlois P, Bonnentien J, Hytch MJ. Science, 2003; 300: 310

[49] Conrad H. Mat Sci Eng A- Struct, 2003; A341: 216

[50] Hansen N, Ralph B. Acta Mater, 1982; 30: 411

[51] Yip S. Nature, 1998; 391: 532

[52] Carsley JE, Fisher A, Milligan WW, Aifantis EC. Metall Mater Trans A, 1998; 29A: 2261

[53] Armstrong RW. Appl Sci, 1983;1

[54] Cai B, Kong QP, Lu L, Lu K. Scripta Mater, 1999; 41-7: 755

[55] Schiotz J, Di Tolla FD, Jacobsen KW. Nature, 1998; 391: 561

[56] Conrad H, Narayan J. Scripta Mater, 2000; 42: 1025

[57] Witkin DB, Lavernia EJ. Prog Mater Sci, 2006; 51: 1

[58] Champion Y, Guerin-Mailly S, Bonnentien JL, Langlois P. Scripta Mater, 2001; 44: 1609

[59] Ebrahimi F, Zhai Q, Kong D. Scripta Mater, 1998; 39-3: 315

[60] Yapici GG, Karaman I, Luo ZP. UFG III The proceedings of the third international symposium on Ultra Fine Grained materials, TMS 2004 Annual meeting, 2004, Charlotte, NC, 433

[61] Robertson J, Im JT, Karaman I, Hartwig KT, Anderson IE. J Non-cryst Solids, 2003; 317: 144

[62] Langlois C, Hytch MJ, Langlois P, Lartigue-Korinek S, Champion Y. Metall Mater Trans A, 2005; 36A: 3451

[63] Lin YJ, Lavernia EJ. Metall Mater Trans A, 2006; 37A: 3317

[64] Xu J, McMeeking RM. Int J Mech Sci, 1992; 43-2: 167

[65] Kawamura Y, Inoue A, Kojima A, Masumoto T. J Appl Phys, 1994; 76 (9): 5545

[66] Segal VM. Sc D Thesis, Minsk, Russia, Physical-Technical Research Institute of the NASB, 1974

[67] Furukawa M, Iwahashi Y, Horita Z, Nemoto M, Langdon TG. Mat Sci Eng A-Struct, 1998; A257: 328

[68] Gibbs MA, Hartwig KT, Cornwell LR, Goforth RE, Payzant EA. Scripta Mater, 1998; 39-12: 1699

[69] Karaman I, Yapici GG, Chumlyakov YI, Kireeva IV. Mat Sci Eng A- Struct, 2005; 410-411: 243

[70] Karaman I, Kulkarni AV, Luo ZP. Philos Mag, 2005; 85-16: 1729

[71] Barber RE, Dudo T, Yasskin PB, Hartwig KT. Scripta Mater, 2004; 51: 373

[72] Ferrasse S, Segal VM, Alford F. Mat Sci Eng A- Struct, 2004; A372: 235

[73] Park KT, Kim YS, Shin DH. Metall Mater Trans A, 2001; 32A: 2373

[74] Furukawa M, Horita Z, Nemoto M, Langdon TG. Mater Sci Tech Ser, 2000; 16: 1330

[75] Shin DH, Park KT. Mat Sci Eng A- Struct, 2005; 410-411: 299

[76] Gubicza J, Balogh L, Hellmig RJ, Estrin Y, Ungar T. Mat Sci Eng A- Struct, 2005; 400-401: 334

[77] Zhilyaev AP, Nurislamova GZ, Baro MD, Valiev RZ, Langdon TG. Metall Mater Trans A, 2002; 33A: 1865

[78] Banghong H. SIMTech Technical report (PT/02/039/FT), Singapore Institute of Manufacturing Technology, 2002, Singapore

[79] Segal VM. Mat Sci Eng A- Struct, 2004; A386: 269

[80] Nagasekhar AV, Tick-Hon Y, Li S, Seow HP. Mat Sci Eng A- Struct, 2006; 423: 143

[81] Wu Y, Baker I. Scripta Mater, 1997; 37-4: 437

[82] Segal VM. Mat Sci Eng A- Struct, 1999; A271: 322

[83] Segal VM. Mat Sci Eng A- Struct, 2003; A345: 36

[84] Cui HJ, Goforth RE, Hartwig KT. JOM-US, 1998; 50-8

[85] Chinh NQ, Horvath G, Horita Z, Langdon TG. Acta Mater, 2004; 52: 3555

[86] Guo Z, Solas D, Etter AL, Baudin T, Penelle R. Mater Sci Forum, 2003; 426-432: 2723

[87] Vinogradov A, Patlan V, Suzuki Y, Kitagawa K, Kopylov VI. Acta Mater, 2002; 50: 1639

[88] Beyerlein, IJ, Li S, Alexander DJ. Mat Sci Eng A- Struct, 2005; 410-411: 201

[89] Cabibbo M, Evangelista E, Latini V. J Mater Sci, 2004; 39: 5659

[90] Jia D, Ramesh KT, Ma E, Lu L, Lu K. Scripta Mater, 2001; 45: 613

[91] ASM International. Metals Handbook 10th edition, Volume 9: Metallography and microstructures, 1990, Materials Park, OH, 709

[92] Han BQ, Ye J, Tang F, Schoenung J, Lavernia EJ. J Mater Sci, 2007; 42: 1660

[93] ASM International. Metals Handbook 10th edition Volume 2: Properties and selection: Nonferrous alloys and special-purpose materials, Materials Park, OH, 1990

[94] Fan GJ, Choo H, Liaw PK, Lavernia EJ. Acta Mater, 2006; 54: 1759

[95] Levina M, Rubinstein MH, Rajabi-Siahboomi AR. Pharm res, 2000; 17-3: 257

[96] Rodriguez L, Cini M, Cavallari C, Passerini N, Saettone MF, Fini A. Tnt J Pharm, 1998; 170: 201

[97] Levina M, Rubinstein MH. J Pharm Sci, 2000; 89: 705

[98] Levina M, Rubinstein MH. Drug Dev Ind Pharm, 2002; 28-5: 495

[99] Kromp W. Powder Metall Tnt, 1985; 17-5: 219

[100] Nam J, Lannutti JJ. J Am Ceram Soc, 2002; 87-4: 557

[101] Tsujino J, Ueoka T, Aoki S. Ultrasonics International, 1981; 81: 313

[102] Siwkiewicz Z, Stolarz S. Powder Metall Tnt, 1986; 18

[103] Dragan O, Protopopescu A. Proceedings of the 1st symposium on High power ultrasonics (IPC Science and Technology Press), 1972, 109

[104] Lehfeldt E. Ultrasonics , 1967; October: 219

[105] Miyata M, Oguma M. J Ceram Soc Jpn, 2000; 108: 656

[106] Masad E, Saadeh S, Al-Rousan T, Garboczi E, Little D. Comp Mater Sci, 2005; 34: 406

[107] Masad E, Jandhyala VK, Dasgupta N, Somadevan N, Shashidhar N, . J Mater Civil Eng, 2002;122

[108] Taud H, Martinez-Angeles R, Parrot JF, Hernandez- Escobedo L. J Petrol Sci Eng, 2005; 47: 209

[109] Yang CY, Fu XY. Powder Technol, 2005; 146: 10

[110] Farber L, Tardos G, Michaels JN. Powder Technol, 2003; 132: 5

APPENDIX A. X-RAY IMAGES OF CANS CONSOLIDATED VIA ECAE

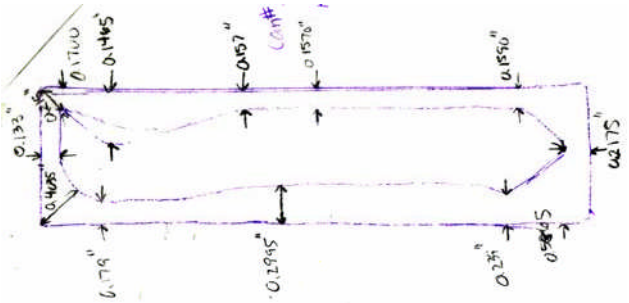

Figure A. 1: Case A2: Al 10.5 Mg 4B 150 C gamma-ray image, showing powder locations in the billet.

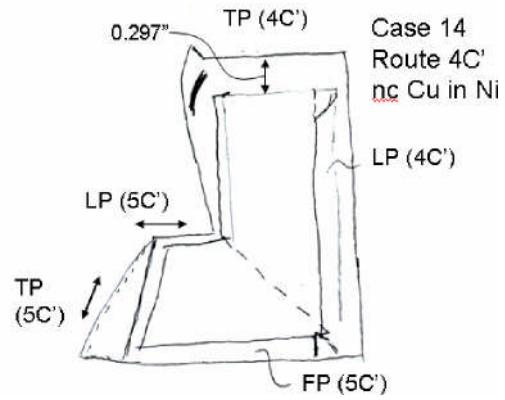

Figure A.2: Case 14 nc Cu 4C' at RT (Could not complete 8C') X-ray image, showing powder location in the Ni can.

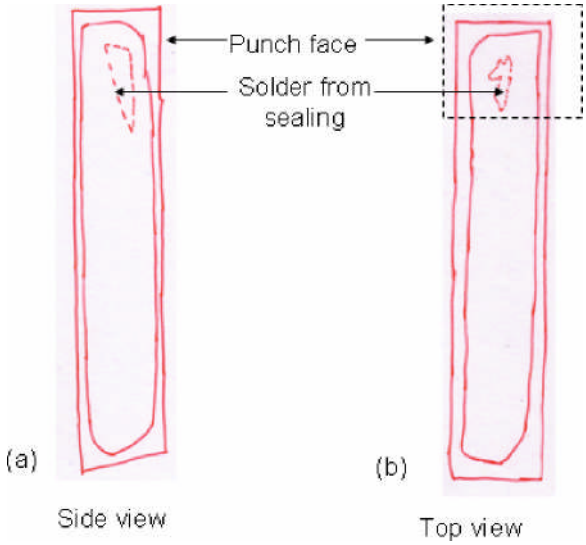

Figure A.3: Case 17 nc Cu 4B 100 °C, showing powder location in the Ni can and solder in cap from sealing, from (a) Side view, and (b) Top view.

APPENDIX B. LOAD-DISPLACEMENT GRAPHS

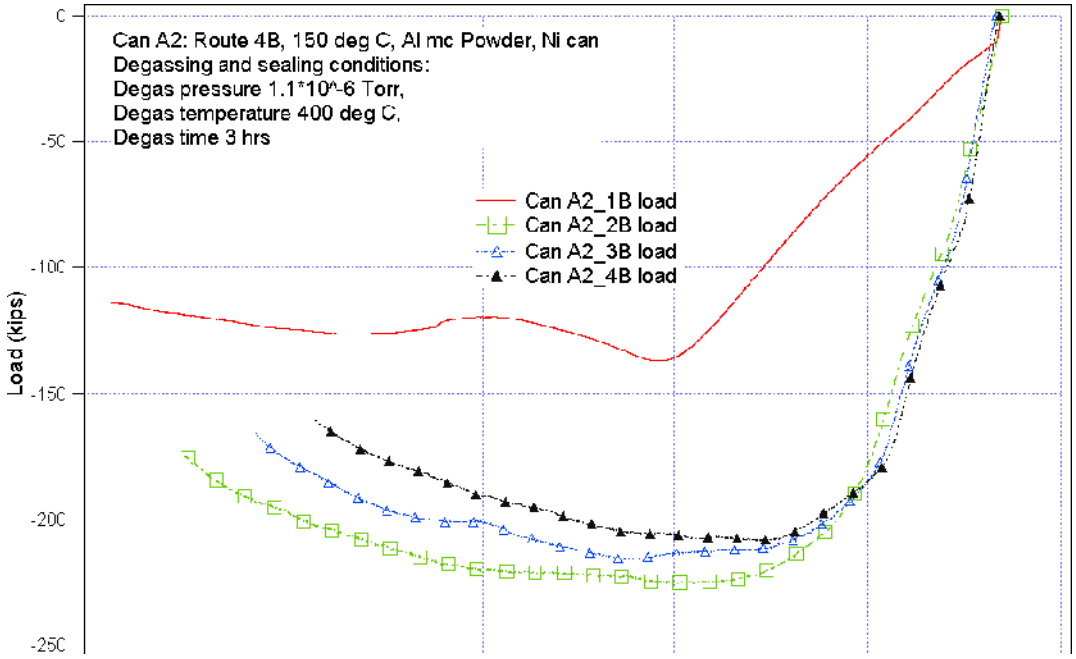

Figure B.1: Load-displacement graph of case A2, 4B 150 C Al mc Powder

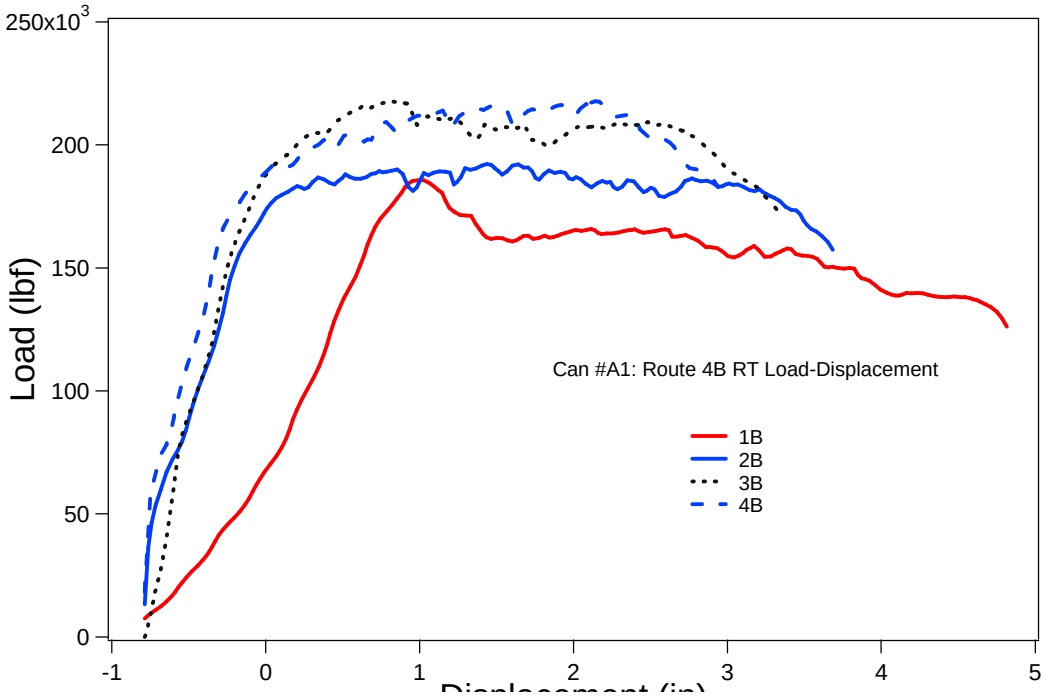

Figure B.2: Load-displacement graph of case A2, 4B 150 C Al mc Powder

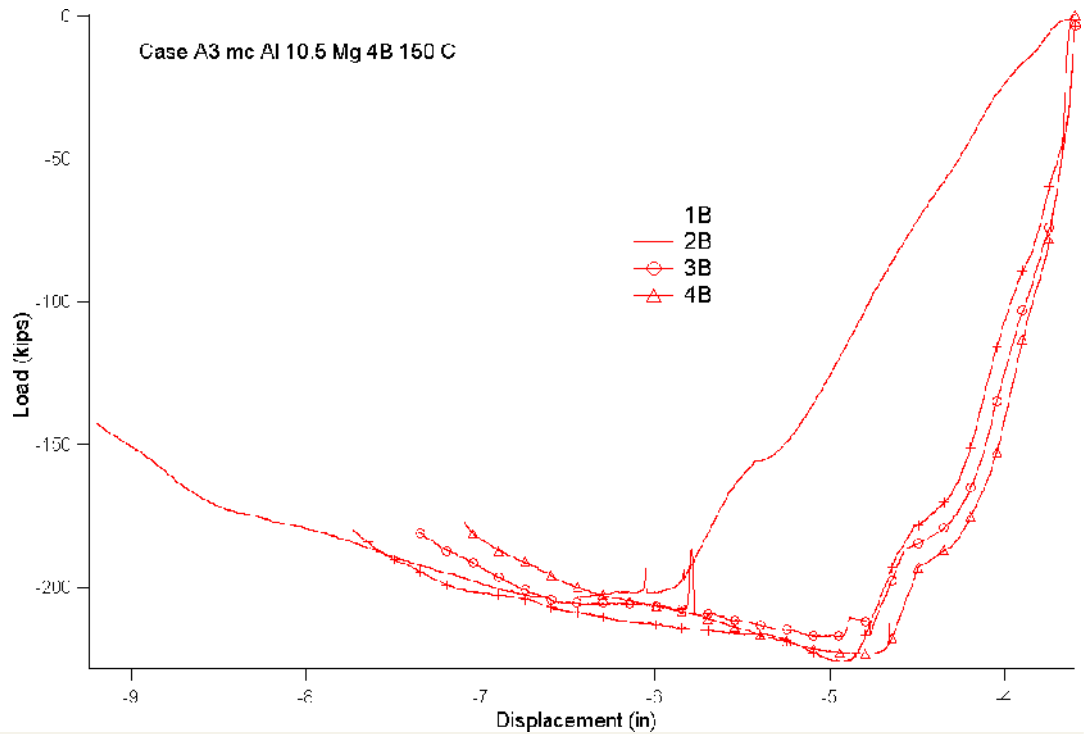

Figure B.3: Case A3 mc Al 10.5 Mg 4B+BP 150 C load-displacement graph Load-displacement curves for nanocrystalline Cu:

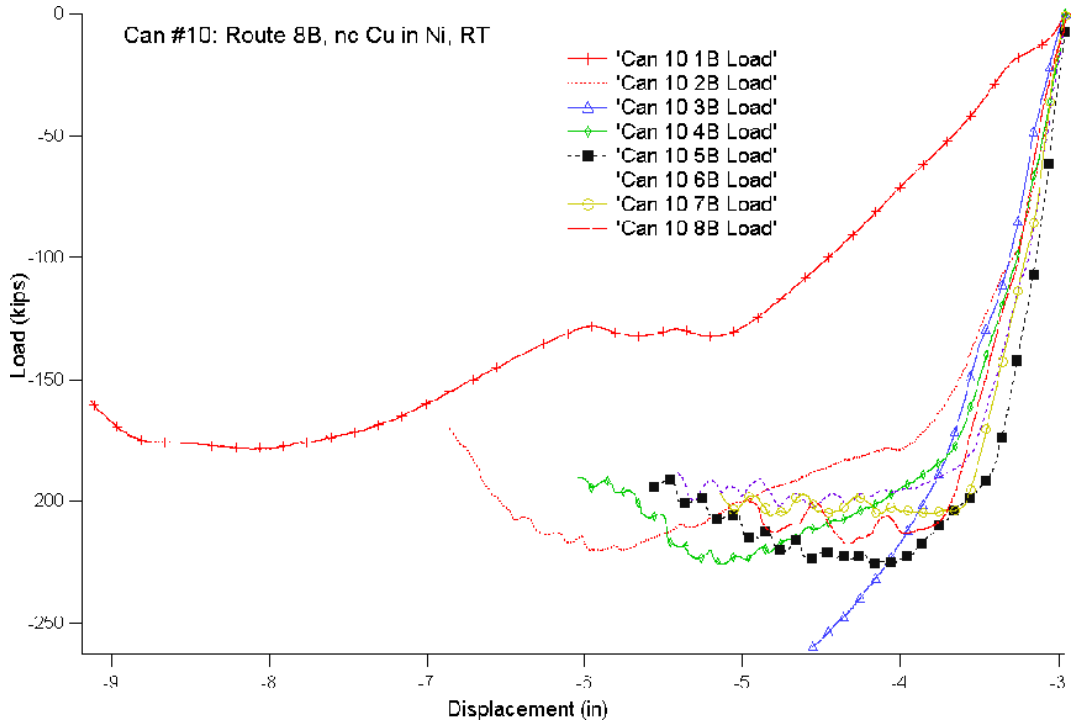

Figure B.4: Load displacement of Case 10 nc Cu 8B RT

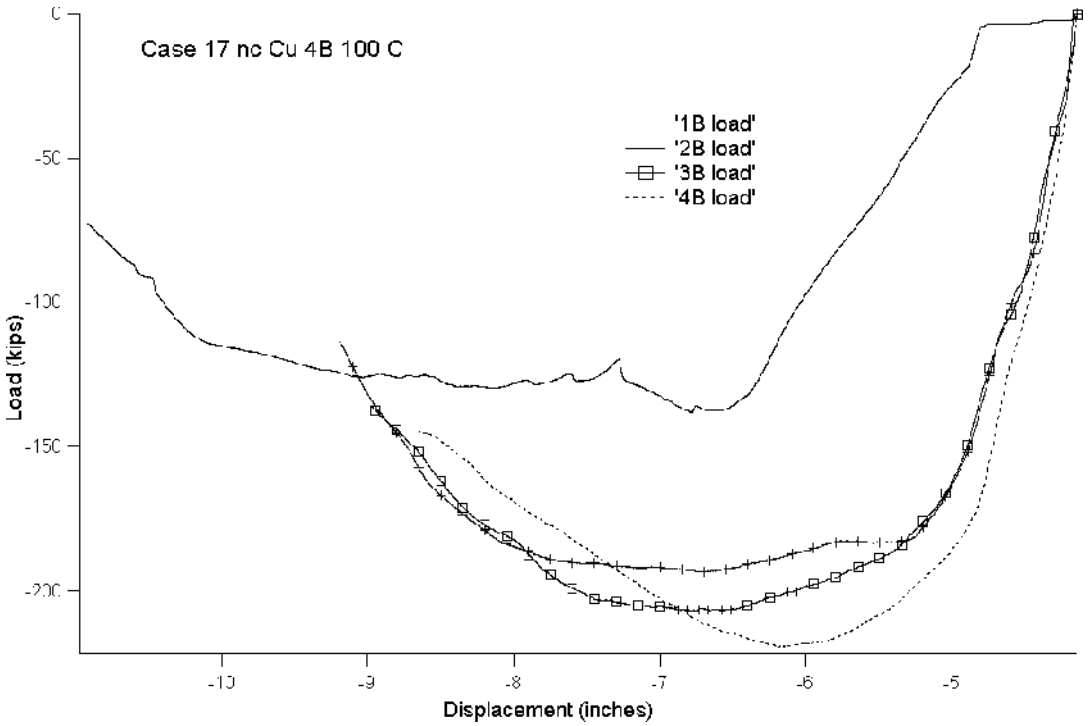

Figure B.5: Case 13 nc Cu 4B 100 C load-displacement graph

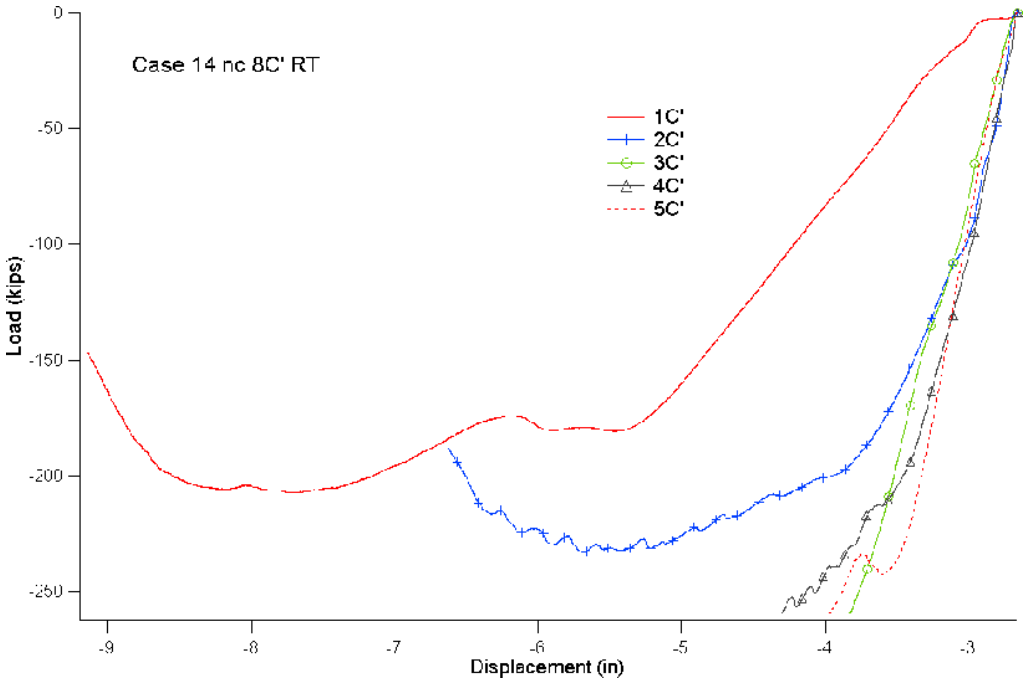

Figure B.6: Case 14 nc Cu 8C' RT load-displacement graph (only went to 5C' before the press was maxed out)

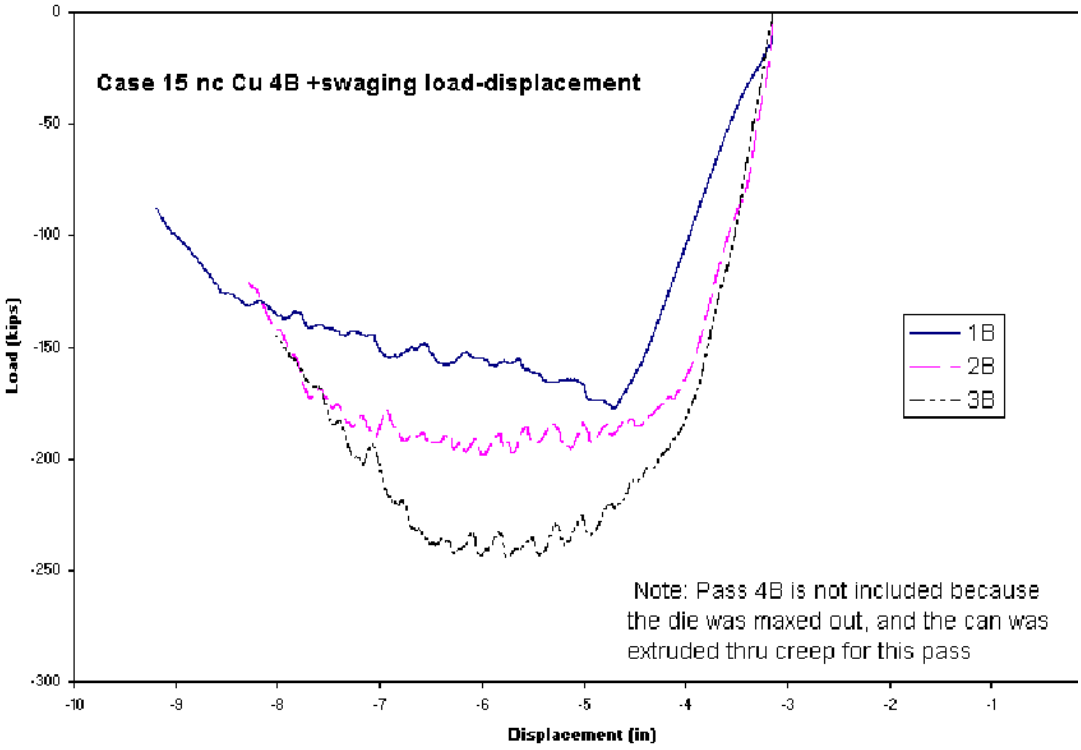

Figure B.7: Load displacement Case 15 nc Cu 4B+swaging RT

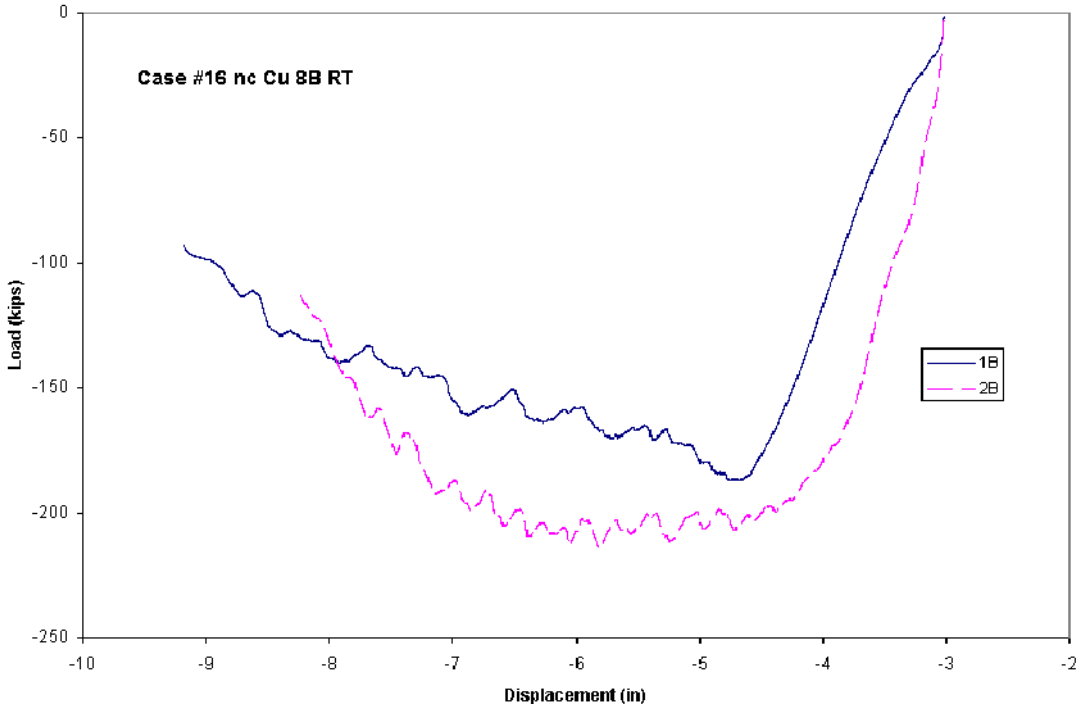

Figure B.8: Case 16 nc Cu 8B RT load displacement graph (only completed 2 passes, can maxed out press at third pass).

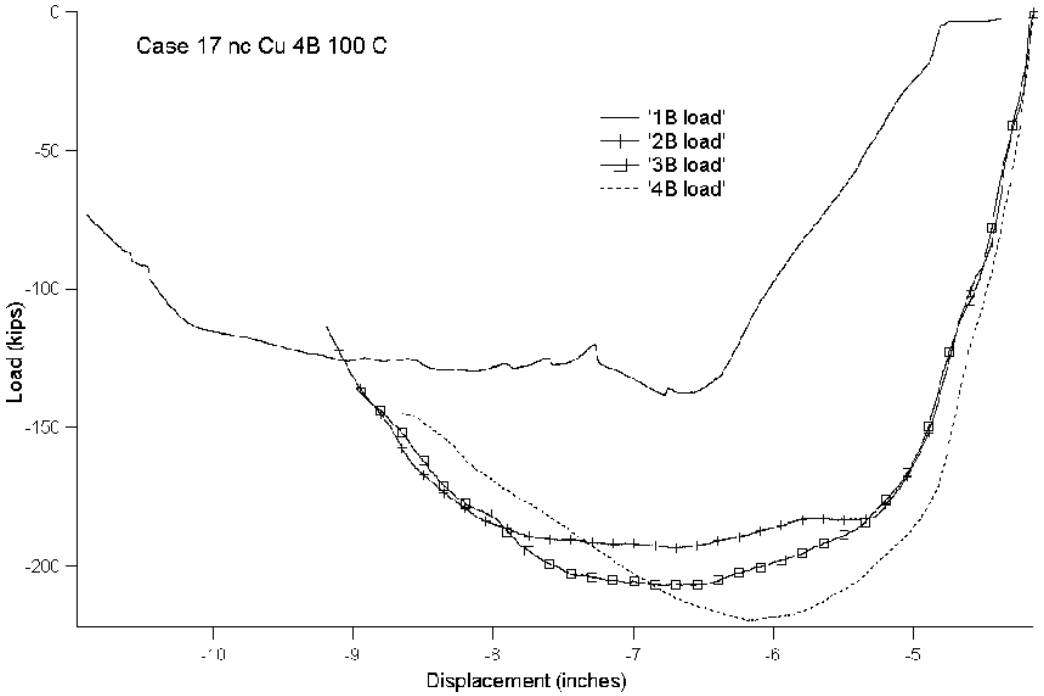

Figure B.9: Load displacement Case 17 nc Cu 4B 100 C

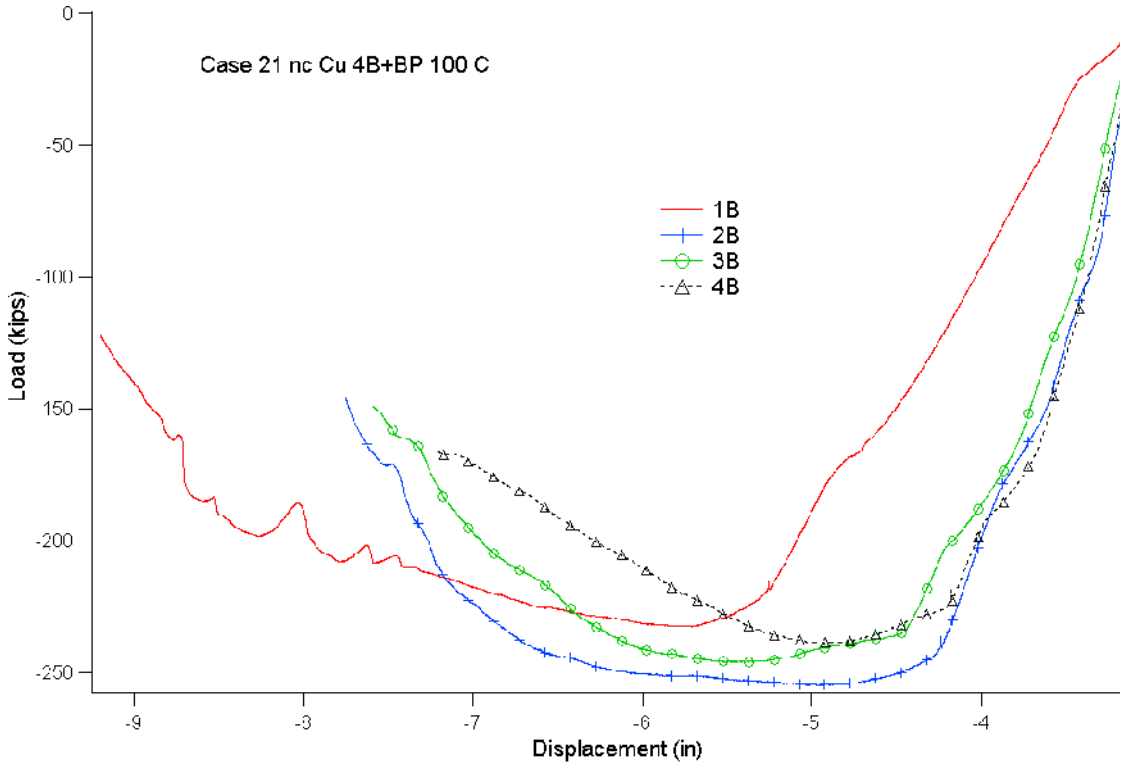

Figure B.11: Case 21 nc Cu 4B+BP 100 C load displacement

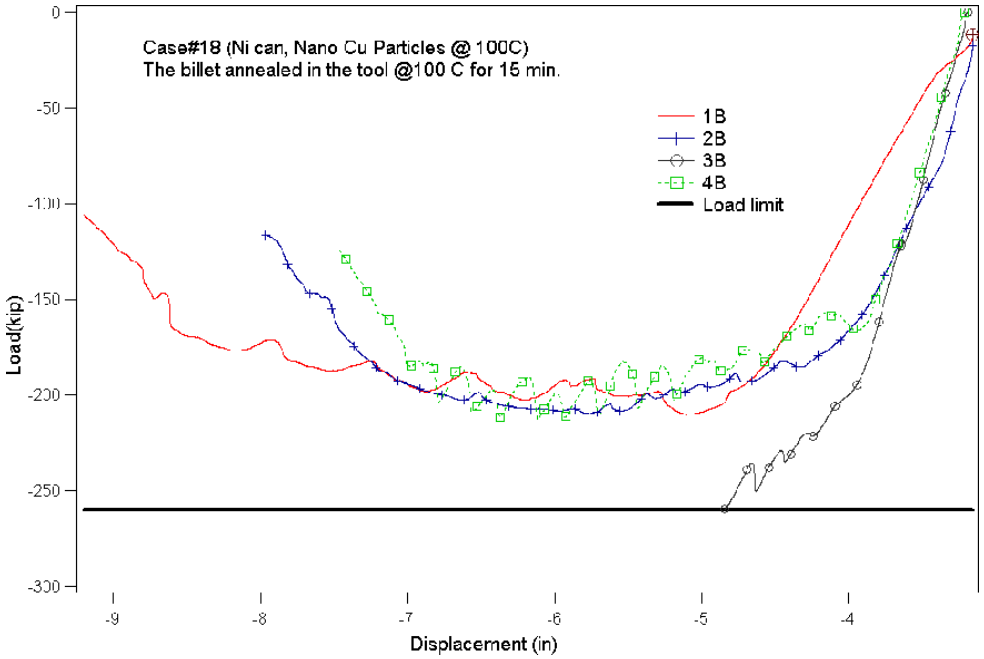

Figure B.10: Load displacement for Case 18 nc Cu 4B, 2 passes at 100 C, 2 passes at RT

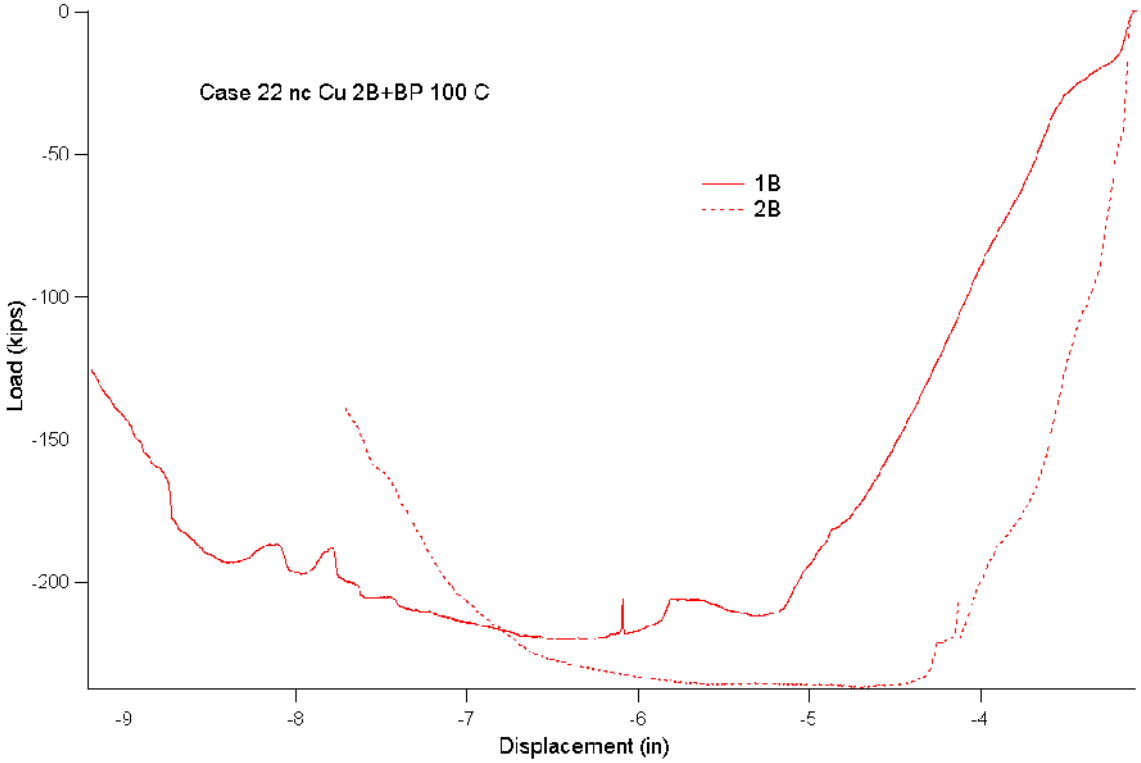

Figure B.12: Case 22 nc Cu 2B+BP 100 C load displacement graph

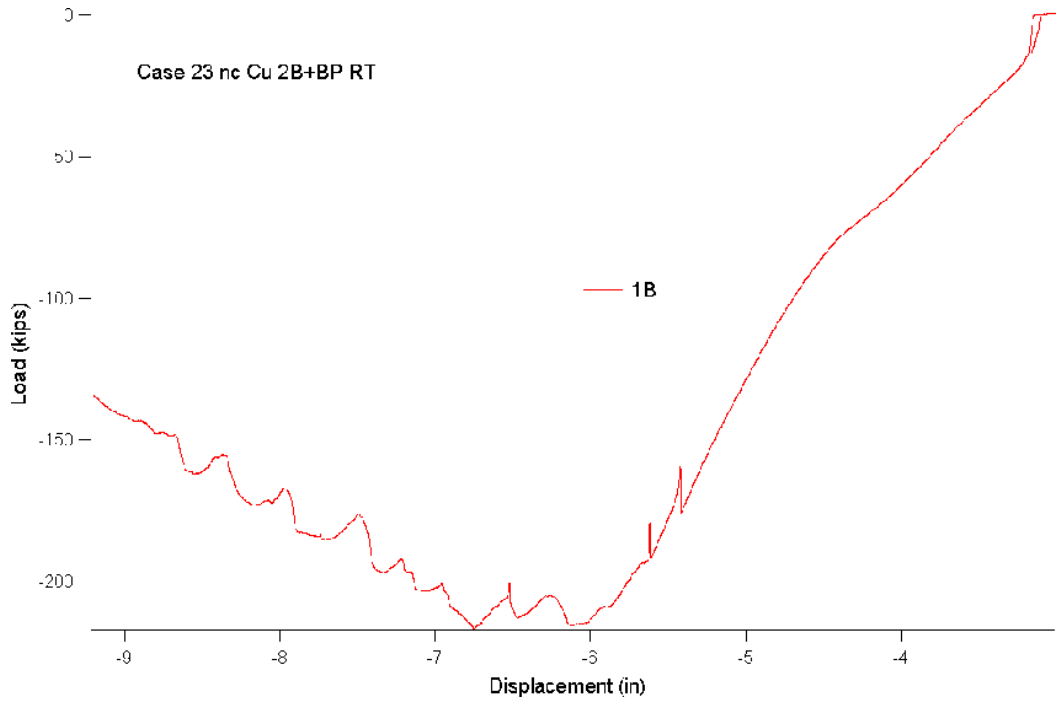

Figure B.13: Case 23 nc Cu 2B+BP RT load displacement graph Load-displacement curves of microcrystalline Cu:

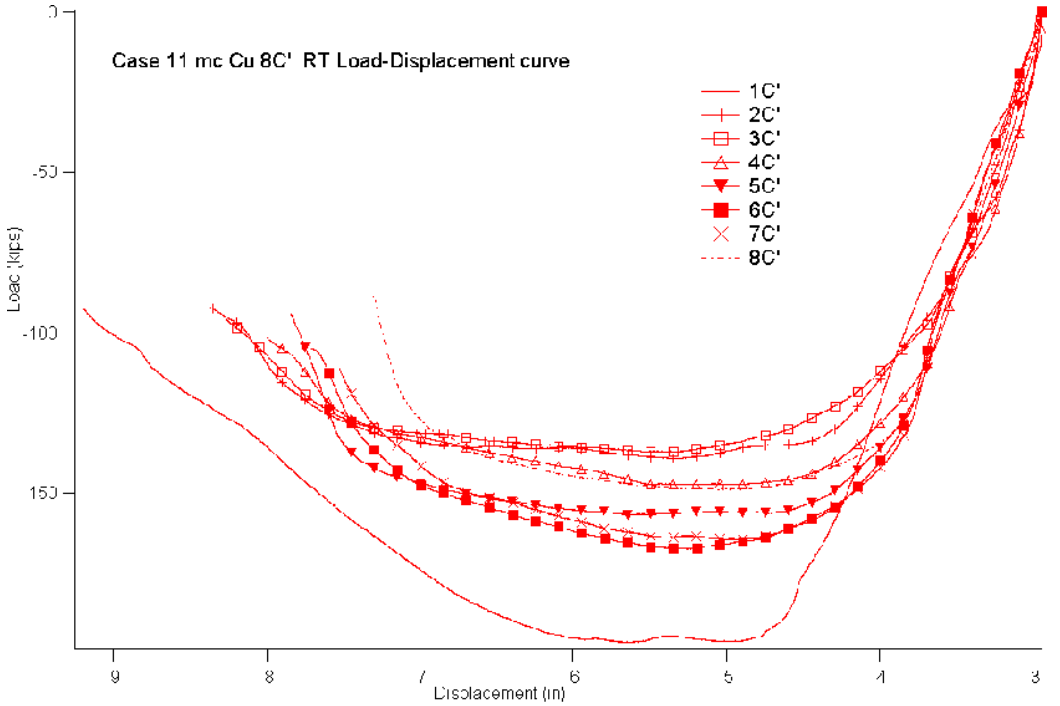

Figure B.14: Case #11 mc Cu 8C' RT load displacement graph

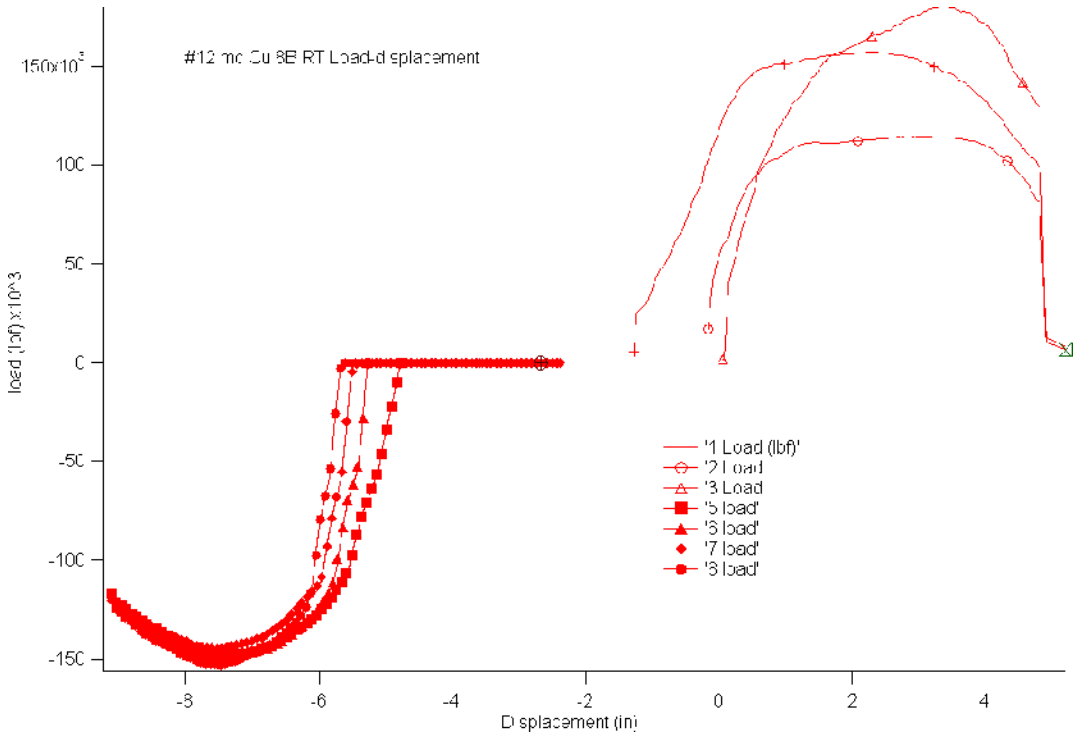

Figure B.15: Case 12 mc Cu 8B RT load displacement graph

Note: The graphs are in two different directions, since halfway thru the ECAE routes, the sensor was upgraded, and the new sensor measured downward movement as negative displacement, and downward force as negative force (used for routes 5-8)

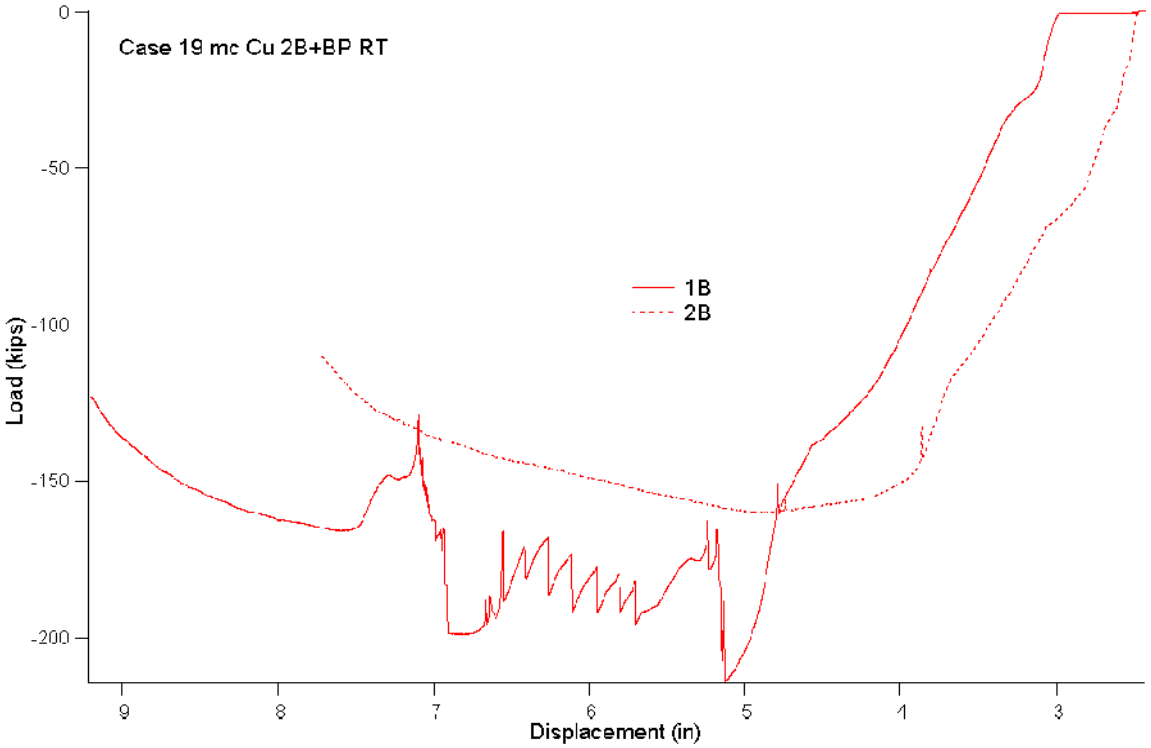

Figure B.16: Load displacement Case 16 mc Cu 2B+BP RT

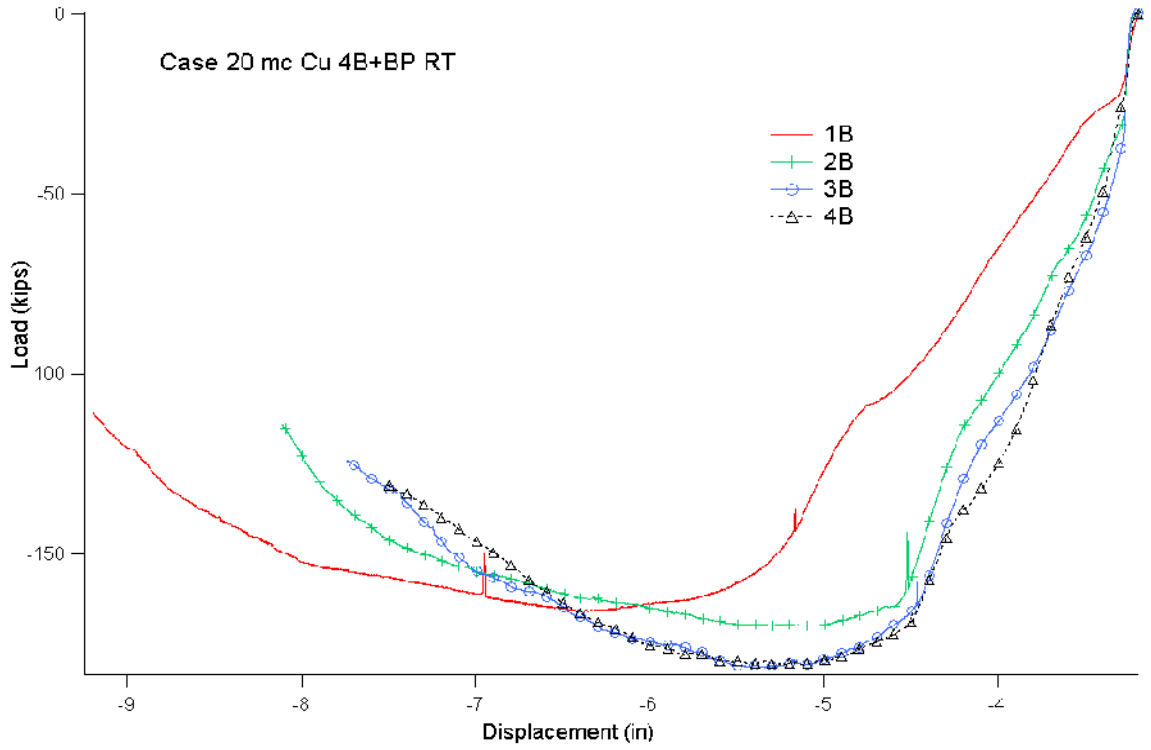

Figure B.17: Load displacement Case 20 mc Cu 4B+BP RT

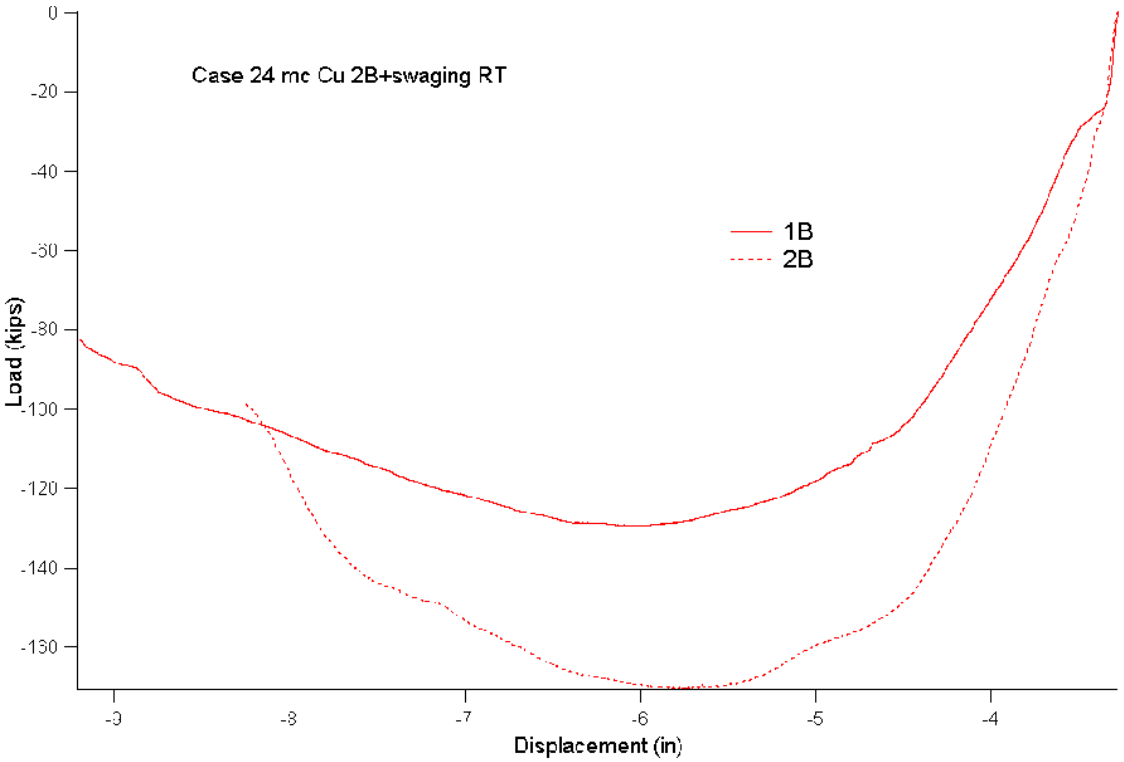

Figure B.18: Load displacement Case 24a mc Cu 2B+swaging RT (and 24b 2B RT)

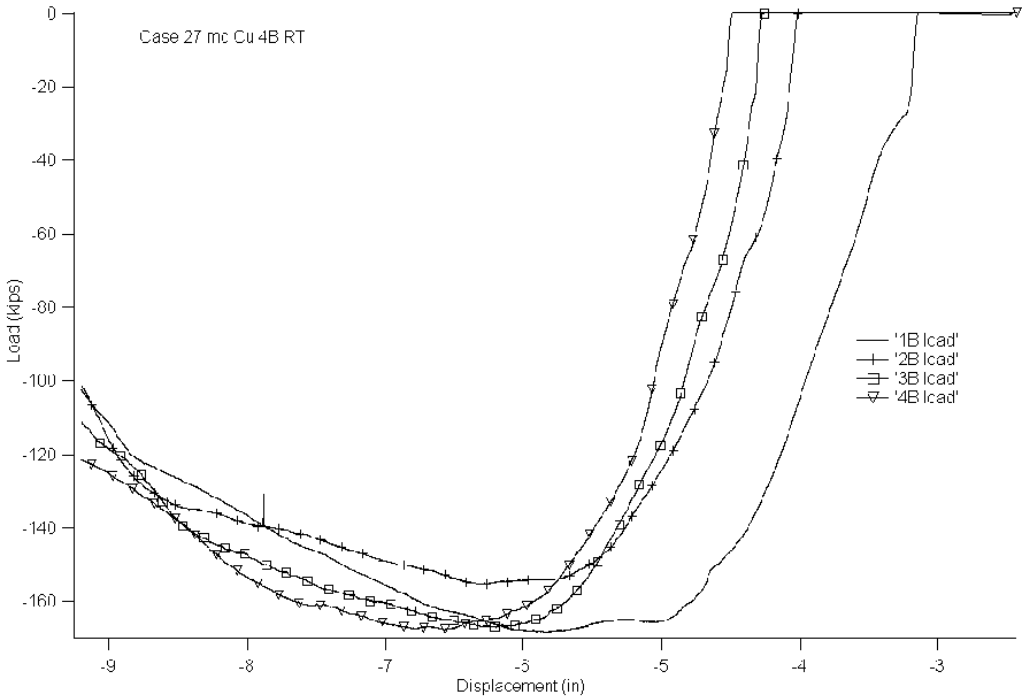

Figure B.19: Load displacement Case 27 mc Cu 4B RT

APPENDIX C. OPTICAL IMAGES OF MICROCRYSTALLINE MATERIAL

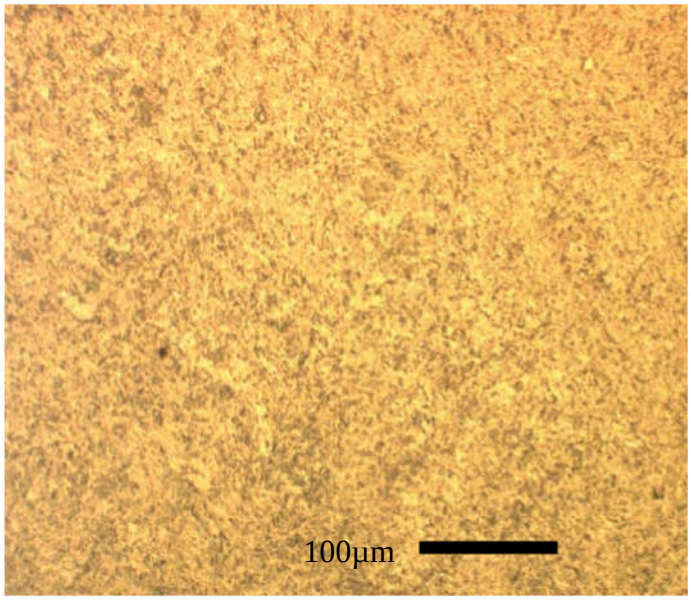

Figure C.1: Case 12 mc Cu 8B RT images, of region 1, etched, at 20x magnification, showing no prior particle boundaries, and no visible grain boundaries.

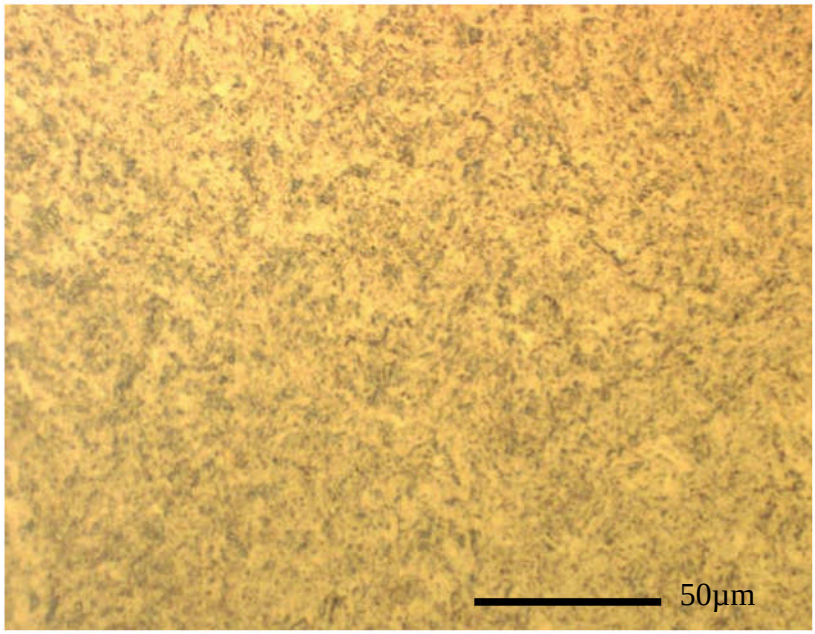

Figure C.2: Case 12 mc Cu 8B RT images, of region 1, etched, at 50x magnification, showing no visible prior particle or grain boundaries

.

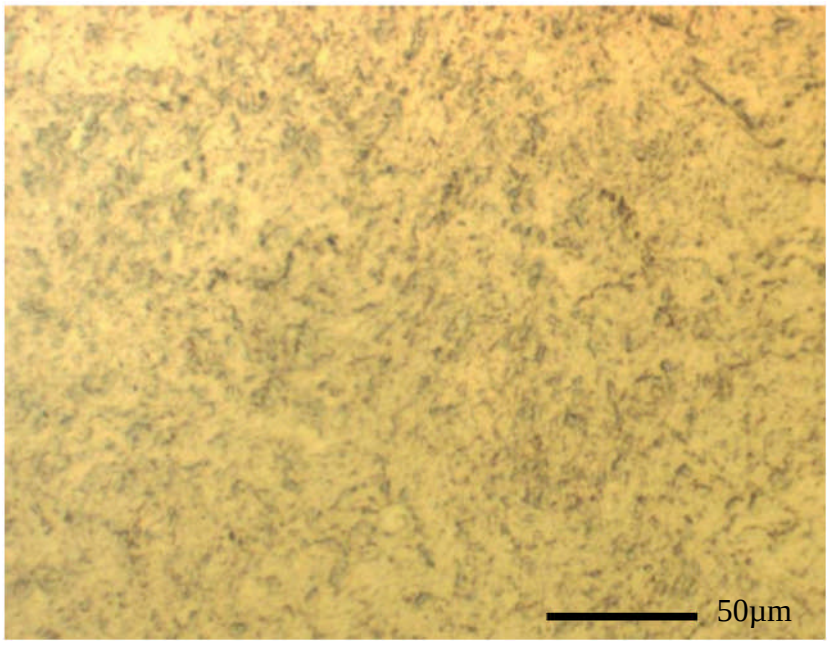

Figure C.3: Case 12 mc Cu 8B RT, of region 1, etched at 100 X magnification, showing no visible prior particle boundaries or grain boundaries

VITA

Name: CATHLEEN RUTH HUTCHINS

Address: Department of Mechanical Engineering
3123 TAMU
College Station TX 77843-3123

E-mail Address: c.hutchins@aggienetwork.com

Education: B.S., Industrial Engineering, Marquette University, 2005
M.S., Mechanical Engineering, Texas A&M University, 2007

Research interests: Failure analysis, metallurgy